Boundary Layer Control and Wall-Pressure Fluctuations in a Serpentine Inlet

by

David K. Harper

Thesis submitted to the Faculty of the
Virginia Polytechnic Institute and State University
in partial fulfillment of the requirements for the degree of

Master of Science

in

Mechanical Engineering

Wing F. Ng, Co-Chair
Ricardo A. Burdisso, Co-Chair
Clint L. Dancey

May 2000

Blacksburg, Virginia

Key words: Serpentine inlet, Separation, Boundary layer control, wall-pressure fluctuations

Boundary Layer Control and Wall-Pressure Fluctuations in a Serpentine Inlet

David K. Harper

(ABSTRACT)

In this thesis, the benefits of boundary layer control (BLC) in improving aerodynamic performance and engine stability were examined in a compact, serpentine inlet exhibiting flow separation. A 1/14-scale turbofan engine simulator provided the flow through the inlet. The inlet's mass flow was measured to be 759 scfm (0.939 lbm/s) with an average throat Mach number of 0.23 when the simulator speed was 40 krpm. Boundary layer suction, blowing, and their combination were used to minimize the inlet's flow separation. The effectiveness of the suction alone and the blowing alone was shown to be approximately equivalent, and the effectiveness of the combined use of both was seen to be better than either one by itself. With blowing and suction flowrates around 1% of the simulator's core flow, the inlet's distortion was lowered by 40.5% (from 1.55% to 0.922%) while the pressure recovery was raised by 9.7% (from 87.2% to 95.6%). With its reduction in distortion, BLC was shown to allow the simulator to steadily operate in a range that would have otherwise been unstable. Minimizing the flow separation within the inlet was shown to directly relate to measurements from flush-mounted microphones along the inlet wall: as the exit distortion decreased the microphone spectrum also decreased in magnitude. The strong relationship between the aerodynamic profiles and the microphone signal suggests that microphones may be used in an active flow control scheme, where the BLC effort can be tailored for different engine operating conditions. Unfortunately, the sensing scheme used in this experiment showed the microphone signal to continue to decrease even when the separation is overly compensated; therefore refinements must be made before it would be practical in a real application.

Acknowledgements

I would like to thank my co-advisors Drs. Wing Ng and Ricardo Burdisso for their wonderful support and technical expertise. I also would like to thank Dr. Clint Dancey for his time and effort as the final member of my advisory committee. I would like to acknowledge that funding for this project was provided through a SBIR Phase I Program given to Technology in Blacksburg, Inc (Techsburg) by the Air Force Research Lab in Dayton, OH under the technical direction of Skip Gridley.

Special thanks should be extended to Stephen Guillot, Randy Hibshman, and Tom Leitch, for they have been both mentors and friends throughout this endeavor. I would like to thank Jinwei Feng, Casey Carter, and Patrick Taylor for their long hours in helping me run the experiments. I am also thankful for Jerome Smith, whose experience and knowledge helped the microphone experiments run smoothly. I am also grateful for David Botos of Techsburg and Bill Songer of the Mechanical Engineering Department for their excellent machining abilities.

Finally, I would like to thank those most special to me. My parents and family have always supported me in all of my dreams and goals, and I truly value their love and friendship. I would like to thank my wife, Andrea, for her encouragement and support—especially during the preparation of this thesis. She understood my long hours and always helped me to keep things in proper perspective. Most importantly, I would like to thank the Lord Jesus Christ for His grace and comfort; I owe any and all of my success to Him.

Table of Contents

List of Figures

List of Tables

Nomenclature

Symbol	Meaning	Value
δ	Boundary layer thickness	~
γ	Ratio of specific heats for air	1.4
$\eta_{\sigma i}$	Incompressible flow index	~
ρ	Density of air	~
σ_i	Standard deviation of a sampled value	~
b_i	Bias error of a measurement	~
BLC	Boundary Layer Control	~
D	Distortion parameter	~
DAQ	Data acquisition	~
I	Distortion intensity	~
IGV	Inlet Guide Vane	~
krpm	Thousands of revolutions per minute	~
$\dot{m}$	Mass flowrate	~
M	Mach number	~
MEMS	Micro-Electro-Mechanical System	~
N	Simulator speed	~
p_0	Stagnation pressure	~
p_s	Static pressure	~
R	Ideal gas constant	53.3 ft-lbf/lbm-R
RCS	Radar Cross Section	~
rms	Root-mean-square	~
sfc	Specific Fuel Consumption	~
T	Temperature	~
TEB	Trailing Edge Blowing	~
TPR	Total pressure recovery	~
UAV	Unmanned Air Vehicles	~
u_i	Total uncertainty a measurement	~
V	Velocity	~
w	Width of inlet	4.1 in
y	Height above inlet floor	~

1.0 Introduction

Today's military aircraft must not only be light and agile, but also maintain a low radar cross section (RCS) that is difficult to detect. Many methods have been developed and proven for minimizing the RCS of the fuselage and wings of an aircraft, but the large metal blades within the engine's compressor easily reflect the radar energy striking it, which drastically increases the RCS of the entire aircraft (Jones 1989, p. 14). Hiding the face of the engine from the incoming radar signal is the best way to keep the RCS small. Therefore, a curved engine intake, known as a "serpentine inlet," is installed to scoop air from the free-stream while the engine is blended into the already-stealthy fuselage. The serpentine inlet diminishes the line-of-sight to the engine so that hostile radar cannot detect the metal surfaces of the blades.

Removing the line-of-sight while minimizing the weight of the inlet requires the development of compact and highly-offset diffusers. The curve in the inlet poses problems, however, to an engine designer because of the distortion created by the adverse pressure gradients. The inlet must possess enough of an offset to hide the fan-face from enemy radar, but Fox and Kline (1962) suggest that if the curved offset is too severe, the inlet will stall and develop flow separation to produce high levels of pressure distortion. A distorted total pressure profile entering the fan face has many drawbacks, but perhaps the most critical is the loss of stability (Williams and Surber 1993). The pockets of air with low mean-velocity may trigger rotating stall for the compressor fan, which decreases its efficiency, but if the distortion is severe enough, the rotating stall will progress into surge, which will fatigue the engine's components.

To combat the flow distortion and separation in a serpentine inlet, a designer has the option of adding an extension to the inlet to allow the flow to reattach and the distortion to attenuate (Williams 1986), or the designer can install a set of vane-type vortex generators to thoroughly mix the low-momentum with the high-momentum regions of the fluid (Anderson *et al*. 1999). Both options have shown success, but involve adding weight and manufacturing expense to the aircraft and are not adaptable to different operating conditions. Boundary layer control (BLC), explored in this thesis, is a

third option at the hands of an inlet designer. For a given inlet, BLC will minimize distortion without the extra weight of an extension or vanes. BLC treats the low-momentum fluid within the boundary layer that promotes separation. BLC can take the form of suction, blowing, or a combination of both. While suction attempts to remove the low-momentum fluid, blowing attempts to re-energize the low-momentum fluid for it to negotiate the strong adverse pressure gradients and remain attached to the inlet wall.

While the weight or complexity of the conventional suction source may have hindered boundary layer suction in the past, vacuum ejector pumps provide a lightweight, small-scale, and inexpensive solution with no moving parts. Long lossy suction lines can be avoided, since ejector pumps can be integrated into the inlet and use high-pressure air from the engine's compressor to provide the vacuum. Furthermore, the exhaust of an ejector pump has the potential to provide the boundary layer blowing, allowing a combined BLC effort for approximately the same amount of bleed from the latter stages of the compressor.

Tactical aircraft must fly in a large number of maneuvers, which adds to the difficulty in minimizing the distortion. Therefore, active flow control has promise to keep a serpentine inlet efficient through a larger range of conditions. Unfortunately, the implementation of active flow control in a serpentine inlet has been hampered by the lack of practical means to sense the effectiveness of the BLC.

Rioual *et al*. (1994) discovered that a microphone, mounted flush with the surface, could sense where the boundary layer transitions on a flat plate. The non-intrusive sensor showed that the pressure signal increased as the boundary layer grew turbulent. Rioual *et al*. used this discovery to actively control where the transition occurred with boundary layer suction. Also, Simpson *et al*. (1987) showed that turbulent pressure fluctuations, measured by microphones, in a separating flow, normalized by the turbulent shear stress, increases to the point of detachment but decreases after detachment. The information provided by Rioual *et al*. and Simpson *et al*. suggests a strong correlation between a flow structure and a microphone signal that can be used for an active BLC scheme.

The work presented in this document attempts to examine the benefits of BLC in a 2-D serpentine inlet in front of a 1/14-scale turbofan simulator. Ejector pumps were

used as the source for the boundary layer suction. The exhaust of current ejector pumps is not suitable for boundary layer blowing, so a regulated high-pressure line was used. Both aerodynamic and microphone experiments were performed to examine the effects of BLC on the flow field. The aerodynamic data showed that distortion decreases and pressure recovery increases as the BLC effort is increased. The microphone experiments were an initial step in developing an active flow control scheme to minimize distortion. The data suggests that as BLC effort is increased, the microphone signal decreases in amplitude within a low-frequency range.

Extrapolating from the results provided by Rioual *et al*. (1994) and Simpson *et al*. (1987), non-intrusive microphones were hypothesized to correlate the effectiveness of BLC on the total pressure profile at the exit of the inlet. An array of ten microphones along the centerline was tested for its ability to detect the degree of separation. It was shown that the microphone data correlated well with the aerodynamic data, but that refinements must be made before microphones could be used in an active flow control scheme to minimize separation.

This thesis is organized into five chapters: (1) Introduction, (2) Literature Review, (3) The Experiment, (4) Results and Discussion, and (5) Conclusions and Recommendations. Chapter 2.0 summarizes the previous work done that motivates the project's direction. Chapter 3.0 describes in detail the experiments performed and the test facilities used. Chapter 4.0 summarizes the results of the experiments and discusses their meaning. Finally, Chapter 5.0 concludes this thesis and provides recommendations for future work.

2.0 Literature Review

Serpentine inlets are gaining importance in tactical aircraft since they hide the engine face from enemy radar. As the push for sleeker, better performing aircraft increases, the development of compact, highly-offset diffusers are becoming critical. Unfortunately, compact serpentine inlets tend to create high levels of distortion and low levels of pressure recovery. The first section of this chapter will discuss how distortion reaches an engine and how it relates to the engine's performance. The next section will demonstrate some previous work to minimize separation and distortion by flow control. The final section will introduce the reader to the subject of aeroacoustics within a boundary layer, which may lead to the formulation of a proper feedback sensor for an active BLC scheme.

2.1 Distortion and Its Effect on Engine Performance

Engine face distortion is a troublesome area for inlet designers. Williams and Surber (1993) points out that the inlet must be robustly designed to ingest the boundary layer formed by the aircraft fuselage and the vortices created by an upstream source such as a wing, while minimizing separation and secondary flow within the inlet itself. Ball (1984) showed that the shape of the entrance boundary layer profile has a strong influence on the total pressure recovery and distortion at the exit. Anderson and Gibb (1998) warn that an inlet designer must be able to account for a wide range of flight conditions and maneuvers. For example, extreme angles of attack tend to separate the flow at the cowl lip, and extreme aircraft acceleration can generate secondary flow within the inlet.

A non-uniform total pressure profile reaching the engine face has many adverse effects on the engine's characteristics. Figure 2.1 shows how the surge margin decreases as the level of circumferential distortion increases. Note that when the circumferential distortion goes above the critical angle of 90°, the surge line changes very little. The figure also shows that a loss of efficiency is created by distortion. Figure 2.2 reiterates

the effect that distortion intensity has in losing surge pressure ratio (Williams and Surber 1993).

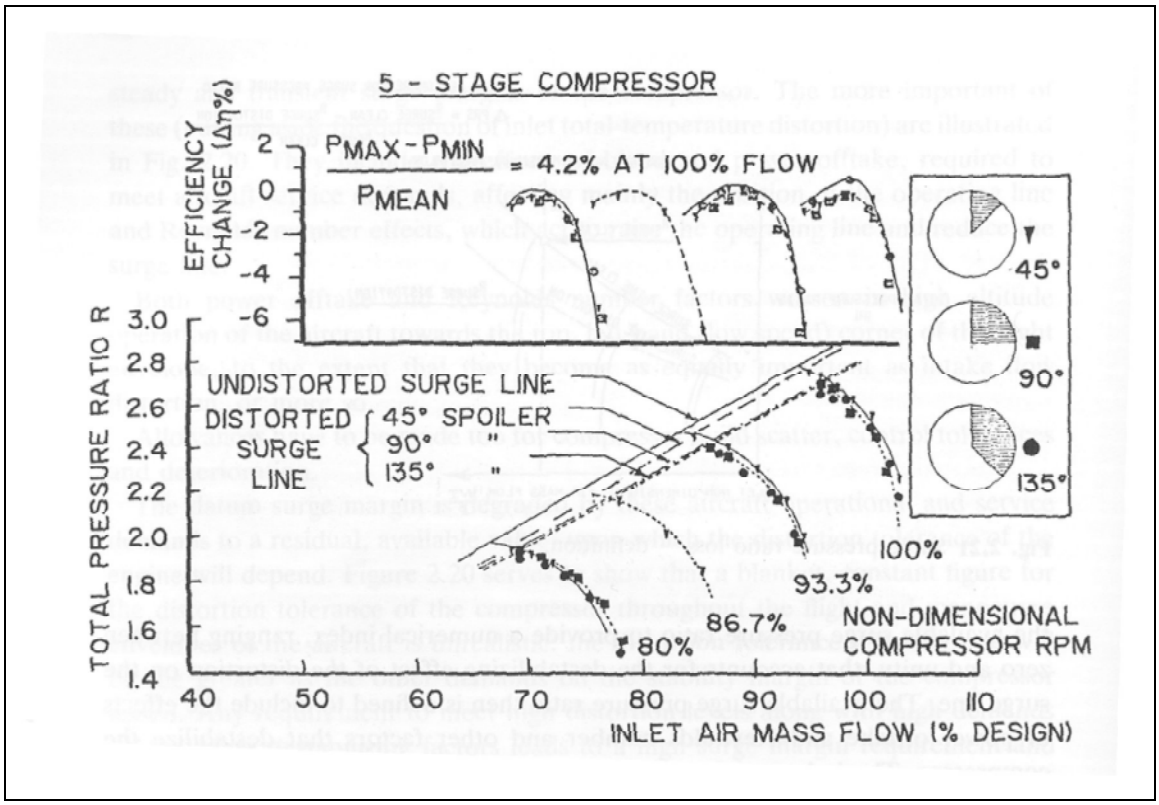

Figure 2.1: Effect of distortion on a compressor map (Williams and Surber 1993)

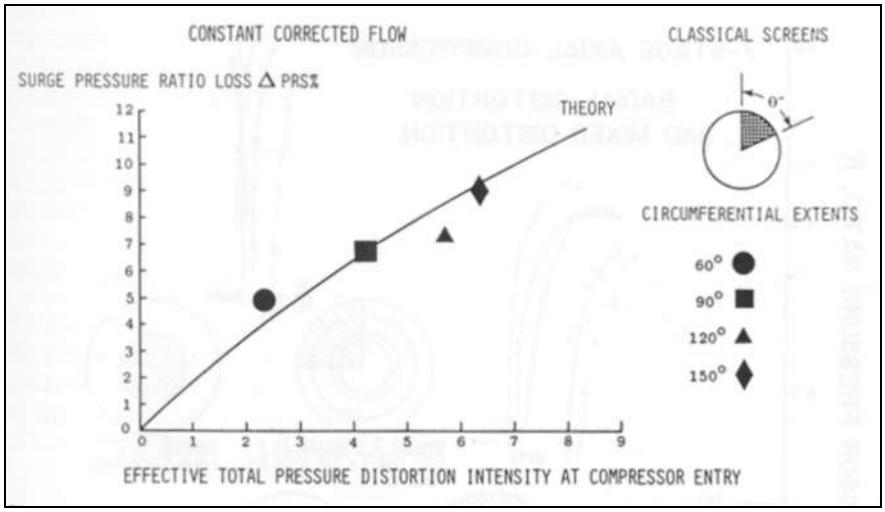

Figure 2.2: The surge pressure ratio's sensitivity to distortion (Williams and Surber 1993)

Due to curvature, even essentially isentropic serpentine inlets can have a non-uniform static pressure distribution at the exit of the inlet, which Williams (1986) claims to directly affect an engine's thrust, demonstrated by Figure 2.3. Williams shows that if short extensions are placed between the exit of the inlet and the engine face, the non-uniformity is attenuated and the thrust is improved by as much as 3% at constant corrected speed or as much as 6% at constant jet-pipe temperature (JPT).

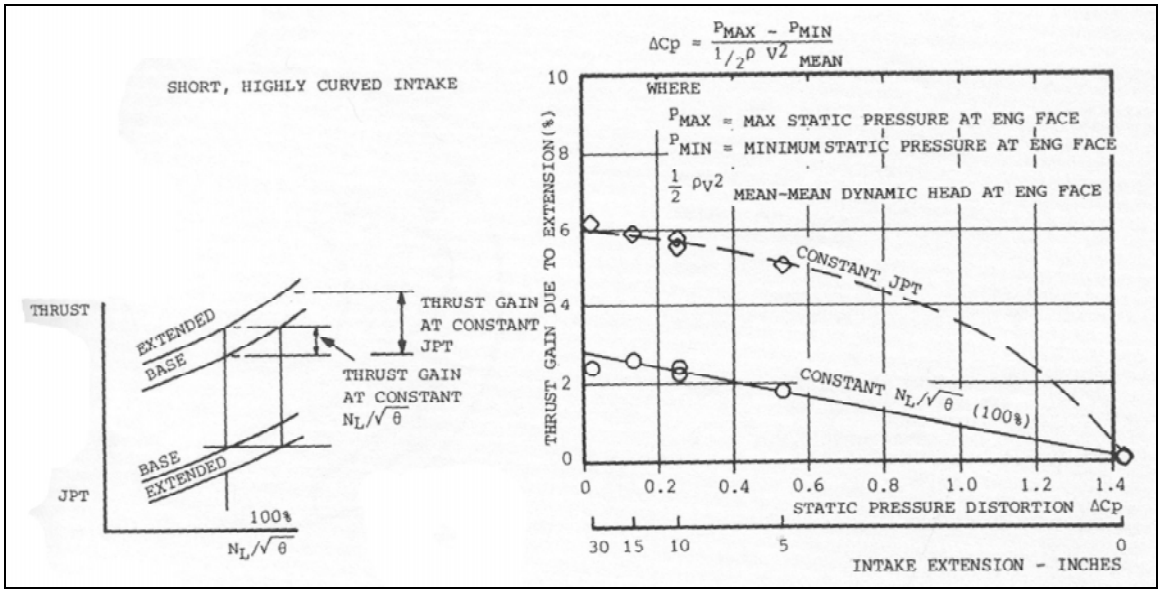

Figure 2.3: Effect of distortion on engine thrust (Williams 1986)

Williams and Surber (1993) explain that it is difficult to correlate distortion with performance since the response to the whole system must be determined, but they mention that distortion can hinder the performance of variable geometry features like tandem stators by creating misalignments with flow sensors. They also show that compressor surge is much more sensitive to distortion than performance quantities such as thrust, specific fuel consumption and air mass flow. Figure 2.4 is a summary of an engine test performed at sea level where the distortion was created with wire mesh screens. Williams and Surber note that any measured changes in the performance parameters shown that are due to distortion are most likely within the range of test uncertainty. Section 4.1.3 of this document will present the aerodynamic distortion data for the different BLC schemes, and Section 4.1.4 will show that BLC enabled the test simulator to operate above its normal surge pressure ratio.

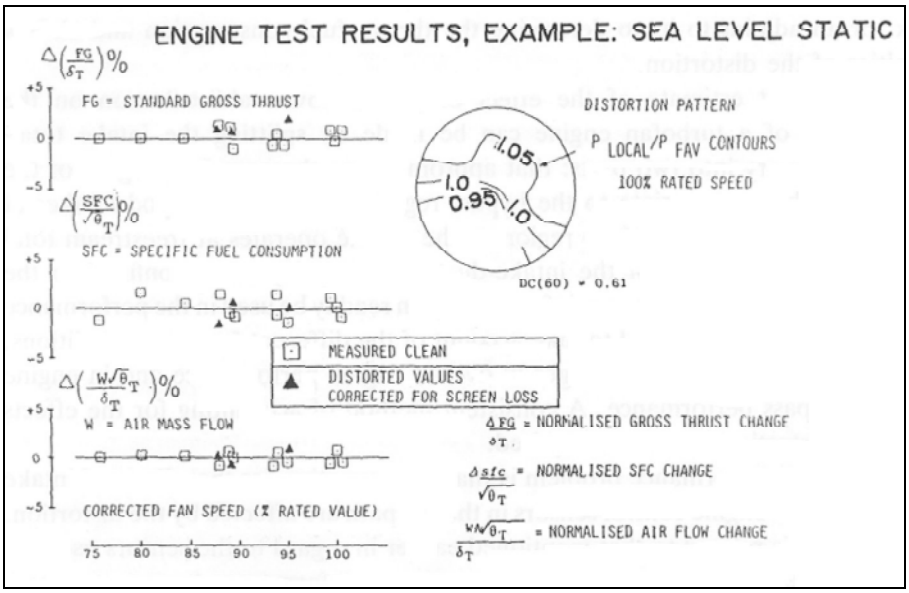

Figure 2.4: Engine performance as a function of distortion (Williams and Surber 1993)

2.2 Previous Flow Control Efforts

Leitch (1997), Rao (1999), and Feng (2000) used trailing edge blowing (TEB) on an inlet guide vane (IGV) to minimize the distortion responsible for a periodic loading of the first compressor rotor. All three used the same test facilities, which included a small turbofan simulator with a constant-area inlet with four flat IGVs. In Figure 2.5 and Figure 2.6, Leitch shows the effect wake management has on aeroacoustics by reducing the circumferential distortion by 22.4%, the engine tones by 8.9 dB, and the overall SPL by 1.0 dB. Using Pitot-Static probes for error signals and MEMS-based microvalves as actuators, Rao introduced active flow control to the TEB system Leitch proposed. Rao lowered the engine tones by as much as 8.2 dB and reduced the sound power by as much as 64%. Feng (2000) replaced Rao's Pitot-Static probes with non-intrusive casing microphones, which empowers active flow control to become an efficient means to manage wake deficits.

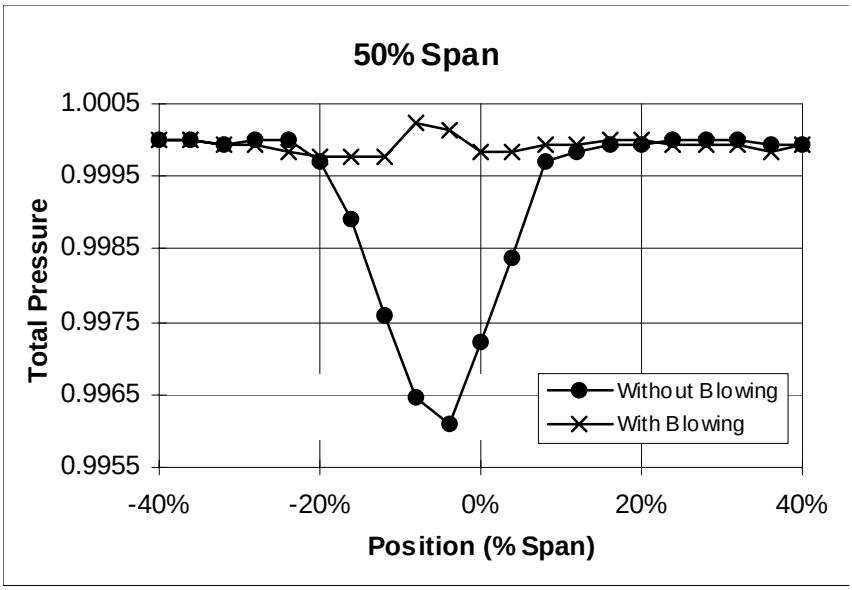

Figure 2.5: Benefit of TEB on the wake profile behind an IGV (Leitch 1997)

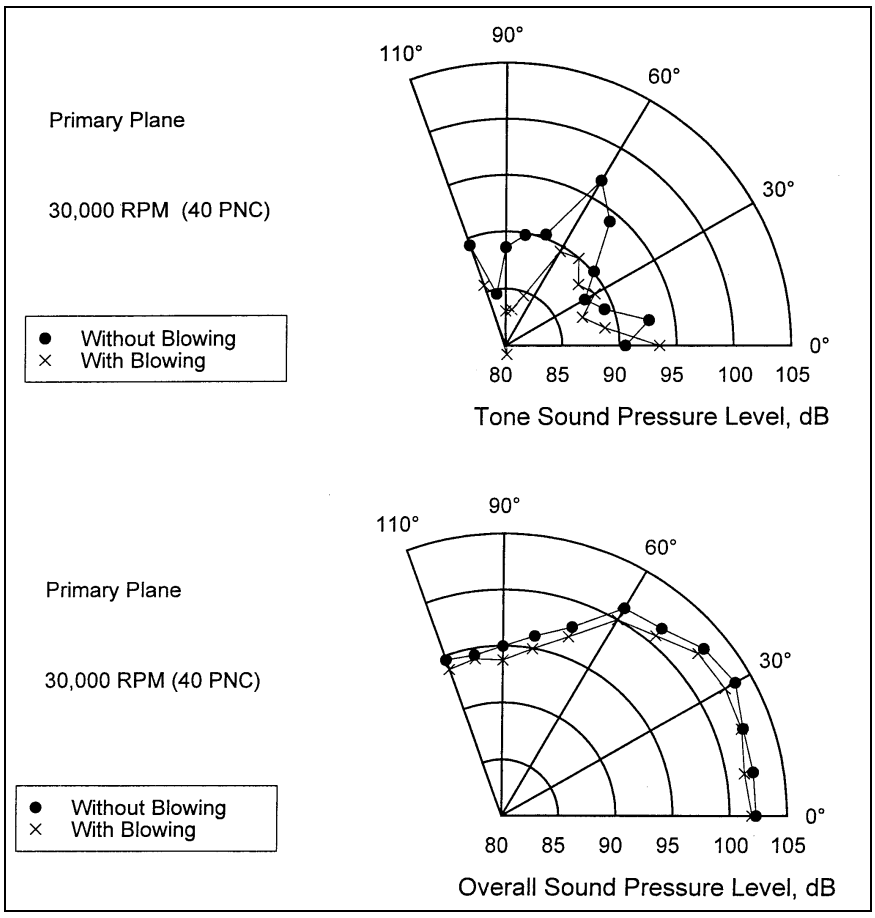

Figure 2.6: Effect of TEB on the directivity of the acoustic signature (Leitch 1997)

Rioual *et al*. (1994) demonstrated active flow control to delay the laminar to turbulent transition of a boundary layer. The test apparatus was a suction panel on a flat plate in a wind tunnel with a free-stream Reynolds number (based on the plate's length) of $2.2(10)^6$. An array of microphones downstream of the suction panel measured the pressure fluctuations as the boundary layer grew turbulent. Figure 2.7 shows the development of turbulent spots that spread into a full-blown turbulent boundary layer as the distance from the leading edge is increased. Each microphone signal was conditioned and then sent to a controller for the centrifugal pump to control the suction flowrate. Figure 2.8 shows the root-mean-square (rms) pressure decreases as the suction flowrate increases. It also shows that as the boundary layer grows from the leading edge, the microphone sees a higher rms pressure. Rioual *et al*. measured the rms pressure of each microphone corresponding to the desired transition point and then programmed the controller to match the microphone signals by varying the suction flowrate.

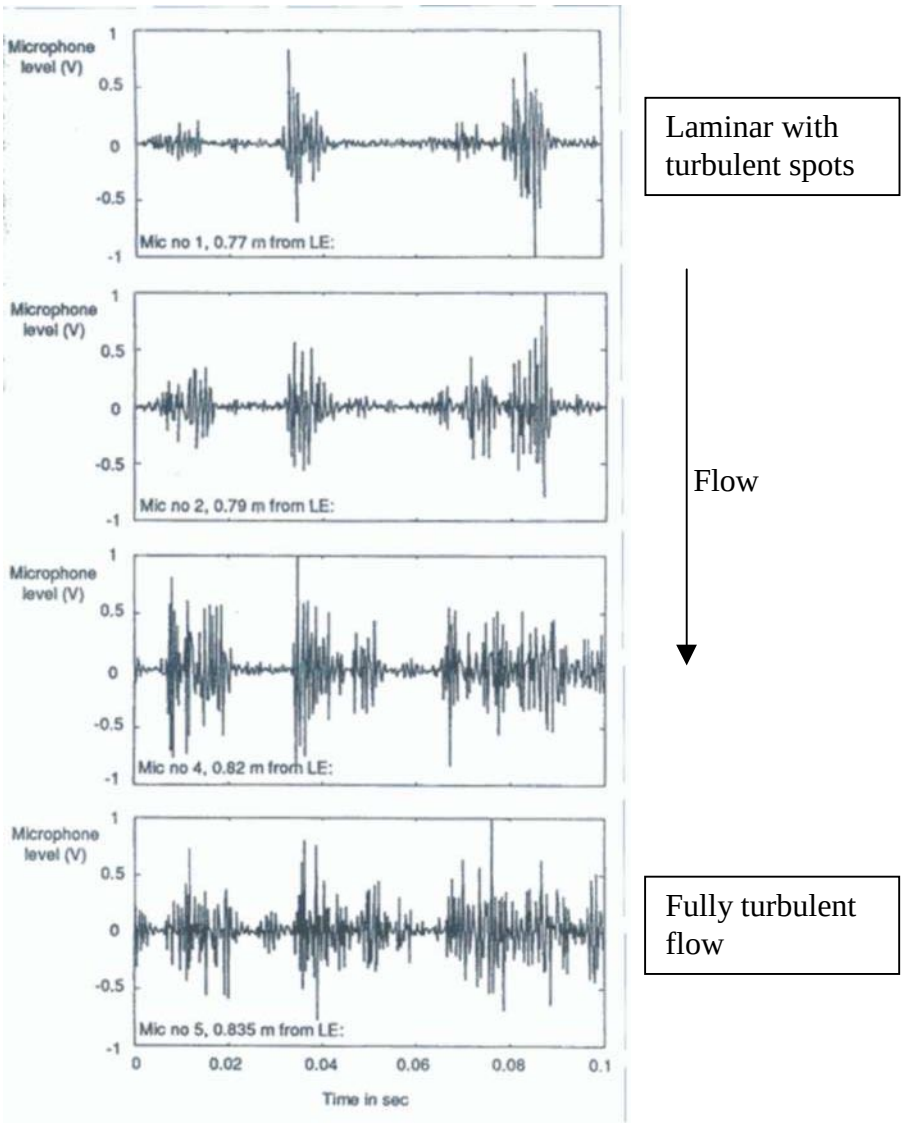

Figure 2.7: Microphone signals in a transitioning boundary layer (Rioual *et al*. 1994)

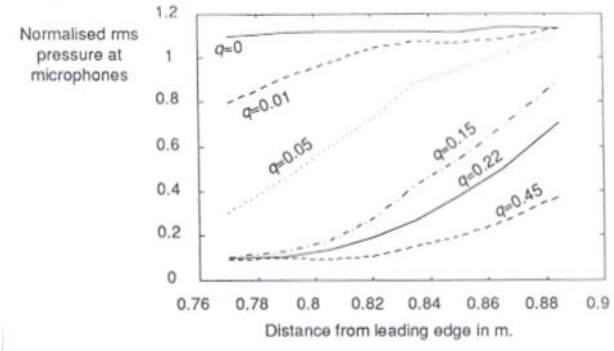

Figure 2.8: Pressure fluctuations with varying amounts of suction (Rioual *et al*. 1994)

Vane-type vortex generators are commonly used to control separation in inlets by locally mixing the low-momentum part of the fluid with the high-momentum part. However, there has been limited success for these vortex generators in serpentine-ducts because of their lack of adapting to off-design flight conditions. To that end, B. H. Anderson *et al*. (1999) attempted to globally control the inlet flow conditions with small vortex generators ideal for compact inlets and MEMS-actuated active control schemes. Their approach is not to prevent separation but to mix the low- and high-momentum parts of the fluid to maximize pressure recovery and minimize distortion. They suggest that vortex flow control is not just a function of how the vorticity is formed, but the overall vorticity strength and distribution to maximize mixing. This concept has sparked a transition from finding the right vane geometry, to finding the right vorticity signature that will be effective on a large range of inlet conditions.

Ball (1983) of Boeing Military Airplane Company performed several experiments in the mid-1980s to show the effects of another type of flow control in serpentine inlets: wall suction and blowing. He used a 3-D serpentine diffuser with area suction and slot blowing and found that with a suction flowrate at 6% of the core flow the total pressure recovery improved by 1.23%. Independently, he also found that with 3.5% blowing the total pressure recovery improved by 1.64%. The effect that suction and blowing have on distortion and total pressure recovery is shown in Figure 2.9, and in Figure 2.10 suction and blowing are seen to improve the total pressure ratio profile at the exit of the inlet. Unlike the work presented in this thesis, Ball did not combine suction and blowing to determine the benefit that both may provide in improving total pressure recovery, distortion, or exit profiles.

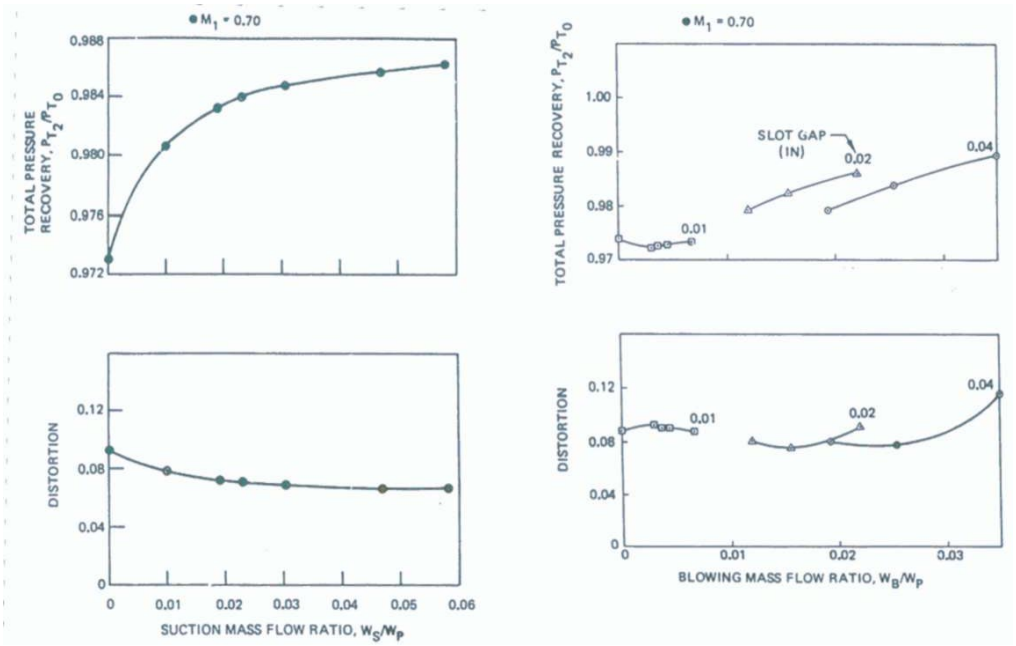

(a) (b)

Figure 2.9: Ball's (1983) results using boundary layer suction and boundary layer blowing.

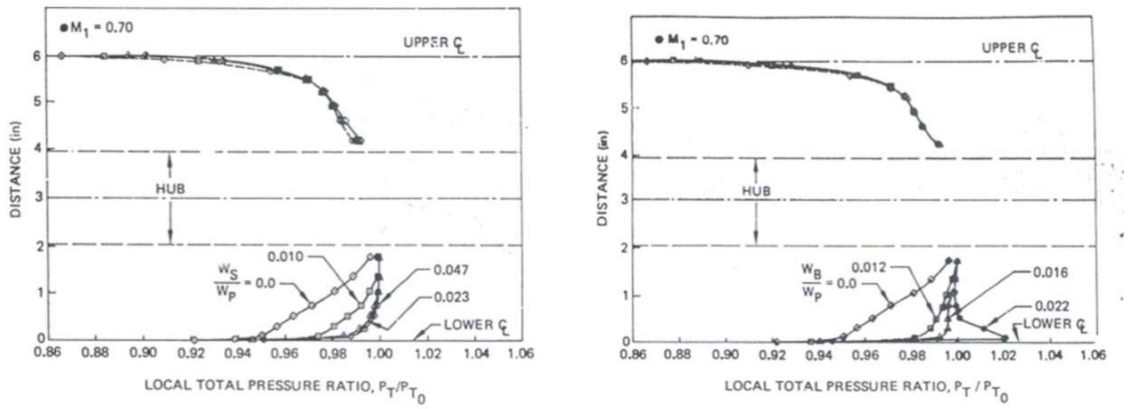

(a) (b)

Figure 2.10: Exit total pressure profiles of serpentine inlet with (a) Suction and (b) Blowing (Ball 1983)

Later, Ball (1984) optimized his blowing scheme by adding different types of blowing jets: discrete tangential jets, slanted holes, vortex generators, and jets aimed at the diffuser corners. He also examined the benefits of directing the jets toward the corners of the walls. He found that the discrete jets provided the best configuration at only 0.6% blowing. Figure 2.11 shows that there is an optimum blowing rate, which Ball speculates to be where the static pressure of the jet matches the wall's local static

pressure, and therefore, the mixing is most efficient. He did not, however, optimize the location of the blowing holes (placed just before the predicted separation point), nor did he perform the same parametric study with boundary layer suction. The blowing scheme chosen for this project used 16 blowing holes slanted directly downstream.

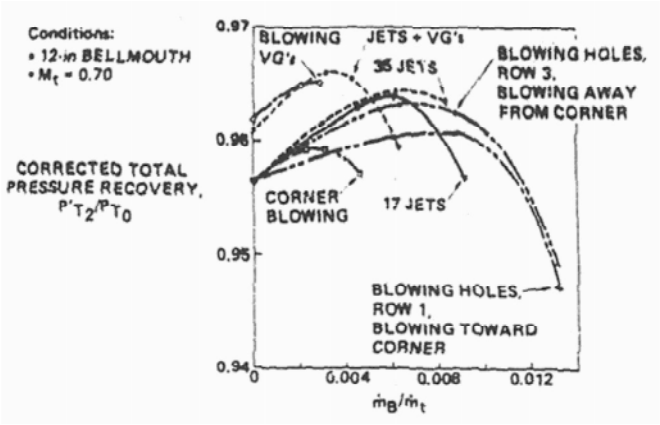

Figure 2.11: Ball's (1984) results using boundary layer blowing

2.3 Sensing of Turbulent, Separated Flow

Microphones in a stream of fluid create a signal with several components. Agarwal and Simpson (1989) explain that a microphone signal represents acoustic pressure, turbulent pressure fluctuations, and wall vibrations. Lighthill (1951) explored the acoustic pressure component, and his theory is explained in the first subsection. The second subsection explains that the turbulent pressure fluctuations and wall vibrations are not governed by the acoustic wave equation. The third subsection shows how the turbulent pressure component is resolved from a set of microphone signals. The work summarized in this section will provide relevance to the microphone data presented in Section 4.2.

2.3.1 Aeroacoustics: Lighthill's Theory

Sir M.J. Lighthill (1951 and 1954) is one of the pioneers in developing a base of knowledge on aeroacoustics. His famous theory models the fluctuating density within an arbitrary fluid motion as a sound propagating through a uniform fluid at rest subject to a

fluctuating external force field. He shows that the physical mechanism for the generation of aerodynamic noise is the fluctuating Reynolds-type stresses associated with turbulence. Since the shearing stresses create a positive displacement in one diagonal direction of the fluid particle and a negative displacement in the other, the sound behaves like an acoustic quadrupole that becomes stronger as the Mach number increases. Lighthill's theory has provided a means to not only identify the source of aeroacoustics, but also its behavior (Laufer *et al*. 1964).

2.3.2 Turbulent Pressure Fluctuations: Pseudo Noise

Besides the acoustic noise created by fluctuating turbulent stresses that Lighthill described, turbulent pressure fluctuations are another component to a microphone signal within a flow. Pressure fluctuations that exist under turbulent boundary layers or within shear layers are caused by eddies and vortices impinging on the microphone diaphragm and are therefore not governed by the acoustic wave equation. Turbulent pressure is sometimes referred to as "pseudo noise," because it may be detected as an acoustic pressure wave, but is actually the varying, instantaneous static pressure within a turbulent flow. The wave speed of the turbulent pressure fluctuation is not the speed of sound but simply the convecting speed of the eddy or vortex that creates it. As seen in Figure 2.12, the pressure fluctuations are generally low-frequency and may peak at a normalized frequency of about 0.2 (Ross 1976, p. 192). At lower frequencies, the turbulent pressure fluctuations are affected by extraneous noises, but at higher frequencies the pressure fluctuations may cancel due to the large size of the microphone compared to the wavelength of the fluctuation (Ross 1976, p. 192). The magnitude of the pressure fluctuations tends to fall with an inverse power of the frequency (Agarwal and Simpson 1989). Ross (1976, p. 193) points out that turbulent pressure fluctuations are related to turbulence levels, which are generally created by wall shear stresses, so minimizing drag will tend to minimize the turbulent pressure fluctuations.

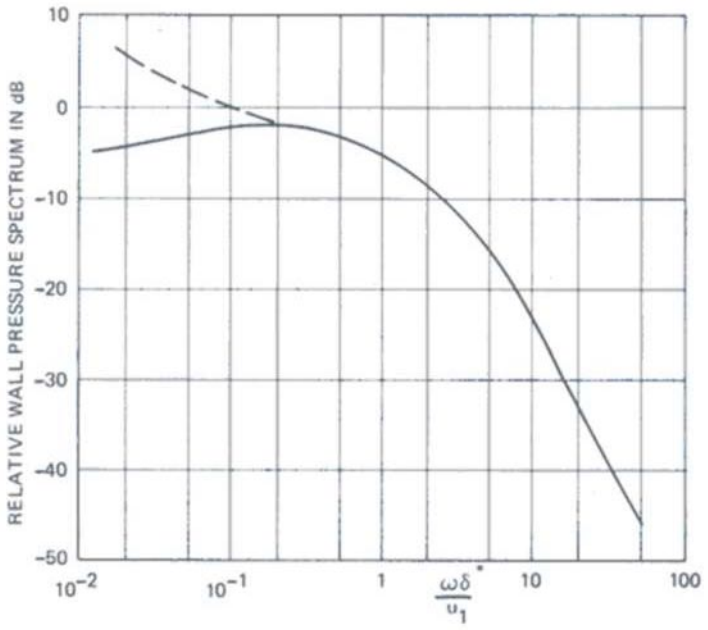

Figure 2.12: Pressure spectrum under detached boundary layer (Ross 1976, p. 192)

2.3.3 Resolving Fluctuating Pressure Components

Measuring pressure fluctuations have increased the understanding of turbulent boundary layers. The methods engineers have developed to measure the turbulent pressure spectrum without the contamination of true acoustic sources, or vice-versa, have relied on the foundation that acoustic pressure and turbulent pressure are incoherent and that acoustic waves are known to be planar below the duct cutoff frequency. Many have been proposed, but only two will be presented here.

Simpson *et al*. (1987) proposed a method to discriminate turbulent pressure from acoustic pressure by separating two microphones in the spanwise direction by at least ½ of the boundary layer thickness, which is said to be greater than the largest local vortex. They assume that the mean-square of the two turbulent pressure components of the microphones are equal, but their cross-correlation is zero since the vortices that create them have the same magnitude but are not in phase. Since the acoustic pressure is the same everywhere, they are able to resolve the true turbulent component by Equation (2.1).

$$\overline{p_{Tn}^2} = \tfrac{1}{2}\overline{(p_{1n} - p_{2n})^2} \quad (2.1)$$

where p_{Tn} is the turbulent pressure at spectral frequency n
p_{1n} is the first microphone signal at spectral frequency n
p_{2n} is the second microphone signal at spectral frequency n
$\overline{(\ )^2}$ represents the mean of the square of $(\ )$

Agarwal and Simpson (1989) were able to refine the previous method by allowing the microphones to be closer together but introducing a time delay, τ, in one of the microphone signals. Since the randomly distributed turbulent pressure component of the delayed microphone signal is uncorrelated with that of the other microphone, Equation (2.2) can find the turbulent pressure for frequencies $1/\tau$ and its higher harmonics.

$$\overline{p_t(t)^2} = \tfrac{1}{2}\overline{[p_1(t) - p_2(t+\tau)]^2} \quad (2.2)$$

where $p_t(t)$ is the turbulent pressure at time t
$p_1(t)$ is the microphone signal at time t
$p_2(t)$ is the second microphone signal at time $t+\tau$
$\overline{(\ )^2}$ represents the mean of the square of $(\ )$

3.0 The Experiment

This chapter will describe the experiments performed during this research project. The first section will describe the turbofan simulator, inlet geometry, ejector pumps, and measurement devices. The second section will describe the research facility, and the final section will describe the test procedure. The results of the experiments are presented in Chapter 4.0.

3.1 Test Setup

This section illustrates the equipment used in performing the experiments. The function and use of the simulator is detailed in the first subsection, and the design of the inlet is found in the second subsection. A description of ejector pumps and the measurement devices are presented in the final two subsections.

3.1.1 Simulator

A turbofan simulator provided the flow through the serpentine inlet. The simulator provides a realistic flow regime that exists in an inlet attached to a bypass turbofan engine found on military aircraft. The simulator has the ability to operate on a wide range of rotational speeds to provide a variable inlet throat Mach number. The simulator is a Tech Development Model 460 and is shown in Figure 3.1. It consists of a single stage fan with 18 rotor blades and a single stage turbine with 29 blades. The turbine, coupled to the fan, is driven by high-pressure air. The fan draws in ambient air that bypasses the turbine. The fan operates at a design speed of 80 krpm with a pressure ratio of 1.60 and a mass flow of 2200 scfm (2.72 lbm/s), but has a wide range of operability. Figure 3.2 and Figure 3.3 show the fan and turbine maps, respectively, with a conventional inlet. The fan diameter is 4.10 inches, and the length of the simulator is 6.57 inches. A magnetic pickup measures the rotational speed, and two thermocouples measure the bearing temperatures for the fan and turbine. The simulator's bearings are kept well-oiled with Exxon 2380 Turbo Oil.

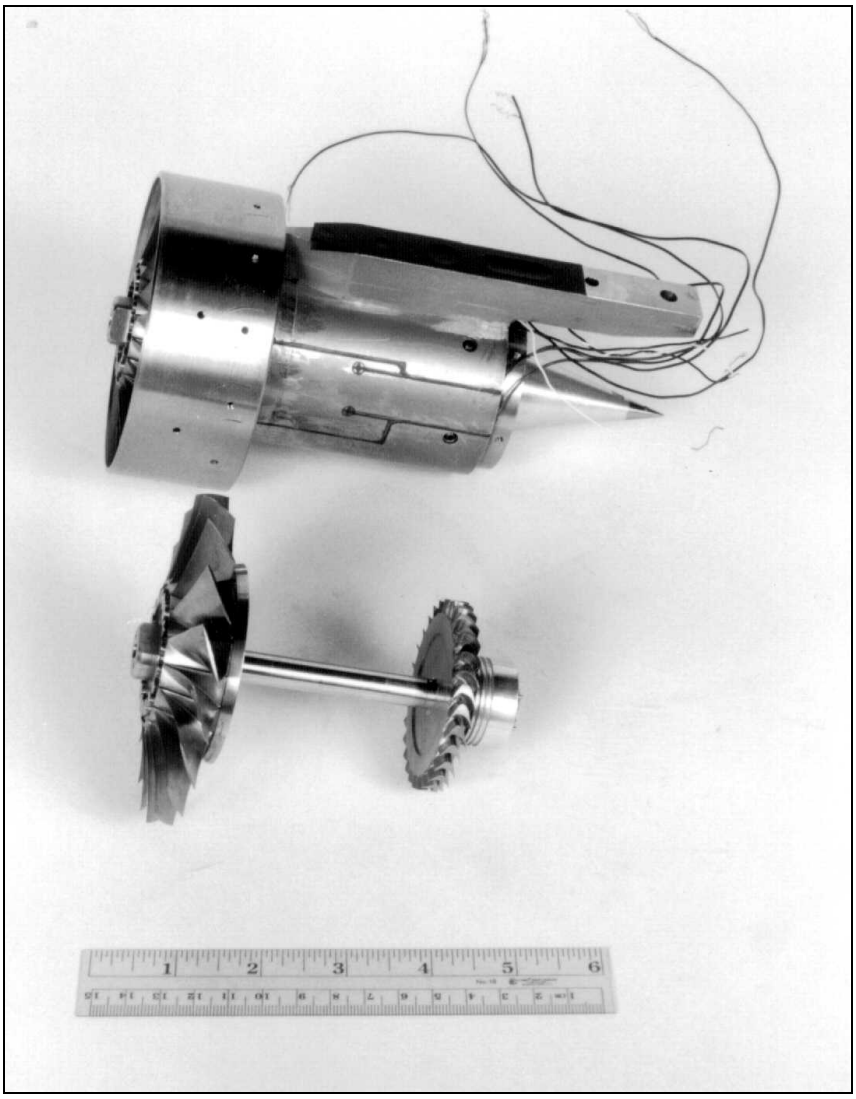

Figure 3.1: The turbofan simulator

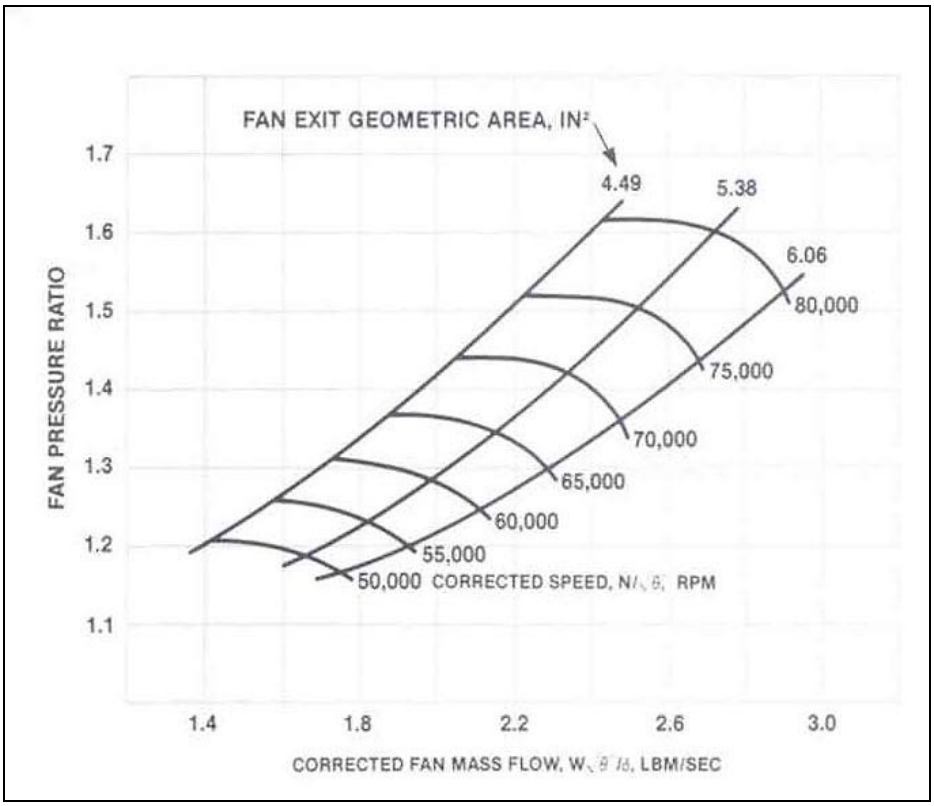

Figure 3.2: Simulator fan map (Model 460)

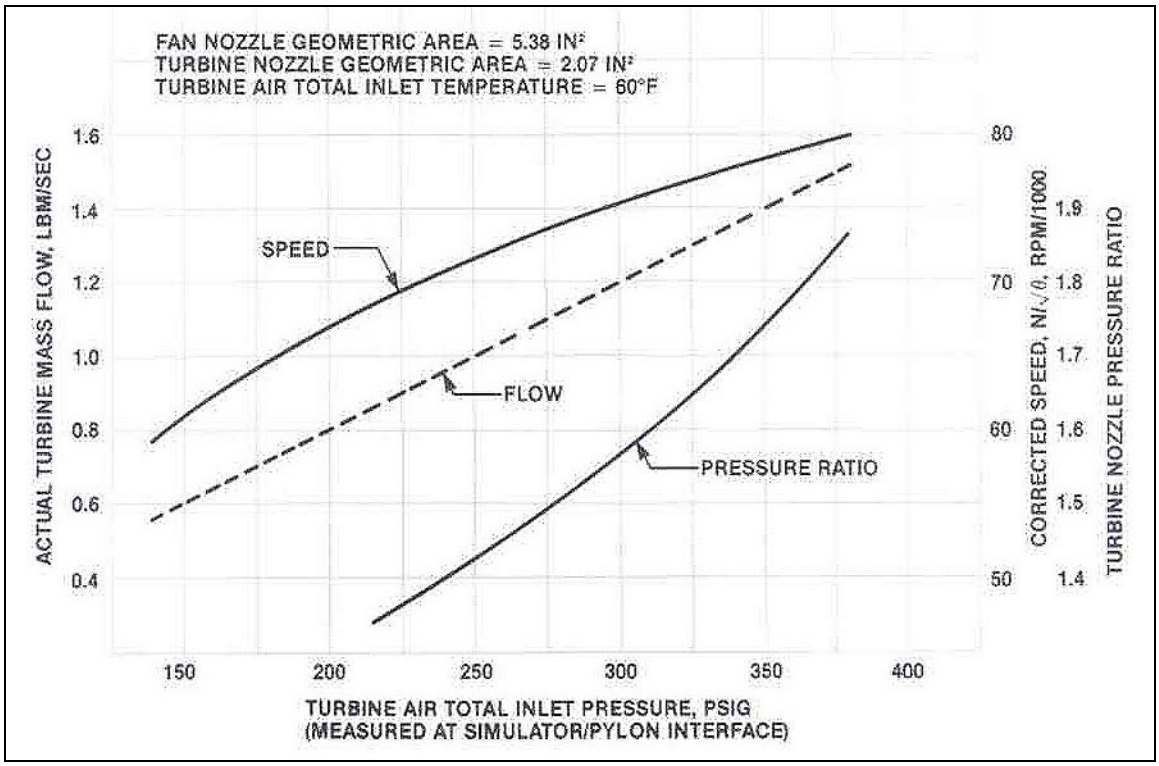

Figure 3.3: Simulator turbine map (Model 460)

3.1.2 Inlet

This subsection describes the inlet used in the experiments and is divided into two parts. The first part describes the design of the inlet, while the second part describes the design of the suction and blowing holes used for the BLC.

3.1.2.1 Geometry of the Inlet

In front of the simulator, an inlet was placed that modeled an inlet found on a modern stealthy, tactical aircraft engine. The inlet is designed to maintain acceptable levels of distortion and pressure recovery while minimizing the radar signature of the engine by reducing the line of sight to the fan-blades. The inlet geometry was based on the geometry used by W.H. Ball (1983) at Boeing Military Airplane Company. Ball used a 2-D model as a working prototype, and then made a comparable 3-D model. Ball found that the 2-D and 3-D models gave similar results. Therefore, the inlet used in this project was the simpler 2-D inlet scaled to the dimensions of the simulator. A picture of the inlet, which will be referred to as the "Techsburg inlet," is shown in Figure 3.4.

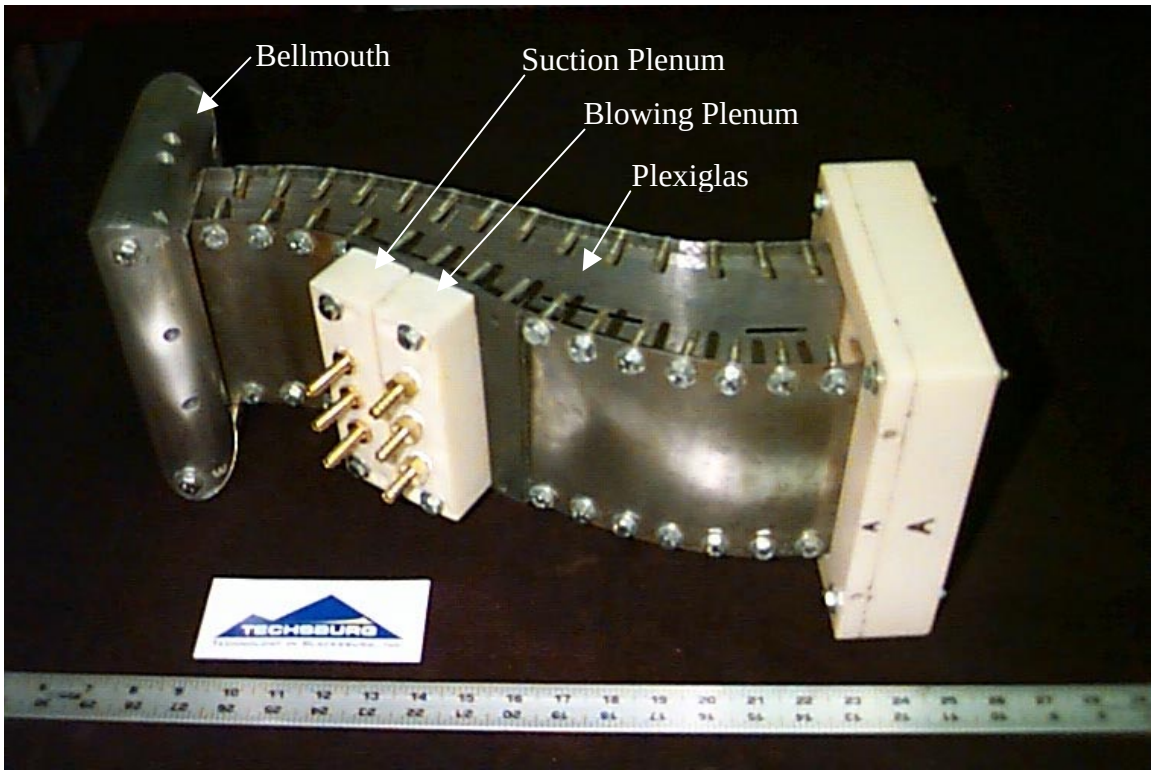

Figure 3.4: Picture of inlet with suction and blowing plenums

Table 3.1 and Figure 3.5 compare Ball's 2-D inlet with Techsburg's prototype inlet. Ball's inlet was scaled down so the width and exit height of the inlet could match the simulator's dimensions. Then, to make the Techsburg inlet more compact, the inlet's length was further shortened by a factor of 0.80. This was done in hopes of showing how BLC can allow for shorter inlets. The shorter inlet, without BLC, promotes stall at lower Mach numbers. A prototype of the Techsburg inlet was tested on the intake to a blower, as described in Appendix A, to ensure that it does indeed separate, but not drastically enough that it could not be delayed or prevented by boundary layer suction and blowing.

Table 3.1: Comparison of Ball's (1983) and Techsburg's inlet

	Ball (1983)		Techsburg
	Actual	Scaled to Size of Simulator	
Length, L [in]	20.4	14.95	12.0
Entrance Height, H_{ent} [in]	2.89	2.12	2.04
Exit Height, H_{exit} [in]	5.32	3.90	3.90
Width, w [in]	5.32	3.90	4.07
Centerline Offset, Δ [in]	7.28	5.33	4.59
Area Ratio, A_{exit}/A_{ent}	1.84	1.84	1.91
Δ/H_{exit}	1.37	1.37	1.18
L/Δ	2.80	2.80	2.61

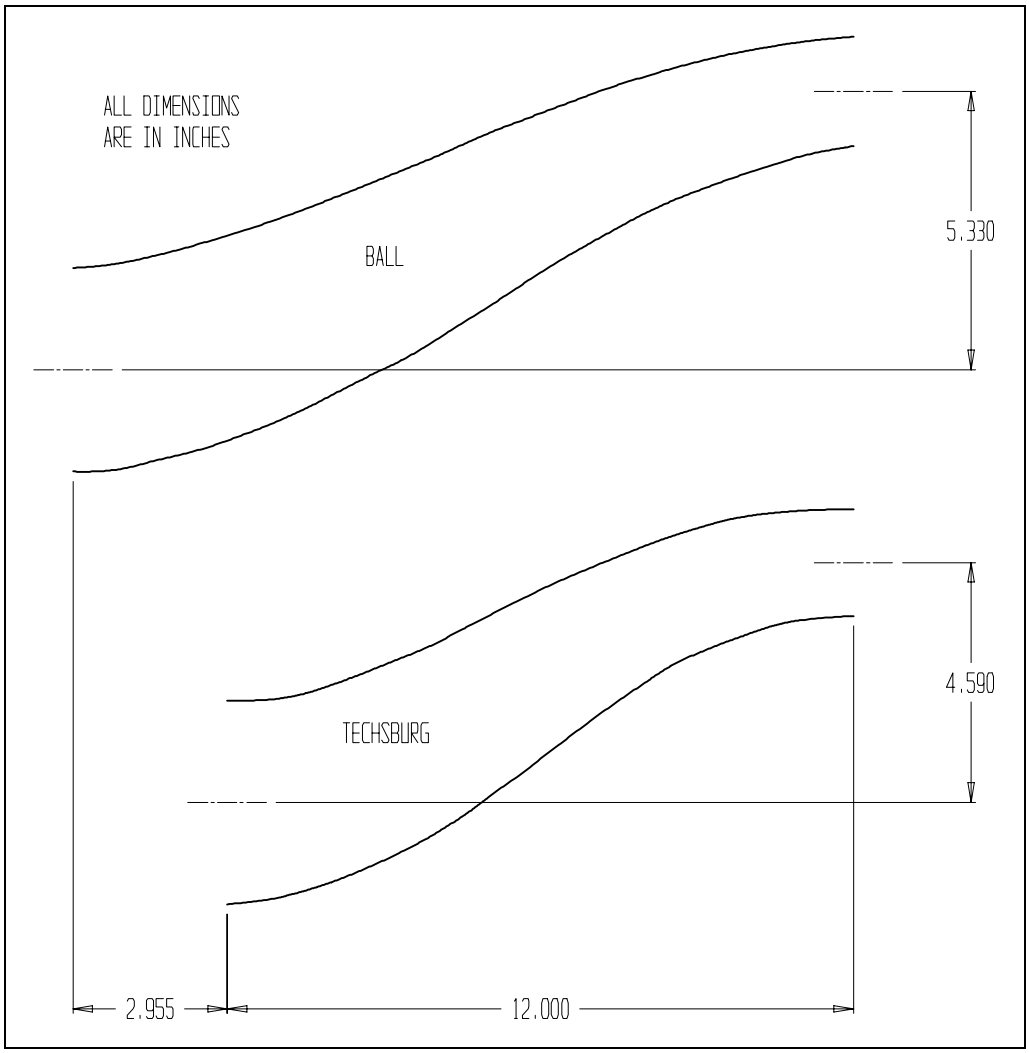

Figure 3.5: Comparison of Ball's (1983) and Techsburg's inlet

The inlet suffers from separation because of two important factors: diffusion and curvature. The inlet diffuses the air to prevent shocks from forming on the rotating blades of the fan, and the inlet curves to "hide" the fan-face from radar signals. The area distribution, showing the rate of diffusion of Techsburg's inlet, is given in Figure 3.6.

Figure 3.6: Area distribution of the inlet used in experiment.

A bellmouth was designed and installed onto the inlet to prevent separation at the entrance. It is made of 2-in aluminum bar stock and has a rectangular entrance with a length-to-width ratio of 2:1. The measurements made at the throat, presented in Section 4.1.2, suggest that the bellmouth provides a well-behaved boundary layer before the diffusion and turning is introduced.

The inlet was made of ¾-in Plexiglas sides for visual inspection of probe position and orientation. The curved surface at the top was made out of a 0.028-in aluminum sheet. The bottom surface was made out of a 0.033-in steel sheet. Aluminum was chosen for the top because of its flexibility, but the steel was chosen for the bottom surface for its ability to weld the blowing apparatus to the curved surface.

The simulator has a circular cross-section, but it was desirable to make the inlet two-dimensional with rectangular cross-sections. A 3-D transition duct that transforms

the rectangular inlet to the circular simulator matched the two different cross-sections. The 7.5-in long transition piece was made out of stereolithographic material.

3.1.2.2 Hole Geometry

The suction and blowing holes had to be designed to effectively control the boundary layer. The number, position, and orientation of the holes had to be determined. Kerrebrock *et al*. (1998) suggested that boundary layer suction is most effective in delaying separation at the point just upstream of the would-be separation point; it is least effective when the flow is well-attached. With this observation in mind, bench tests were performed to determine the separation point so that the suction holes could be placed just upstream of it. Iterations on the hole design were also made on the bench tests, described in Appendix A. A detailed parametric study to find the optimum configuration was not performed in this experiment.

High- and low-pressure plenums were placed directly on the inlet to provide a source for the blowing and suction holes. The plenums were reamed-out ABS plastic blocks. The suction and blowing plenums each had three 3/8-in polyethylene flexible lines attached to the respective source. The plenums were intended to stagnate the air immediately next to the inlet so that the blowing or suction would be evenly distributed across all of the holes. The plenums were bolted against the bottom surface and sealed with a ¼-in soft rubber (Sorbothane) gasket.

The design for suction holes is summarized in Table 3.2. The bench tests showed that this configuration was the most effective of all configurations tried. Figure 3.7 shows a drawing of the suction and blowing holes. The suction holes were kept as large as possible to minimize losses, but as Poisson-Quinton and Lepage (1961) noted, a finely perforated suction surface provides the best means to control separation.

Table 3.2: Description of suction and blowing hole geometries

	Suction	Blowing
Number of Holes	17	16
Hole Diameter [in]	0.055	0.035
Space Between Holes [in]	0.125	0.125
Span of Holes Across Inlet Surface [in]	2.00	1.875
Angle from Surface [°]	90.0	≈10.0

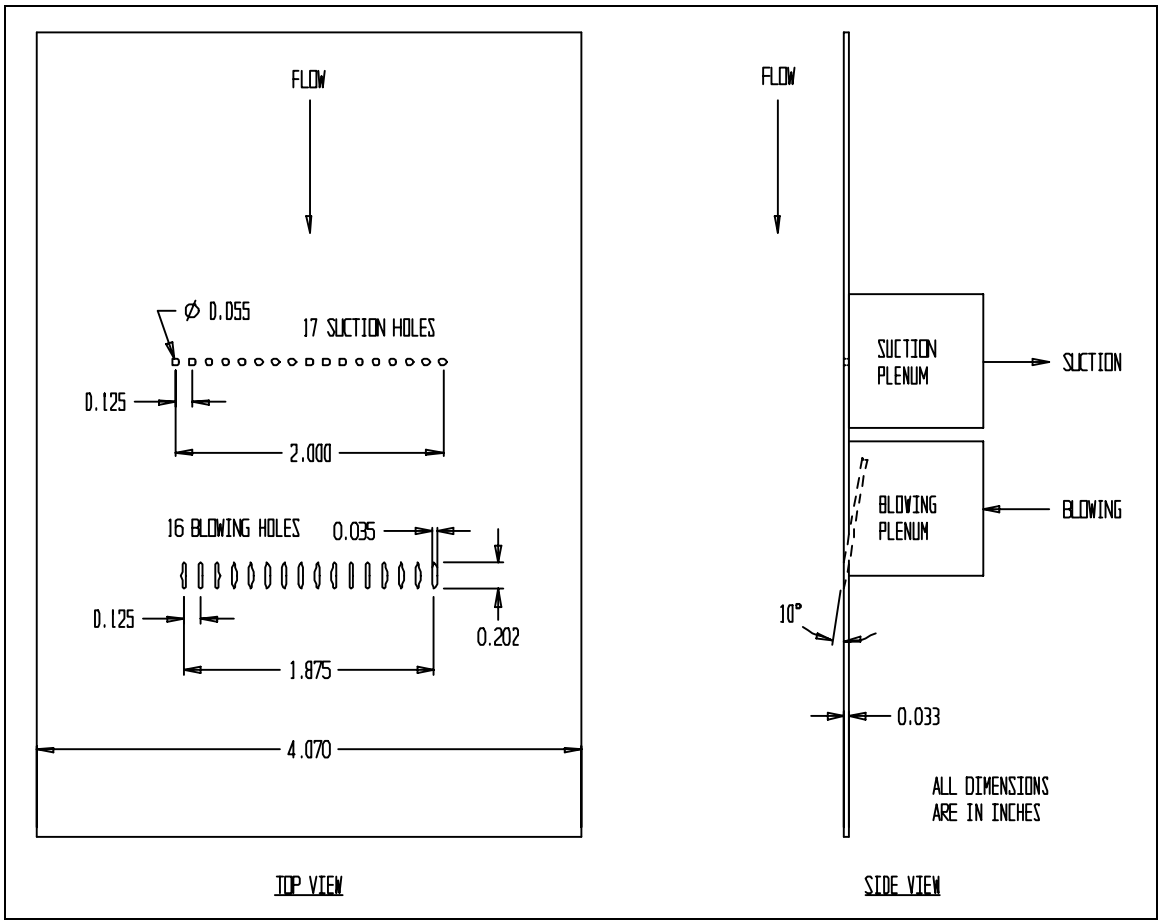

Figure 3.7: Blowing and suction hole geometry for the inlet

The blowing hole designs were less critical because the bench tests showed that the blowing worked well without much design iteration. Based on previous experience, it was critical that the blowing holes were as tangential as mechanically possible to the surface. This was done to give the fluid an increase in momentum tangential to the inlet surface, while giving it as little as possible momentum normal to the surface.

The blowing holes were given direction by welding short 0.035-in steel tubes at the appropriate angle. The tubes were pierced through the steel sheet of the curved surface, then ground flat to the surface. The tubes are held in place by weld and epoxy.

For this preliminary project, the suction and blowing holes did not cover the entire width of the control surface. Therefore, for a more general set of comparisons, the suction and blowing flowrates were normalized to the flow that passed over the holes only. This method allows any suction or blowing width to be compared to these results. In the Techsburg inlet, for example, the suction and blowing holes covered only half the width of the inlet, so the BLC flowrates were compared to only half the core flow.

3.1.3 Ejector Pumps

Ejector pumps provided the suction for the boundary layer control. Ejector pumps, shown in Figure 3.8, are devices that use high-pressure air to provide a region of low pressure. The high-pressure air is accelerated to supersonic speeds through a converging-diverging nozzle. When the high-pressure air diffuses, it entrains low-pressure flow behind it. The two streams of air (high-pressure and low-pressure) combine to form a mixed jet.

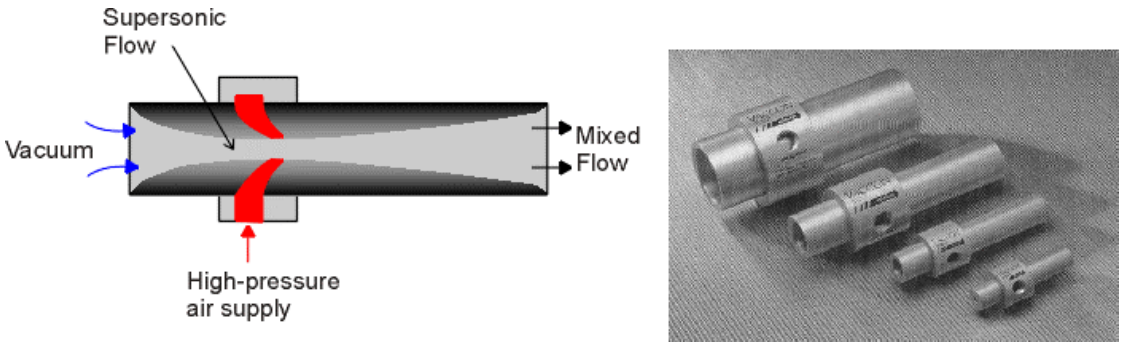

Figure 3.8: Schematic of a typical ejector pump is shown on the left; on the right, is a picture of an assortment of ejector pumps. (Leitch, 1999)

Ejector pumps are ideal sources of suction for flow control because they are capable of the large flow rates required to control high velocity flow. Changing the high-pressure supply and the exhaust backpressure can independently control the ejector pump. Furthermore, the ejectors used in this project feature a variable throat position of

the converging-diverging nozzle to allow an additional degree-of-freedom in setting the suction flowrate (Vaccon).

Ejector pumps are well-suited for flow control on aircraft. They have no moving parts to provide little additional complexity, and they are made of lightweight material (Leitch 1999). The Vaccon VDF model ejector pumps used in this project are robustly designed to handle any contaminants that could come through the device (Vaccon). Most importantly, the actuating force of the ejector pump is high-pressure air, which can easily come from the latter stages of the compressor. With further developments, ejector pumps could be integrated into the inlet's surface to allow short suction lines, which will minimize Fanning-type losses.

The ejector pumps used in this project were Vaccon VDF models. The bench tests used the VDF-250 model while the tests on the simulator used the more powerful VDF-375 model. The motive air supply was regulated to 90 psig. The back-pressure seen by the ejector pump was always ambient pressure. The throat position was changed until the optimum flowrate and suction pressure were found. A differential pressure transducer across a laminar-flow element flowmeter measured the flowrate. A silencer, properly tuned to not hinder the ejector's performance, was placed on the exhaust end of the ejector pump to minimize ambient noise.

3.1.4 Measurement

This subsection describes the equipment used in the measurements made in these experiments to evaluate the effectiveness of BLC. The subsection is divided into three parts that describe the pressure measurements, microphone measurements, and suction and blowing flowrate measurements.

3.1.4.1 Pressure Profile Data

The flow within the inlet was characterized with the use of pressure probes. All Mach number measurements were taken at the entrance to the inlet with a 0.063-in Pitot-Static probe, measuring both total and static pressures. Pitot-Static probes are only accurate when placed parallel to the flow, otherwise the stagnation point moves away from the end of the probe. Therefore, all of the total pressure measurements taken at the

exit of the inlet were taken with a 0.063-in Kiel probe to eliminate sensitivity to orientation with the flow. A Kiel probe has a converging nozzle to direct the stagnation point to the proper measurement point. Kiel probes are insensitive to a yaw angle of ±40° and to a pitch angle of +40°/-30°. The range of insensitivity to misalignment only decreases slightly at Mach numbers above 0.3 (United Sensor). Figure 3.9 shows a picture of the Pitot-Static and Kiel probes used in this research project.

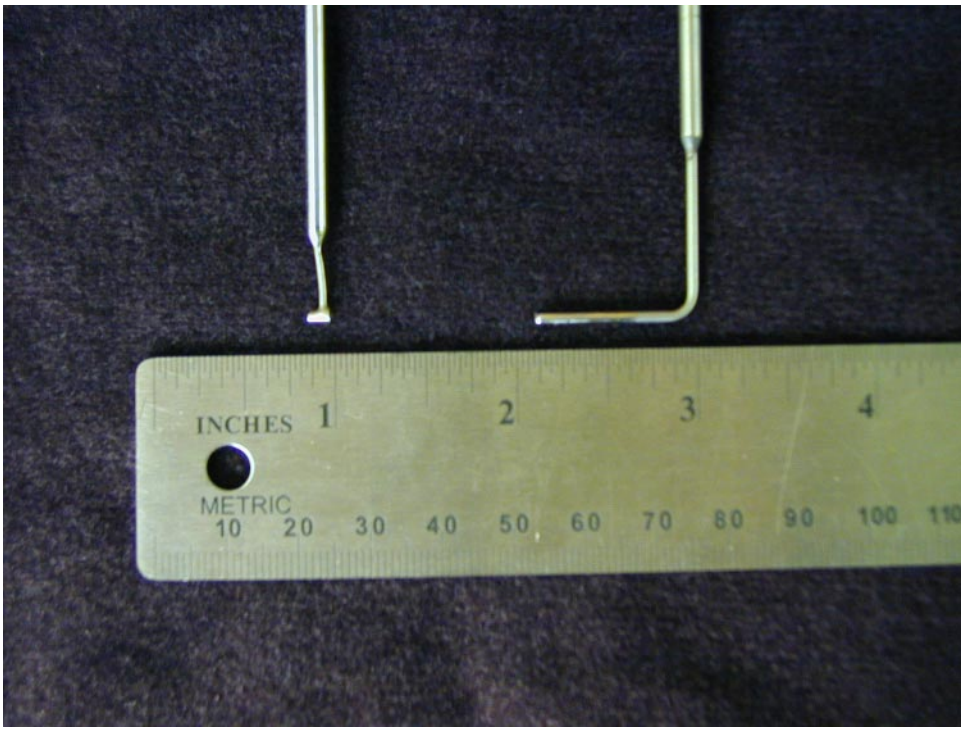

Figure 3.9: Pressure probes used in this project. The Kiel probe (left) was used for total pressure measurements, and the Pitot-Static probe (right) was used for Mach number measurements

Pressure-measurement systems with Pitot-Static and Kiel probes can have poor dynamic characteristics. The transducer and tubing act as a spring-mass-damper system that can act as a low-pass filter. The cavities and elasticity of the air and tubing introduce magnitude and phase differences between the measured and actual pressure. The time response of a pressure probe and transducer is usually slow (Beckwith *et al*., p. 595-596), so only steady-state pressures can be measured accurately. The measured settling time of the system used in this project was only 0.11 s, so some of the dynamics of the flow may be resolved.

The pressure probes were connected to a Validyne variable reluctance transducer model DP15. They possess a very high natural frequency and are very durable. They have an accuracy of ±0.25% of the full-scale value (DP15 Transducer). A key advantage to using the DP15 transducer is its ability to change pressure ranges by installing different diaphragms. The total-pressure transducer was set to ±0.5 psig, while the static-pressure transducer was set to ±1.25 psig.

A data acquisition (DAQ) system was used to measure the output voltages of the pressure transducers. A LabVIEW module was written to manage the DAQ system. The DAQ board has 8 channels, but an analog multiplexer (AMUX) allows the system to sample 32 independent signals. The sampled signal was then analyzed with either MATLAB or Microsoft Excel.

3.1.4.2 Microphones

Rioual *et al*. (1994) showed that microphones could be used to detect the transition from laminar to turbulent boundary layers. The microphones in this project examined the difference between attached and separated flow. Active flow control is made more practical by using microphones that can sense large-scale flow structures without disturbing the flow. Two configurations of microphones were used for this project to examine their non-intrusive sensing abilities.

The first configuration was an array of ten microphones placed along the spanwise centerline of the bottom surface of the inlet. In this configuration the flow was studied to see the effects of suction and blowing on the microphone signal. Two microphones were used near the entrance of the inlet to reference a well-behaved, attached boundary layer. Downstream of the separation point and blowing holes, eight more microphones were used to describe the flow as it separates. Figure 3.10 shows a schematic of the test setup. Extrapolating from the results provided by Rioual *et al*. (1994), the amplitudes of the microphone signals were expected to increase as the flow separates and larger, stronger turbulence develops.

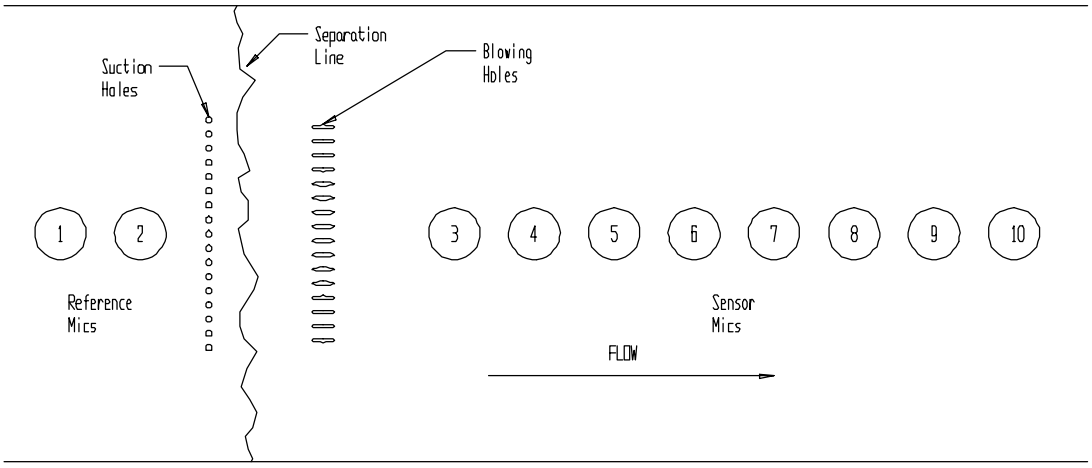

Figure 3.10: The bottom surface of the inlet with one array of ten microphones installed (Figure is not drawn to scale)

The other microphone configuration used two arrays of three microphones to resolve acoustic pressure fluctuations from turbulent pressure fluctuations. The first array, upstream of the holes, was used for a reference to an attached flow, and the second array at the exit of the inlet examined the effect separation and BLC have on the different components of the microphone signal. Figure 3.11 shows a schematic of the test setup, and Table 3.3 describes the function of each microphone within a set.

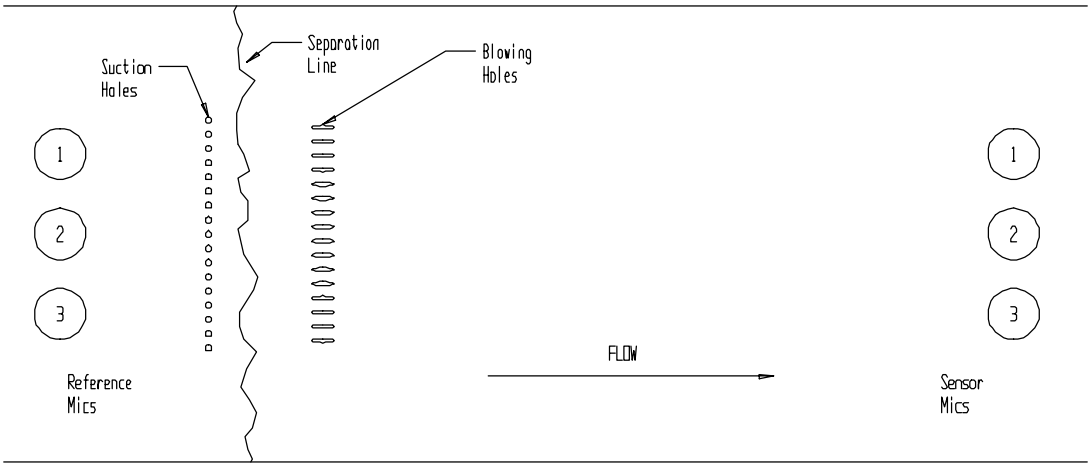

Figure 3.11: The bottom surface of the inlet with two arrays of three microphones installed (Figure is not drawn to scale)

Table 3.3: The microphone's function in each set shown in **Figure 3.11**.

Microphones	**Function** (see Section 2.3.3)	**Source**
1 and 2	Time filter	Agarwal and Simpson (1989)
2 and 3		
1 and 3	Spatial filter	Simpson *et al*. (1987)

The microphones used in this experiment were PCB Piezotronics model number 106B. The 316L stainless-steel diaphragm has a diameter of 0.435 in. Their sensitivity is 300 mV/psi with a resolution of 0.0001 psi. The microphones are compensated for mechanical vibration and possess an acceleration sensitivity of less than 0.002 psi/g. They have a resonant frequency above 60 kHz (PFS pressure catalog). A low-pass digital filter, with a variable cut-off frequency, was used to eliminate power noise in the acquisition.

3.1.4.3 Flowmeters

The suction and blowing flowrates were monitored to keep within a practical range. Typically, 1% is the maximum percentage of the core flow that could be available for flow control in any physical application. The source of high-pressure air on aircraft is the latter stages of the compressor where a lot of work has been added to the air, so the use of compressed air has a large potential to affect the performance and efficiency of the engine. BLC may improve performance and efficiency, but bleeding too much compressed air can limit the performance of the engine. Since the source of suction in this project is an ejector pump powered by high-pressure air, both the suction and blowing flowrates were important to keep around 1%.

The blowing air flowrate was passed through a Lambda-Square orifice meter, and the differential pressure was measured with a ±3.2 psid Validyne transducer. A static pressure gage and thermocouple upstream of the orifice plate measured the upstream static pressure and temperature so the density could be calculated to find the mass flowrate. A choice of three meters with orifice diameters of 0.18 in, 0.28 in, and 0.44 in were used to increase the range of accuracy. Equation (3.1) was used to find the flowrate through the orifice meter.

$$\dot{m} = \frac{\pi}{4} C_d d_o^2 \sqrt{2\rho \Delta p} \cdot \sqrt{\frac{1}{1-\beta^4}} \tag{3.1}$$

where $\dot{m}$ is the mass flowrate
C_d is the discharge coefficient
d_o is the orifice diameter
ρ is the average density across the orifice plate
Δp is the measured differential pressure
β is the ratio of the orifice diameter to the bore diameter

The suction flowrate was measured by a Meriam Instrument laminar-flow element. A ±8.9-inH_2O Validyne transducer was used to measure the differential pressure across the element, and a ±20-psid Validyne transducer measured the upstream static pressure. The mass flowrate is found by Equation 3.2 (Meriam Instrument)

$$\dot{m} = \rho\left(B\Delta p + C\Delta p^2\right) \tag{3.2}$$

where $\dot{m}$ is the mass flowrate
ρ is the average density across the element
B is a calibration constant
C is a calibration constant
Δp is the pressure difference across element

3.2 Research Facilities

This section describes the facilities used in the experiments and is divided into two parts. The first part describes the anechoic chamber where the experiments were performed, and the second part describes the source of compressed air for the ejector pumps, blowing supply, and simulator power.

3.2.1 The Anechoic Chamber

With the exception of the bench tests, all of the experiments for this project were performed in front of the simulator described in Section 3.1.1. The simulator is installed inside the anechoic chamber, owned by the Vibration and Acoustics Laboratories, at Virginia Tech. The anechoic chamber was designed to absorb the sound waves that

strike its walls. The chamber acoustically simulates free-space since there are no reflected sound waves. The chamber is constructed so that 3.0-ft thick Owens Corning Type 705 industrial fiberglass wedges cover the floor, ceiling, and all four walls. A false-floor made of metal grates provides a walking surface over the fiberglass wedges. The chamber's normal door was removed to provide sufficient airflow into the simulator. The chamber's dimensions are 13.1 ft $\times$ 8.9 ft $\times$ 6.6 ft. The chamber is considered anechoic above 200 Hz with an ambient noise of 30 dB (Leitch, 1997). Figure 3.12 shows the experiment installed in the anechoic chamber.

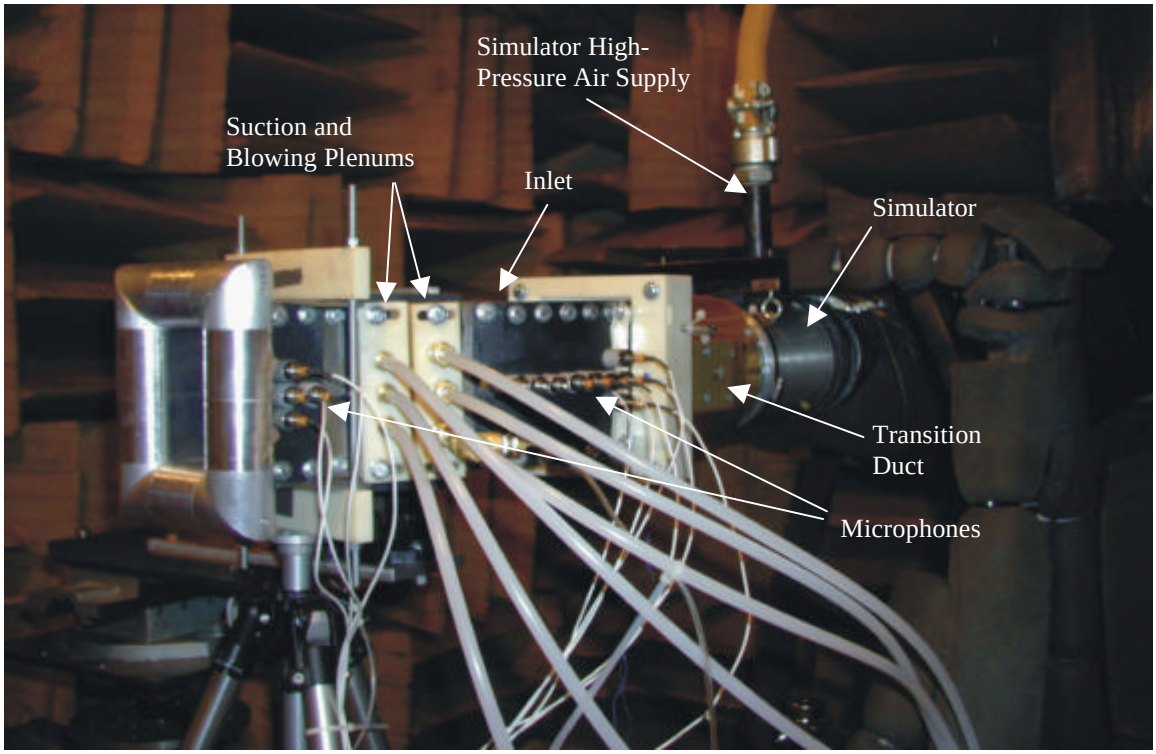

Figure 3.12: Experimental setup inside anechoic chamber

The simulator and inlet was installed onto a steel truss to support the axis of the simulator rotation at 48 in above the working surface in the center of the room. The test facility is static, so it does not allow for the simulation of the forward flight of an aircraft. The simulator is attached to the rig truss by two ¼-in bolts. The simulator's turbine receives its high-pressure air from a 2-in diameter flexible hose attached to the rig by a flange. An oil-soaked cork gasket provides a seal at the flange. The exhaust air is sent to

the atmosphere via a 12-in diameter pipe. The inlet is clamped to the simulator rig, with a tripod providing vertical support.

A pressure probe is held by another rig next to the simulator-inlet rig and is actuated by a stepper motor. The 200-step/rev stepper motor with a 16-tpi screw allows 2.65 in of travel in only one-direction. An arm attached to the stepper motor holds the pressure probe at the desired location. A two-dimensional sliding table supports the traversing assembly. A tripod supports the sliding table and allows for height and horizontal angle adjustments. The tripod is held fixed to the floor by a short table clamped to the floor.

3.2.2 Compressed Air Supply

As described in Section 3.1.1, the turbofan simulator is energized by high-pressure air expanding across the turbine. An Ingersoll-Rand four-stage reciprocating compressor supplies the air to the simulator. To prevent water vapor from hitting the turbine blades, the compressed air is passed through a heat exchanger and an activated-alumina drying unit to dry the air.

As Figure 3.13 shows, as the air leaves the air compressor module, it is plumbed to the anechoic chamber by way of a 2-in pipe. A digitally controlled valve is inline with the simulator supply line and controls the simulator to ±500 rpm. A secondary line is tapped off of the main line and regulated to 90 psi for the control valve's pneumatic power. Two quarter-turn valves—one upstream of the control valve and one downstream—act as emergency shutoff valves.

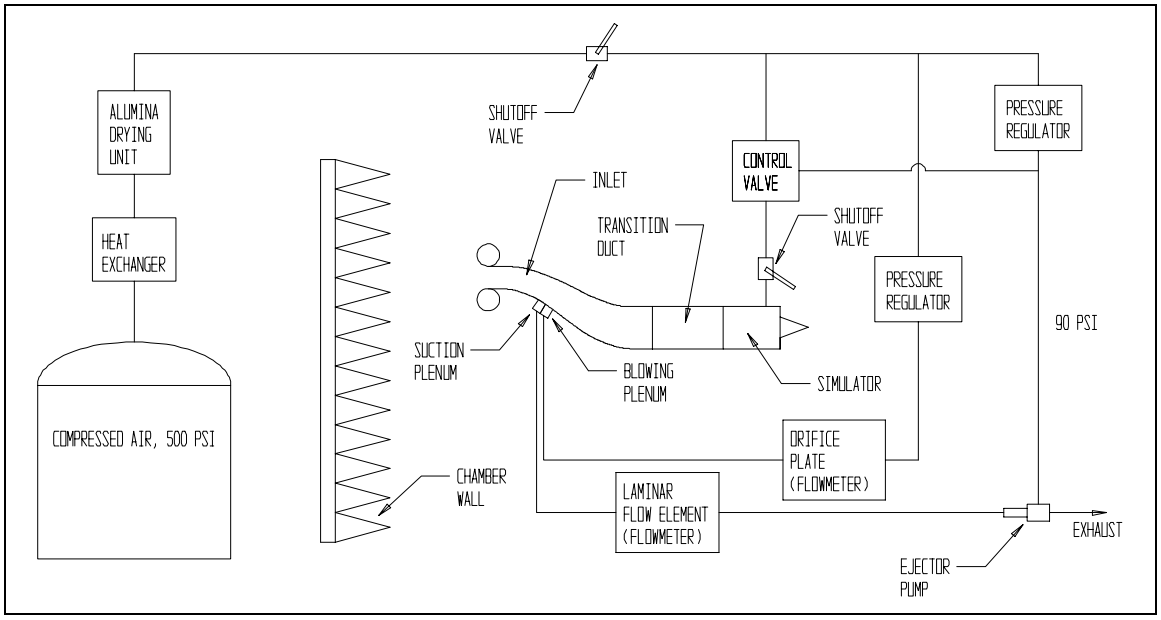

Figure 3.13: Schematic of experimental setup

The compressed air lines also supply air to the ejector pumps and blowing supply lines. The ejector pump line is directly tapped off of the 90-psi secondary line, while the blowing supply line is regulated to various pressures depending on the required blowing flowrate.

3.3 Test Procedure

In this section the procedures used to obtain data will be explained. Two separate sets of data were taken: aerodynamic and microphone. The aerodynamic data were used to evaluate the effectiveness of the boundary layer flow control, while the microphone data were used to examine the ability of a microphone to provide feedback for actively controlling the flowrates of the suction and blowing.

3.3.1 Aerodynamic Measurements

Several kinds of aerodynamic data were taken in this research project. Table 3.4 describes their purpose and configurations. The results of the experiments are presented in Chapter 4.0.

Total pressure measurements were made at the exit of the serpentine inlet just before the transition piece. A stepper motor was used to traverse the pressure probe from the bottom surface to the free-stream, 3.4 in away. Since this work is only a preliminary assessment, measurements were only taken along the spanwise center of the inlet.

Pressure measurements were also taken at the entrance of the inlet to measure the throat Mach number and simulator mass flowrate. The stepper motor again traversed the Pitot-Static probe along the centerline just downstream of the bellmouth. The traverse covered the 1.90 in of the entire 2.04 in of the entrance.

The traversing motor was programmed to stop at certain locations to measure the pressure for a reasonable amount of time. The average and standard deviation of the data measured at that specific location would be calculated, recorded, and later used for uncertainty analysis. The recorded data also provided insight as to how the pressure fluctuates with different BLC schemes.

Table 3.4: Description of aerodynamic experiments.

Description	Section	Purpose	Speed [krpm]	BLC Configurations
Inlet Throat Speed	4.1.1	Find Mach number versus simulator speed	22.3 – 55.5	No control
Inlet Intake Traverse	4.1.2	Mass flowrate and Effectiveness of bellmouth	40	No control, 1% suction & blowing
1% Control	4.1.3	Effectiveness of practical BLC	40	No control, 1% suction, 1% blowing, 1% suction & blowing
Surge Margin	4.1.4	Effectiveness of BLC to increase surge margin	60	No control, 1% suction & blowing
Overblow	4.2.2	Assess microphones as feedback sensors	30	Blowing only (0% to 2.43%)

3.3.2 Acoustic Measurements

The acoustic experiments were taken to examine the worthiness of using a non-intrusive measuring device to give feedback to a BLC scheme. The array of ten microphones examined the difference in microphone signals along the inlet as the flow separates. The results presented in Section 4.2 will show a correlation with the aerodynamic data presented in Section 4.1. The two arrays of three microphones were

used to examine the different components of the microphone spectrum, and their results are presented in Appendix C. The array of three microphones was designed based on the papers of Agarwal and Simpson (1989) and Simpson *et al*. (1987).

4.0 Results and Discussion

In this chapter the results of the experiments described in Chapter 3.0 will be discussed. The chapter is divided into two sections: Section 4.1 describes the aerodynamic results, and Section 4.2 describes the microphone results. The aerodynamic section will attempt to show how BLC improved the entrance and exit pressure profiles, distortion, pressure recovery, and stability. The microphone results will show the effect BLC has on the signal of a microphone, which is then compared to the distortion of aerodynamic profiles. The assessment of microphones as a feedback sensor for an active flow control scheme is also given in Section 4.2.

4.1 Aerodynamic Results

In order to determine the success of the suction and blowing in the inlet, aerodynamic measurements had to be taken. Total pressure measurements were taken with a Kiel probe because of its insensitivity to direction, but Pitot-Static probes were used to measure velocity. Figure 4.1 shows where the pressure measurements were taken in the inlet. All measurements were taken at the spanwise center of the inlet. The next four subsections will describe the results of the aerodynamic measurements. The first two subsections will show and analyze the results of the experiments done at the throat of the inlet; the third subsection will show and analyze the results of the experiments done at the exit of the inlet. Finally, the last subsection will document BLC's ability to delay compressor instability.

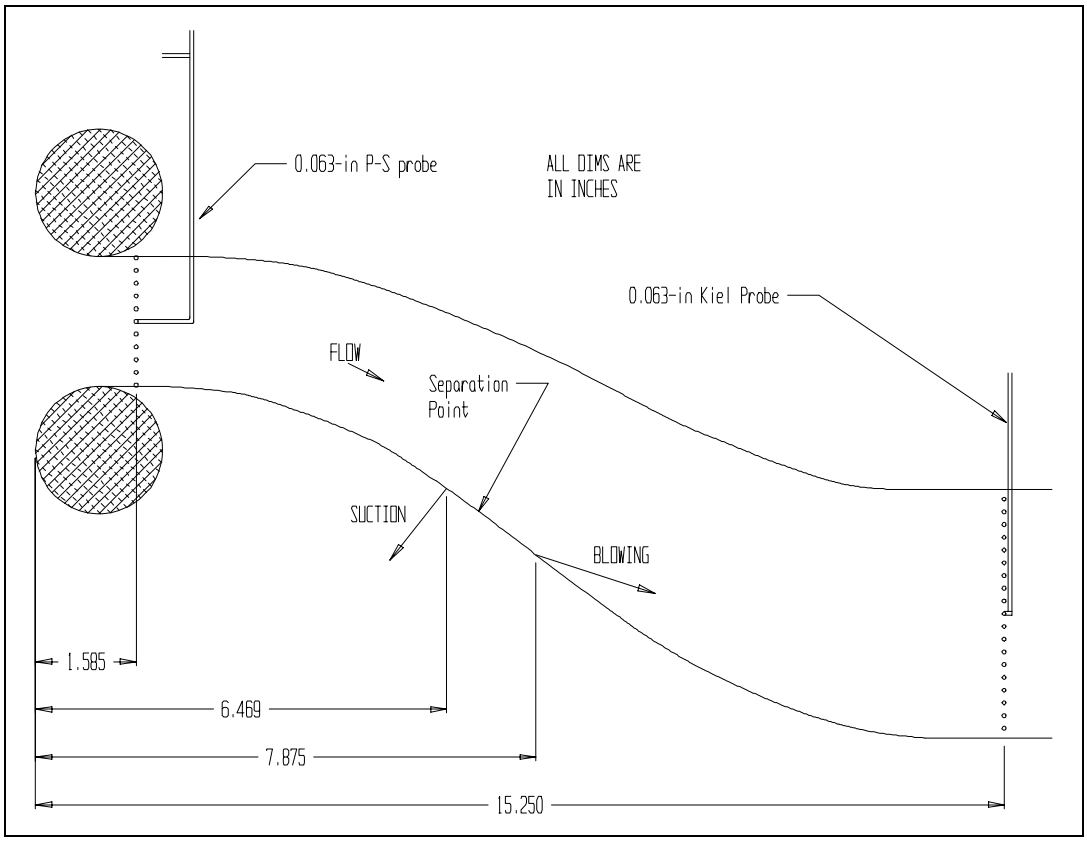

Figure 4.1: Schematic showing where pressure measurements were taken

4.1.1 Throat Mach Number

The first set of experiments run on the simulator was to measure the Mach number at the entrance of the inlet. The measurement of the Mach number was important to ensure that experiments presented later in this document would be meaningful to compare to real-life applications. For example, the ability to provide a blowing jet with sufficient momentum to control a boundary layer from separating is difficult if the free-stream velocity is too high

A Pitot-Static probe was placed in the geometric center of the intake and held facing the flow while the simulator speed was stepped from 22.3 krpm to 55.5 krpm. A wider range of speeds was not possible because below 22.3 krpm the simulator speed is hard to control and near 60 krpm the simulator enters an unstable region. One transducer measured the static pressure while the other measured the total pressure. Given the

pressure ratio, the Mach number was calculated with Equation (4.1). Figure 4.2 shows the results of the experiment. The throat Mach number was found to have an approximately linear relationship with simulator speed.

$$M = \sqrt{\left[\left(\frac{p_0}{p_s}\right)^{(\gamma-1)/\gamma} - 1\right]\left(\frac{2}{\gamma-1}\right)} \tag{4.1}$$

where M is the Mach number
p_0 is the total pressure
p_s is the static pressure
γ is the ratio of specific heats

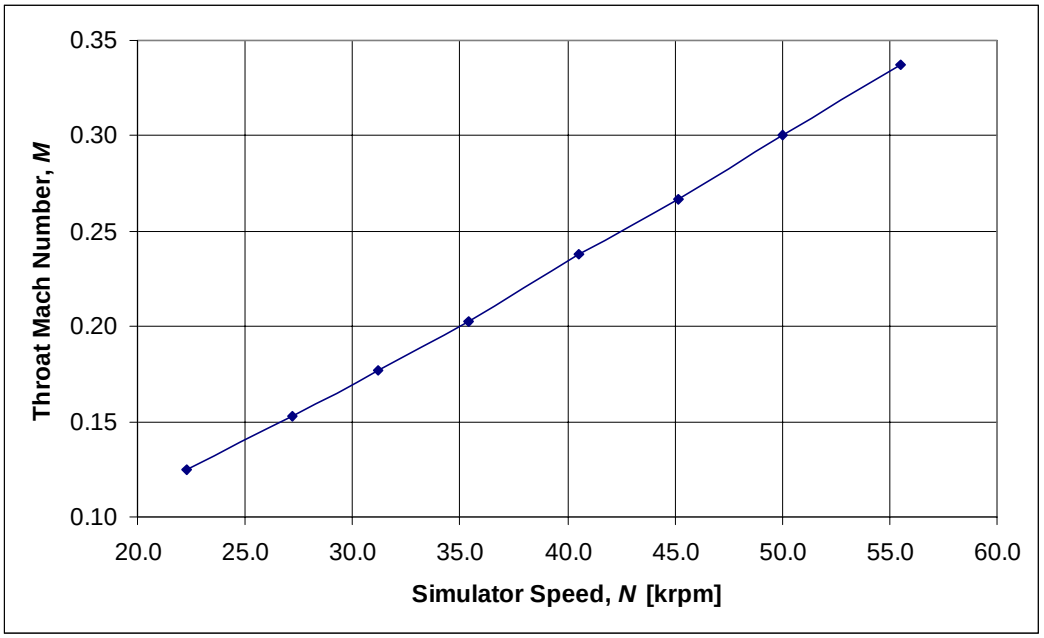

Figure 4.2: The variation of the throat Mach number with simulator speed

4.1.2 Mass Flowrate

The mass flowrate of the simulator was measured at the intake of the inlet. The mass flowrate is important because the flowrates of the suction and blowing will be normalized to the flowrate of the simulator. The experiment was performed in a similar way as the throat Mach number measurements were done in Section 4.1.1, but now the Pitot-Static probe was traversed from the bottom of the inlet to the top. During each

pause, the DAQ system sampled the data at 100 Hz for 10 s to provide a better estimate of the true value. The traverse moved 0.14 in with each step over 1.90 in of the entire height of the intake, 2.04 in. The probe was unable to get closer to the surfaces because of the danger of damaging the probe by striking the inlet surface. The no-slip condition, however, requires the velocity near the wall to be zero, so little mass is added in the small, unprobed region.

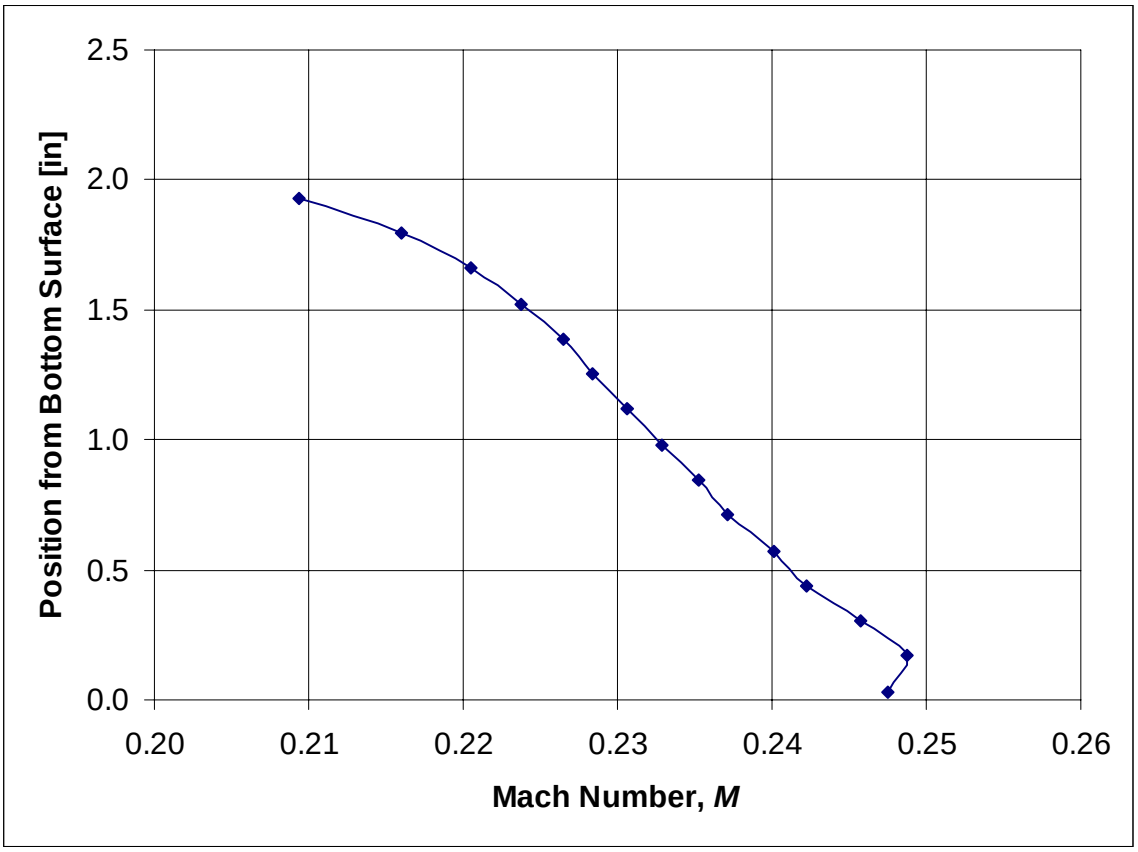

Figure 4.3: Mach number profile of the intake of the inlet with a simulator speed of 40 krpm.

The Mach number profile was converted to a velocity profile by the equation $V = M\sqrt{\gamma RT}$, and the mass flowrate was calculated from this traverse by Equation (4.2), which numerically integrates (using trapezoids) the velocity profile over the area. Measurements were only taken along the spanwise center of the inlet, so it is assumed that while the velocity varies across the height of the inlet, it is constant across the width

of the inlet. The clean flow at the entrance was chosen for the mass flow measurements since the pressure probe is uni-directional and could not resolve the chaotic velocity vectors inside a separated region.

$$\dot{m} = \sum_{k=2}^{n} \tfrac{1}{2}\left[(\rho V)_k + (\rho V)_{k-1}\right](y_k - y_{k-1})w \qquad (4.2)$$

where $\dot{m}$ is the mass flowrate through the inlet
ρ_k is the static density of each element
V_k is the velocity measured in each element
y_k is the height above the inlet floor
w is the width of the inlet, 4.1 in
n is the number of elements

Williams and Surber (1993) noted that distorted flow might hinder an aircraft engine's mass flow but that experimental data shows the loss to be within test uncertainty (see Section 2.1). To examine the effects of the distortion on the simulator the experiment above was performed again with the 1% BLC turned on. Because the flowrate measurements were taken well upstream of the BLC, the change in the flowrate can only be due to the reduction in distortion. The 1000 data points taken at each step of the traverse, were used for a propagated error analysis using the method presented by Beckwith *et al*. (1993, p. 82) encompassing both the standard deviation of the measurement and the bias associated with the measuring devices. Appendix B summarizes the method. Figure 4.4 shows the two profiles with error bars attached to the data points signifying the uncertainty in the measurement. Figure 4.5 shows that the mass flow improves by 1.74% when BLC is used.

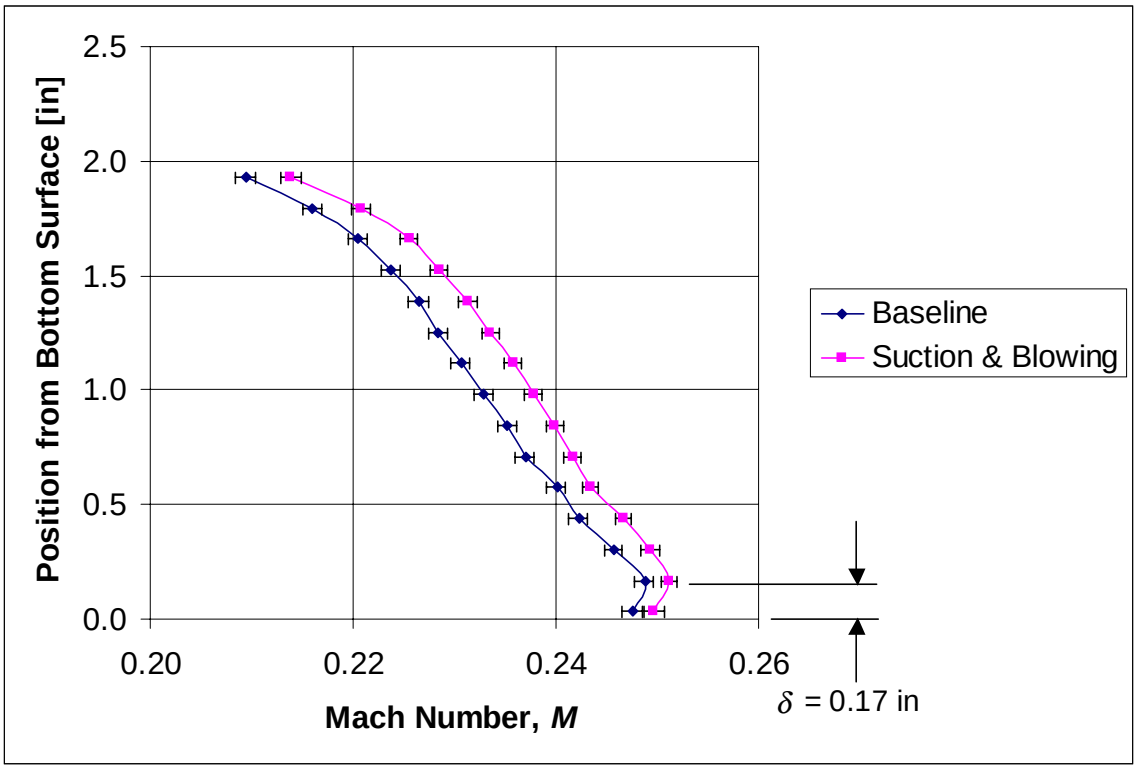

Figure 4.4: Profile of the entrance to the inlet at 40 krpm.

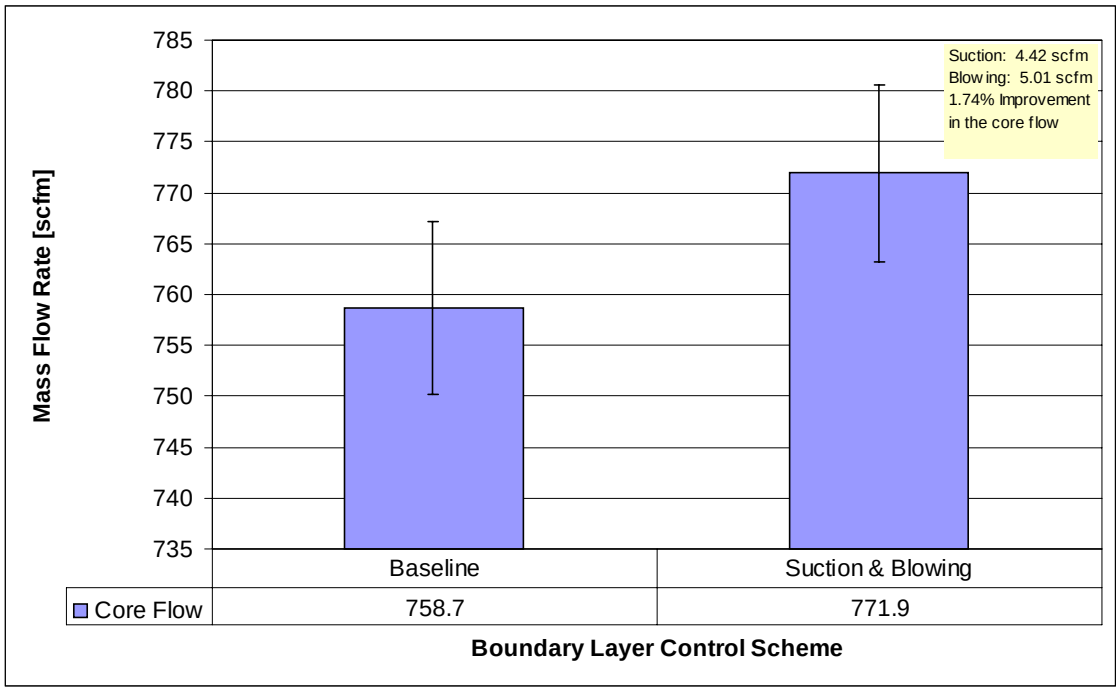

Figure 4.5: Mass flow rate through inlet at 40 krpm with no BLC and with 1% BLC

Figure 4.4 shows that the improvement in Mach number is consistent across the whole entrance to the inlet. The error bars do not overlap to suggest that the difference is significant enough to overcome the uncertainty in the measurement of the Mach number. Even though the significantly stronger Mach profile suggests an improved mass flow, the error bars in Figure 4.5 suggest that the difference is within the bounds of uncertainty, as Williams and Surber (1993) predicted. While no conclusive claims may be made on the improvement of mass flow with BLC from these experiments, the Mach number profiles in Figure 4.4 suggest that if more precise measurements could be made, the mass flow would show clear improvements.

Figure 4.4 also shows that the bellmouth was properly designed. For 40 krpm the boundary layer is less than 0.17 in and appears to be well-behaved and attached. Therefore any distortion measured in the flow at the exit of the inlet is due directly to the curvature and diffusion of the inlet. The skewed Mach number profile outside of the boundary layer is an effect of the turning passageway just downstream of the measurement location, and therefore should not be blamed on the bellmouth or the inlet flow conditions.

4.1.3 Practical Flow Control

Because of its thermodynamic cost in a real engine the use of high-pressure air must be kept to around 1% of the core engine flow. Too much above 1% and the gains of BLC is overpowered by the loss in performance. Since even the source of suction in this research project is high-pressure air, both BLC flowrates were kept as close to 1% of the core flow as possible. This section will show the results to the experiments done with only 1% suction and blowing based on the mass flow of the simulator at 40 krpm. Since this research is only a preliminary study, measurements were only taken along the spanwise center of the inlet. As described in Section 3.1.2.2, the BLC flowrates were normalized to half of the simulator flowrate since the control effort is concentrated in the center half of the inlet. Table 4.1 tabulates the flowrates used in the boundary layer suction and blowing. Section 4.1.3.4 will offer a summary of the rest of this subsection.

Table 4.1: Flowrates used for boundary layer suction and blowing during aerodynamic experiments

		Flowrate	
		[scfm]	**[%-core flow]**
Suction		4.250	1.12
Blowing		4.736	1.25
Suction & Blowing	Suction	4.210	1.11
	Blowing	4.726	1.25
Simulator at 40 krpm		758.7	

4.1.3.1 Profiles

Total pressure traverses with the Kiel probe were done at the exit of the inlet to show the effect of suction and blowing on the simulator. The simulator was maintained at 40 krpm and the traverse moved from 3/32 in from the bottom surface to 3.4 in above it with steps of 0.13 in. After each step, the traverse was held for 10 s and the DAQ-system sampled the total pressure at 100 Hz. After the baseline traverse, the suction was turned on to the 1% rate and the traverse was repeated. Another traverse was performed for 1% blowing. Then, one final traverse was performed with both the suction and blowing turned on. The results are shown in Figure 4.6. The total pressure measured by the Kiel probe was normalized by the ambient pressure.

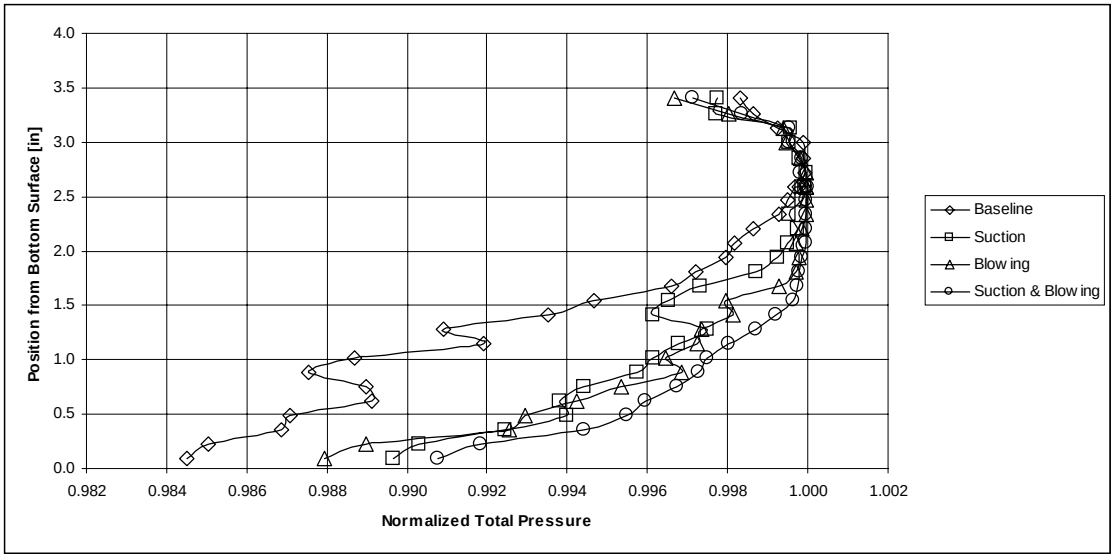

Figure 4.6: Test results with simulator speed at 40 krpm showing the effects of 1% BLC

An error analysis was performed on the normalized total pressure data based on the methods of Beckwith *et al*. (1993, p. 82) and Kline and McClintock (1953). Appendix B provides a summary of the error analysis. Error bars placed on the data will show the significance of the improvement by comparing the uncertainty of the measurement with the value of the measurement. In Figure 4.7 the suction and blowing case is clearly an improvement over the baseline case: the error bars only overlap in the freestream. Figure 4.8 and Figure 4.9 show that suction alone and blowing alone improve the profile over the baseline. However, blowing alone is shown in Figure 4.10 to be only a slight improvement over suction alone, with the improvement focused in the 1.0 in to 2.0 in range. Figure 4.11 shows that suction and blowing together is an improvement compared to using just suction alone, especially in the 0.5 in to 2.0 in range. Figure 4.12, however, shows that suction and blowing together is only slightly better than blowing alone even though every suction and blowing data point below the free-stream is consistently better than the corresponding blowing data point.

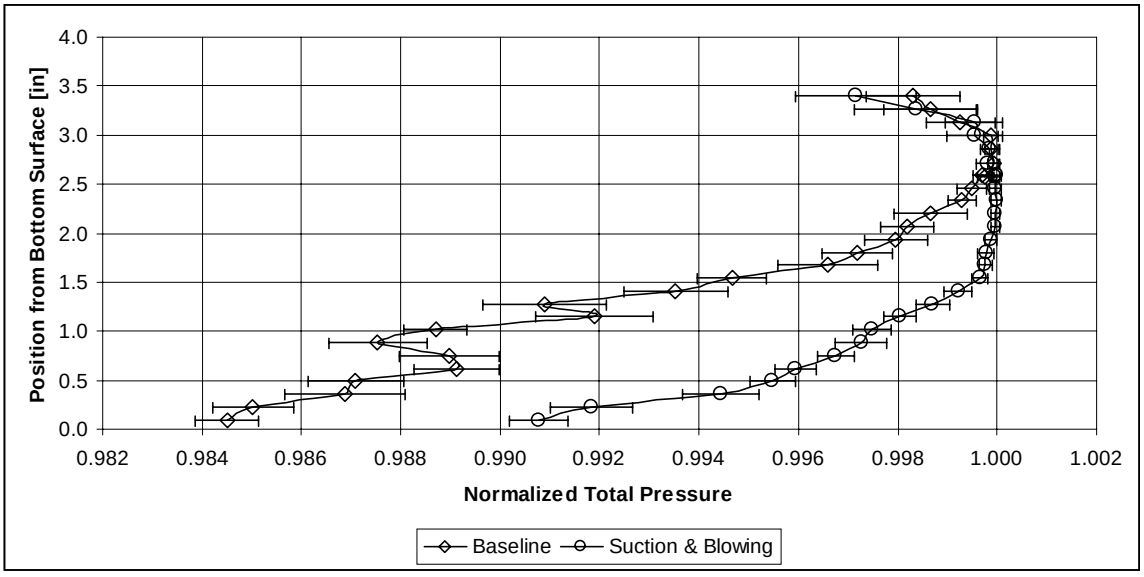

Figure 4.7: Comparison of Baseline and Suction and Blowing traverses with error bars

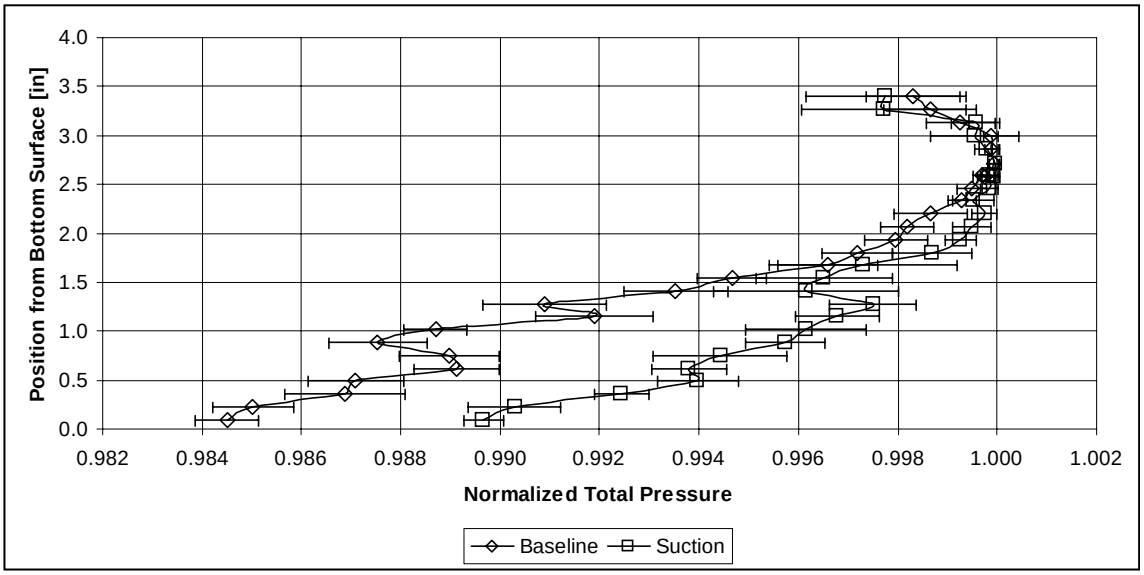

Figure 4.8: Comparison of Baseline and Suction traverses with error bars

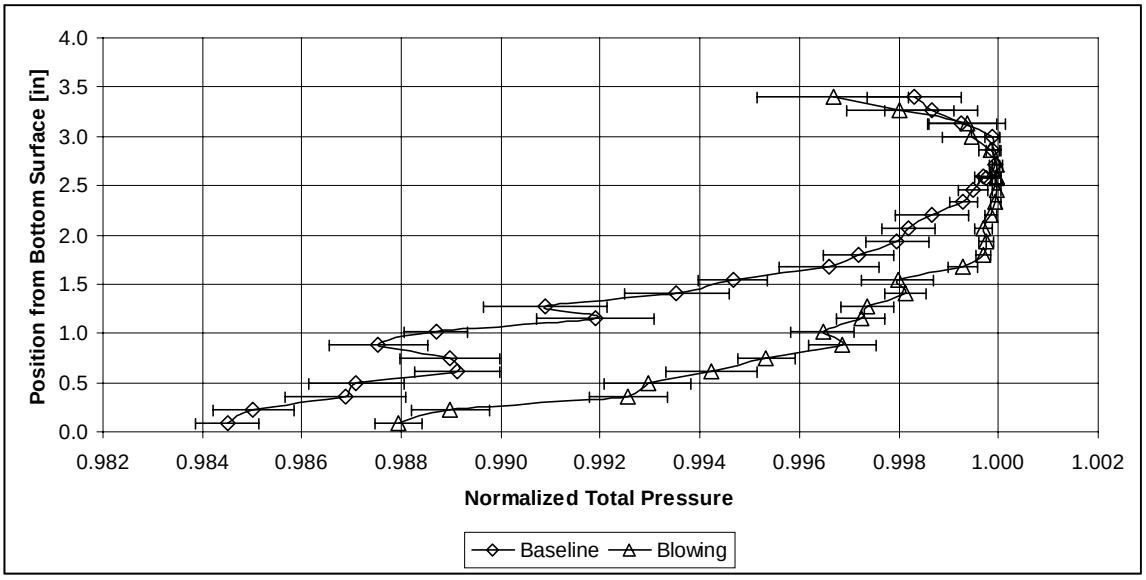

Figure 4.9: Comparison of Baseline and Blowing traverses with error bars

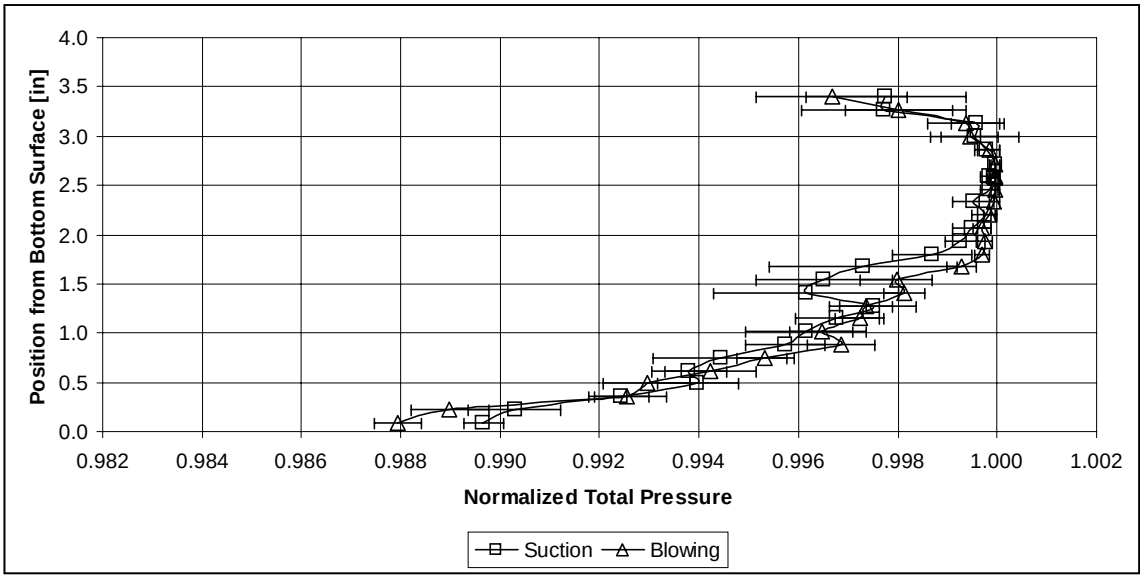

Figure 4.10: Comparison of Suction and Blowing traverses with error bars

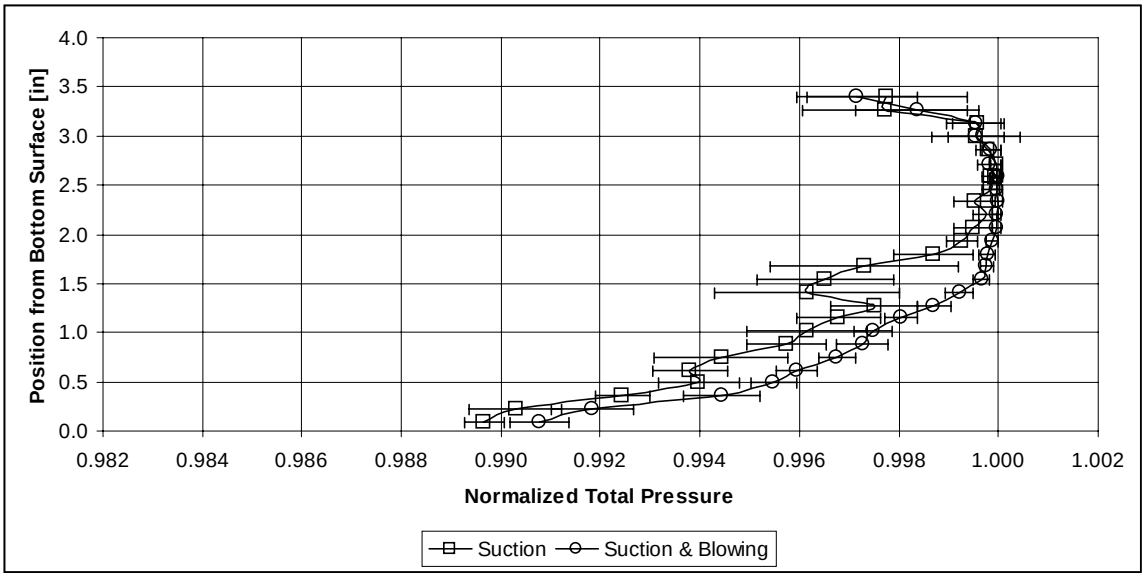

Figure 4.11: Comparison of Suction and Suction and Blowing traverses with error bars

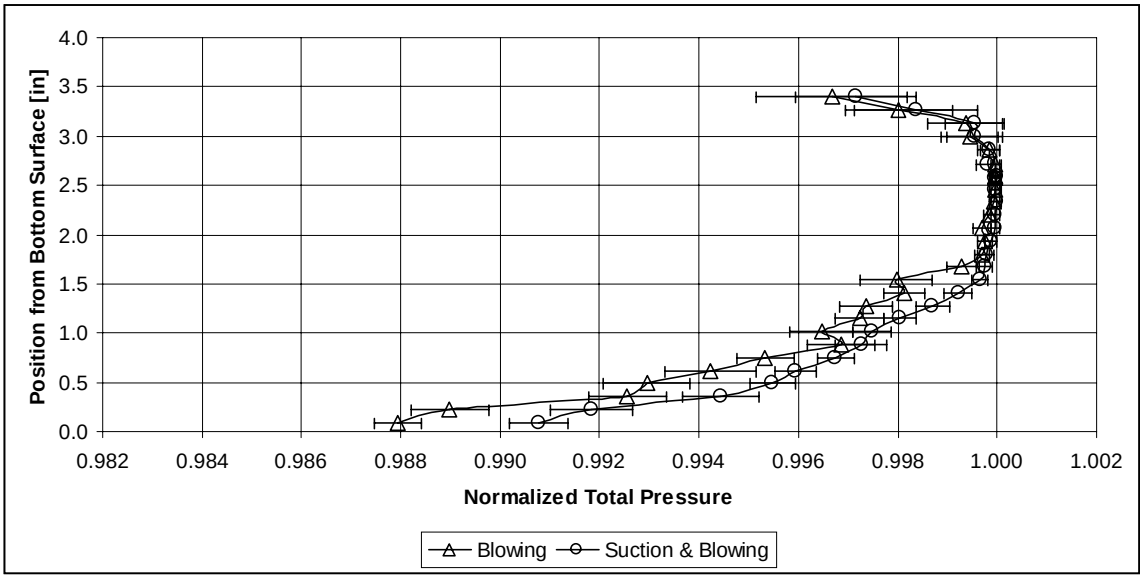

Figure 4.12: Comparison of Blowing and Suction and Blowing traverses with error bars

Simpson *et al*. (1981) showed that a large-scale eddy and vortex structures is associated with a separating turbulent boundary layer, which translates to high unsteadiness in the pressure field within the separated region. While no measurements were taken to concretely determine the existence of the eddy and vortex structures within the inlet, the large error bars seen in the previous figures, especially close to the wall and for the baseline case, suggest that the unsteadiness associated with the structure is present in this inlet. Table 4.2 shows the distribution of the 1000 measured pressure data points at positions above the inlet surface. At positions near the wall, the baseline distributions are wider while the flow control cases show a more narrow distribution. The baseline distribution appears to be bi-modal, especially at 0.09, 0.36, 0.62, 1.15, and 1.67 in. This could be a result of the speculated vortices within the separated region that the pressure probe senses as an alternating high (less-negative) and low (more-negative) pressure. With flow control, the bi-modality disappears suggesting that the vortices are weakened with flow control.

Table 4.2: Distribution of normalized total pressure data at the exit of inlet for various positions from the wall with different BLC schemes

Position [in]	Profile	Histogram
0.09	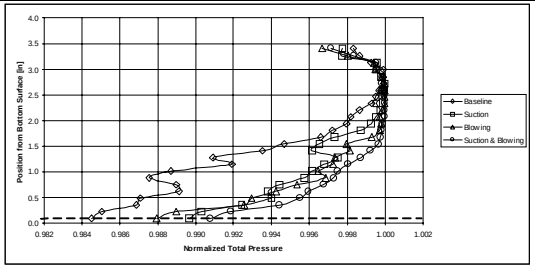	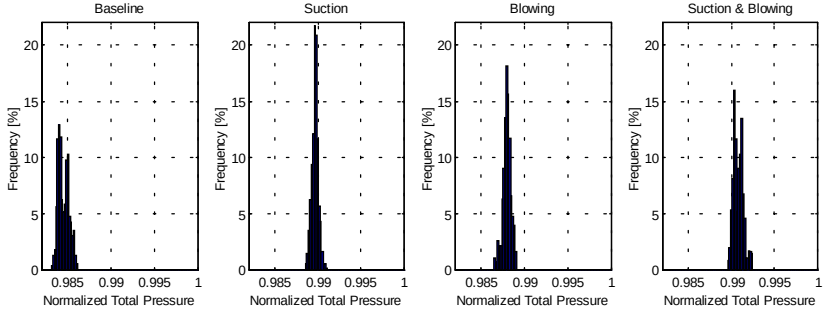
0.36	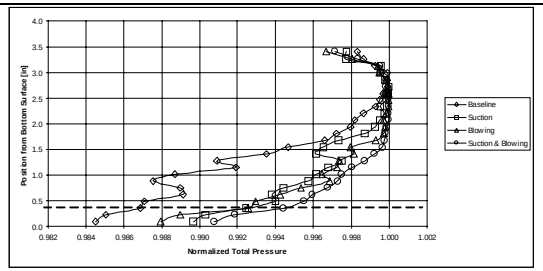	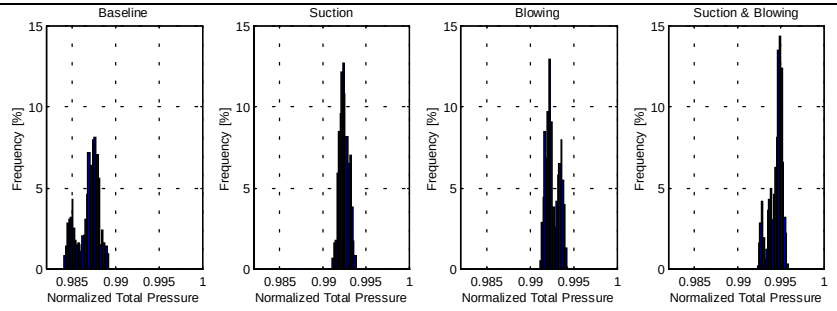
0.62	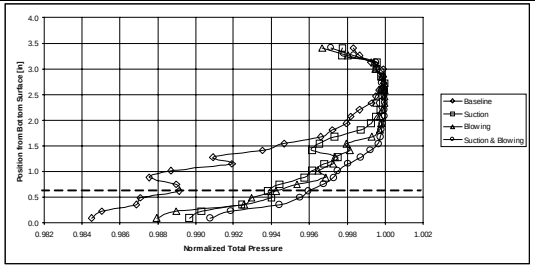	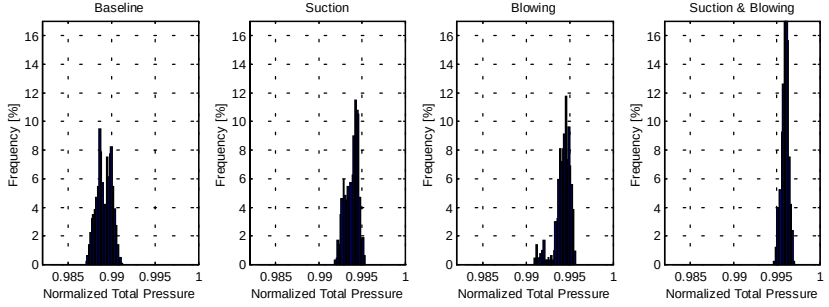

Position [in]	Profile	Histogram
0.88	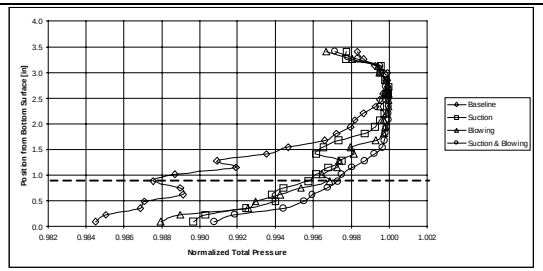	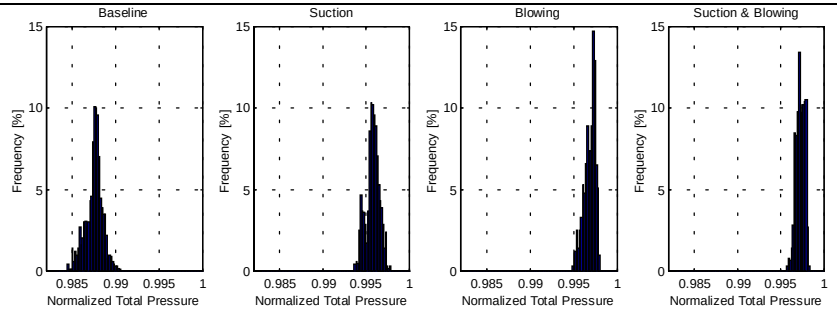
1.15	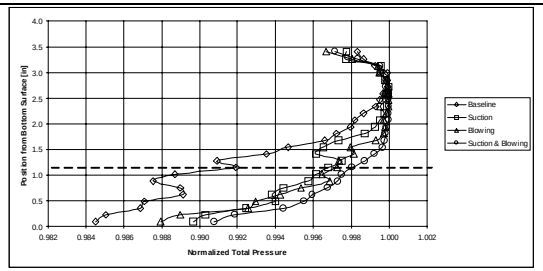	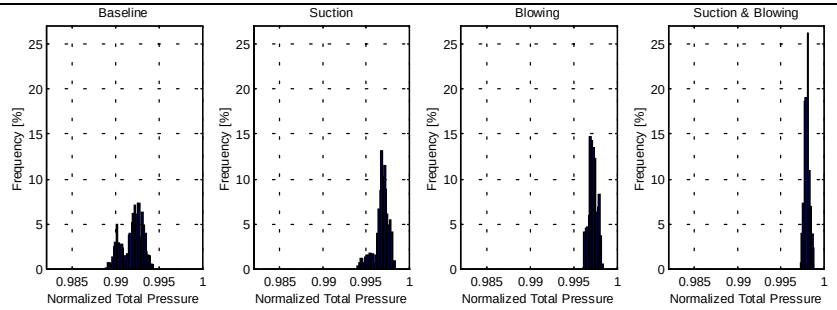
1.41	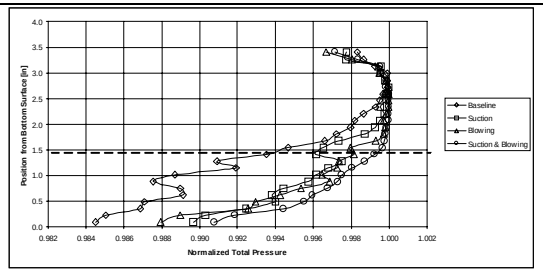	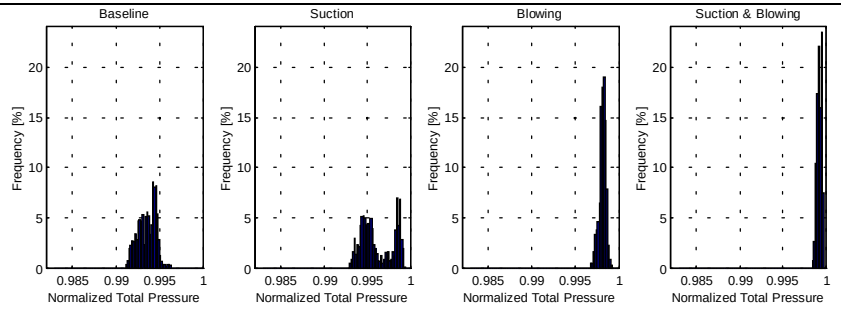

Position [in]	Profile	Histogram
1.67	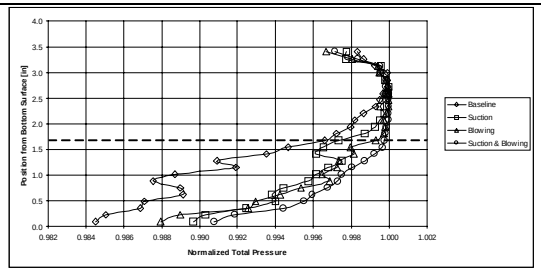	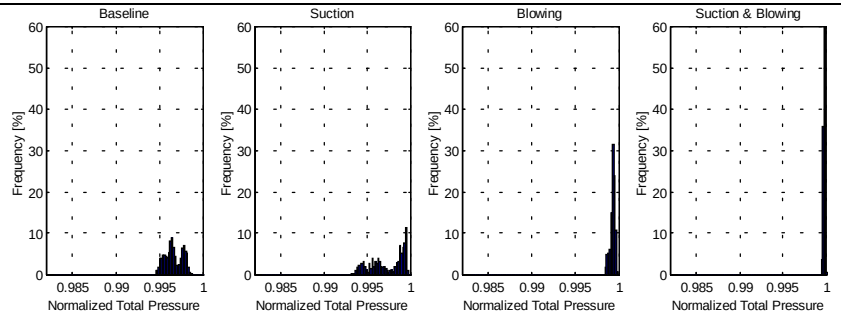

The bi-modal distributions seem to be associated with the anomaly that appears on the baseline profile between 0.5 and 1.0 in and on the suction and blowing profiles between 1.0 and 1.5 in. This suggests some instability in the flow in those regions where a vortex might produce a locally lower or higher total pressure. With the suction or blowing, the instability is attenuated; the instability is not found in the suction and blowing profile. This illustrates that BLC improves the flow conditions within the inlet allowing for a more stable and uniform total pressure distribution. As BLC minimizes separation, the vortices that may exist within the separated region are forced to shrink in size and strength, thereby decreasing the total pressure variations.

The depth of the aerodynamic pressure profiles of Figure 4.6 suggests separated flow along the bottom surface. As BLC effort increases, the depth of the profile decreases. The top leg of the pressure profile, however, is not affected by the BLC. Furthermore, the top leg does not have nearly the deficit that the bottom leg does, which suggests that the top surface does not separate—at least not to the degree of the bottom surface. The boundary layer is fairly thick along the top surface, however, at approximately 0.75 in. It should be noted that the pressure probe did not fully reach the top surface due to the danger of damaging the probe.

Another set of traverses was taken at the exit, but the probe was moved at a constant 0.05 in/s while the DAQ system sampled the total pressure at 10 Hz. The same BLC flowrates that were given in Table 4.1 were also used for these traverses. Since the response time of the probe is relatively slow, the continuously moving traverse is not necessarily accurate, but the data provides some insight to the unsteadiness of the total pressure within the inlet. Figure 4.13 shows the results of these traverses. Note that the trends seen in Figure 4.6 are present here including the anomaly between 1.0 in and 1.5 in for the suction case. The baseline data shows a vertical slope near the wall, which suggests that the flow is indeed separated without BLC. The other cases—especially the blowing and suction & blowing—do not show the vertical slope.

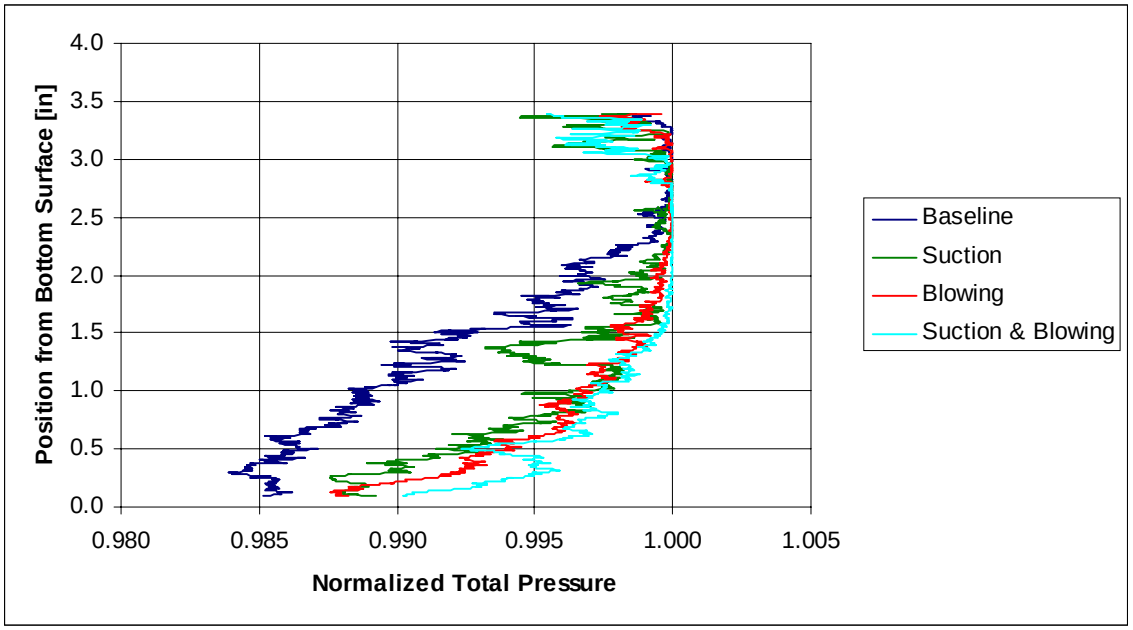

Figure 4.13: Profile of normalized total pressure at the exit, using a continuously moving traverse

4.1.3.2 Distortion

There are various measures of the effectiveness of an inlet in diffusing the incoming flow to an engine. One method is the circumferential distortion intensity described in the SAE Aerospace Recommended Practice (ARP) 1420 and is given in Equation (4.3). In an isentropic inlet, the intensity would be zero. This method, generally applied at the circular plane directly in front of the engine face, examines the distortion within constant radius rings. Unfortunately, the exit of the inlet in this project is rectangular and measurements were taken only with a centerline traverse. Since the flow has already been assumed to be two-dimensional, however, the well-defined meaning of Equation (4.3) was modified in the framework of this project to represent the distortion along the traverse at the centerline of the inlet. Algebraically, it is the same equation. Figure 4.14 gives a visual description of the distortion intensity.

$$I = \frac{\overline{p_0} - \overline{p_{0,lo}}}{\overline{p_0}} \tag{4.3}$$

where I is the distortion intensity parameter
$\overline{p_0}$ is the average of the total pressure at the exit of the inlet
$\overline{p_{0,lo}}$ is the average of the total pressure below $\overline{p_0}$

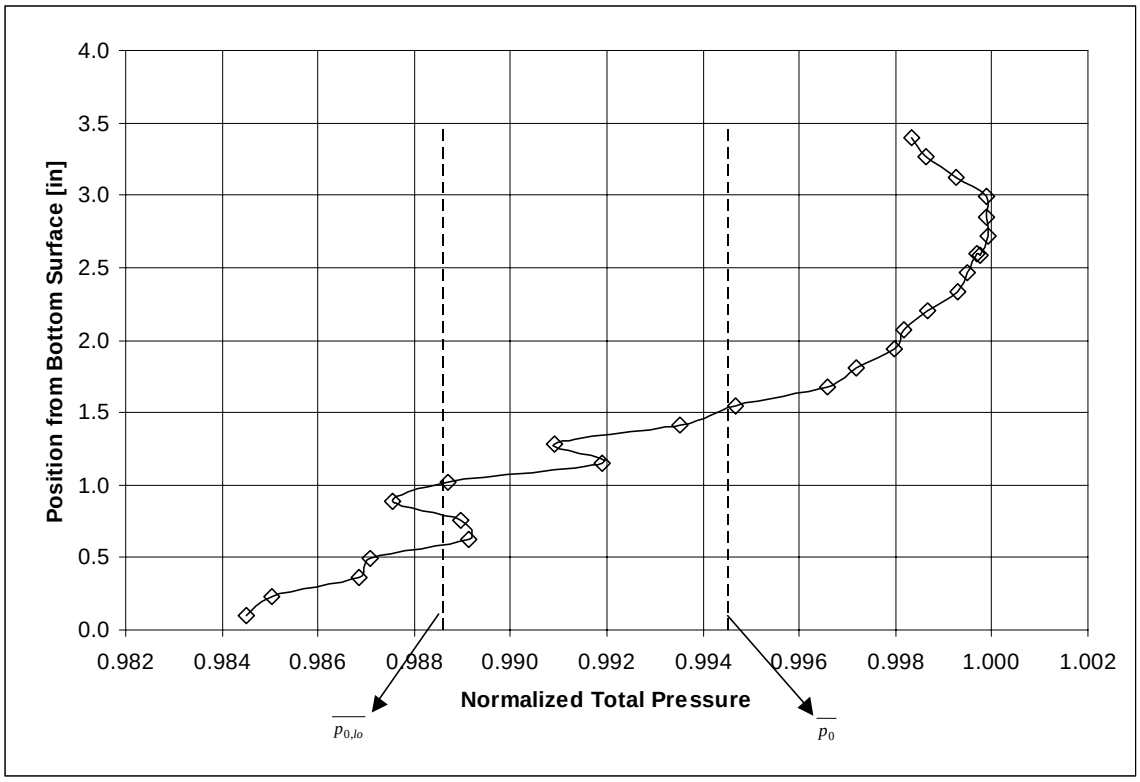

Figure 4.14: Visual description of distortion intensity based on SAE ARP 1420

Figure 4.15 shows how the distortion intensity changes with different BLC schemes. All of the tested schemes of BLC drastically improve the distortion intensity over the baseline case. The combined use of suction and blowing is better than just using blowing, but the combined use of suction and blowing together over just suction does not significantly improve the inlet distortion intensity. Distortion intensity is a measure of the uniformity of the pressure profile, and only drastic changes in the shape of the profile will result in significant changes in intensity. Figure 4.6 showed the overall shape of the profile does not drastically change for different BLC configurations, even though the depths of the profiles do change.

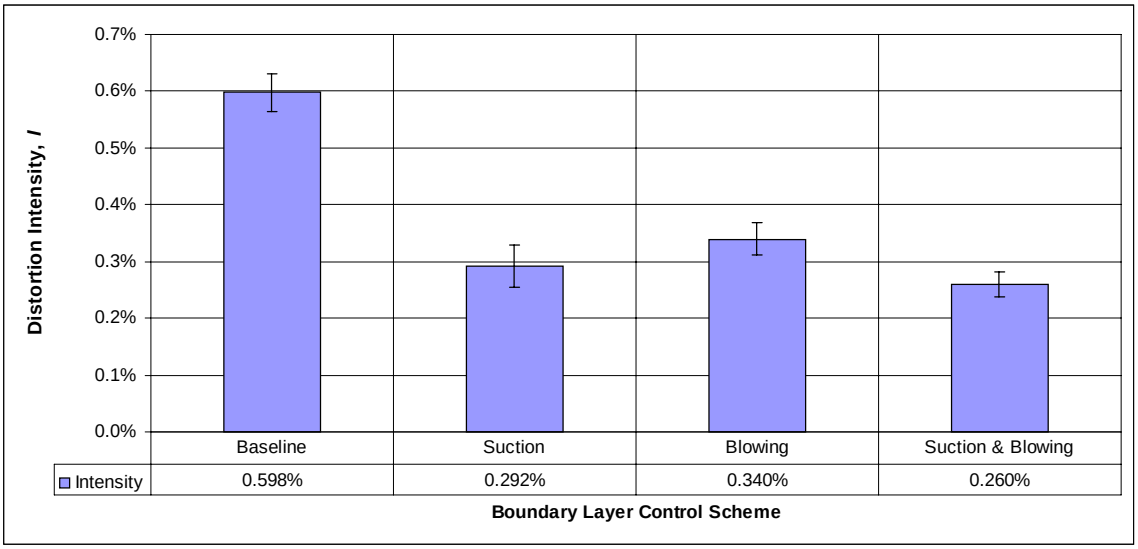

Figure 4.15: Distortion intensity parameter, *I*, with different BLC schemes

Another way to describe distortion, given in Seddon and Goldsmith (1985, p. 301), is shown in Equation (4.4). This parameter does not consider circumferential or radial distortion even in its general use. For an isentropic inlet with a uniform inlet profile, the distortion would be zero since the total pressure would be constant across the exit plane. While the distortion intensity, *I*, attempts to describe how the pressure profile is distributed, the distortion, *D*, only looks at the range of the pressure profile.

$$D = \frac{\Delta p}{\overline{p_0}} = \frac{p_{0,\max} - p_{0,\min}}{\overline{p_0}} \tag{4.4}$$

where D is the distortion

$p_{0,\max}$ and $p_{0,\min}$ are the maximum and minimum total pressures

$\overline{p_0}$ is the average of the total pressure at the exit of the inlet

Figure 4.16 shows the distortion, *D*, for different BLC schemes. The baseline case has significantly higher distortion than any of the other cases. Applying suction alone drastically improves the distortion parameter, and while blowing alone improves distortion it is not as effective as suction alone. When blowing and suction are used simultaneously, there is an even further improvement over the suction alone case.

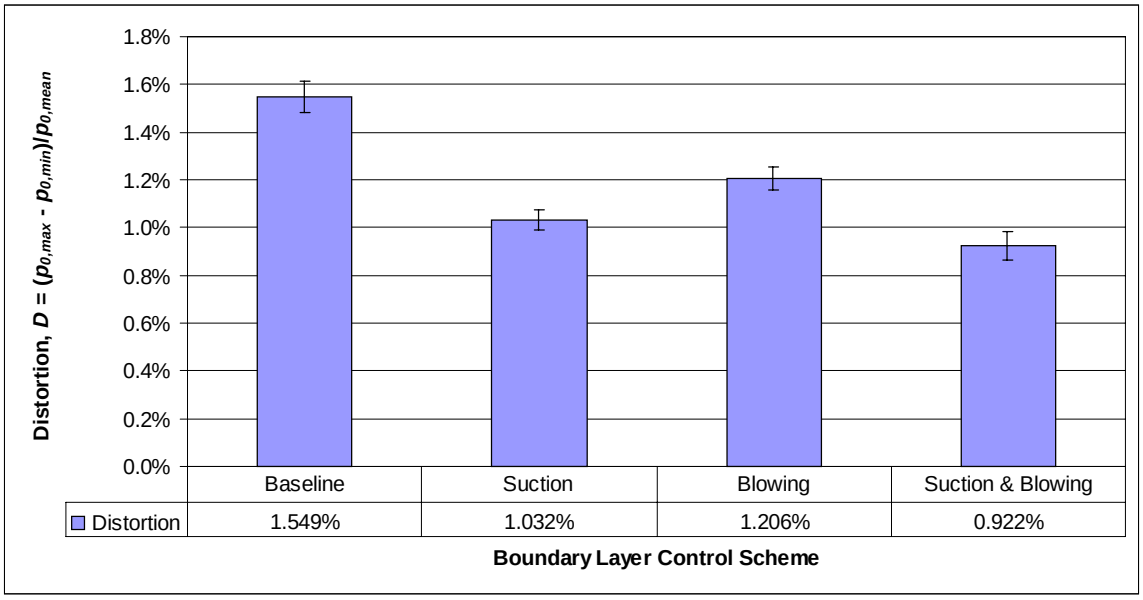

Figure 4.16: Distortion, *D*, for different BLC schemes.

4.1.3.3 Pressure Recovery

Another way to describe the effectiveness of a diffusing inlet is to describe the pressure recovery of the inlet. In an isentropic inlet, the total pressure recovery (TPR) would be unity since no losses would be associated with the inlet. Inevitably, however, losses will accrue in any physical inlet with boundary layers, shock waves, turbulence, and separated regions. The most common way to describe total pressure recovery is by the equation given as Equation (4.5).

$$TPR = \frac{\overline{p_0}}{p_{0,\infty}} \tag{4.5}$$

where TPR is the total pressure recovery
$\overline{p_0}$ is the average total pressure at the exit of inlet
$p_{0,\infty}$ is the total pressure of the freestream

The TPR was calculated for the data taken at the exit of the inlet, and a chart summarizing the results is shown in Figure 4.17. The suction case and the blowing case are equivalent in significantly improving the TPR of the inlet. Compared to the error bars, the combined suction and blowing case shows additional improvement of TPR over

just suction or just blowing. Realizing that minimizing the depth of the normalized total pressure profile will produce a TPR closer to unity, an examination of Figure 4.6 can confirm the TPR results presented in Figure 4.17. The suction case and the blowing case produce similar profiles with smaller deficits than the baseline case, while the suction and blowing case produces an even better profile with a smaller deficit to yield a TPR closer to unity.

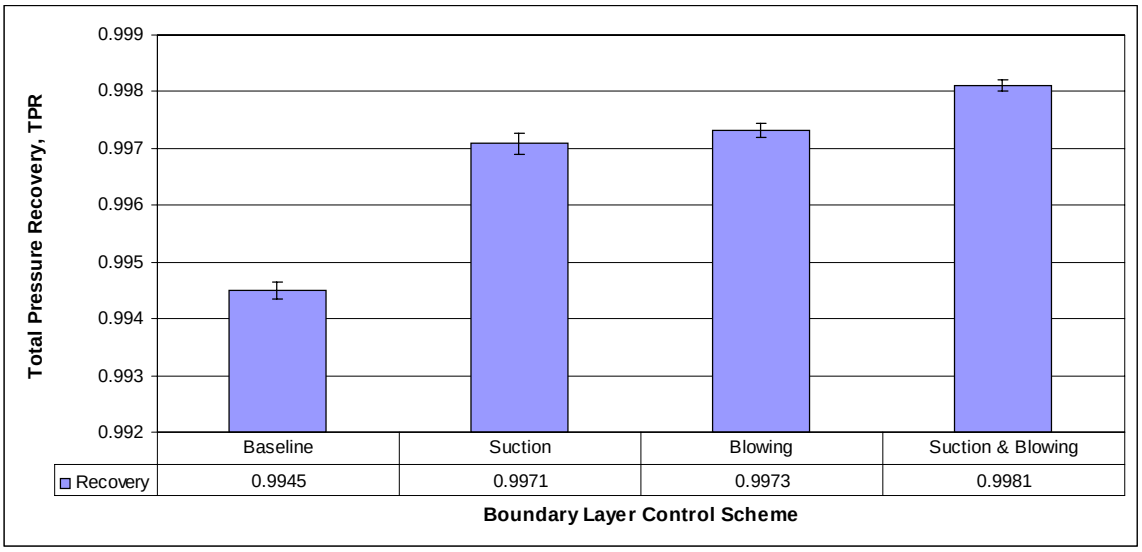

Figure 4.17: Total pressure recovery of the inlet at 40 krpm

Seddon (1993) claim that a change in the intake pressure recovery is directly proportional to a change in thrust for a given engine. They suggest Equation (4.6) approximates the gain in thrust by increasing the total pressure recovery. The proportionality constant, *K*, is greater than 1.0 and usually close to 1.5. Assuming K=1.5, the estimated improvement of thrust is 0.54% by using suction and blowing together. A Pratt & Whitney F100-PW-220 engine has a maximum thrust of 23 700 lbf (Pratt & Whitney). If the same increase in pressure recovery were seen on this engine as was seen by the simulator, an increase of 127 lbf of thrust would result.

$$\frac{\Delta X}{X} = K\left(TPR_{BLC} - TPR\right) \tag{4.6}$$

where X is the nominal engine thrust
ΔX is the change in thrust
K is a proportionality constant, assumed to be 1.5
TPR_{BLC} is the total pressure recovery with suction and blowing
TPR is the total pressure recovery

Seddon (1993) points out that while Equation (4.5) is valid for subsonic or supersonic conditions, the TPR approaches unity for small Mach numbers regardless of the amount of losses accrued within the inlet. They go on to suggest that the incompressible flow ratio, $\eta_{\sigma i}$, given as Equation (4.7), is a more discriminating parameter for small flight Mach numbers.

$$\eta_{\sigma i} = \frac{\overline{p_0} - p_\infty}{p_{0,\infty} - p_\infty} \tag{4.7}$$

where $\eta_{\sigma i}$ is the incompressible flow ratio
p_∞ is the static pressure of the (un-diffused) freestream
$\overline{p_0}$ is the average total pressure at the exit of inlet
$p_{0,\infty}$ is the total pressure of the freestream

The incompressible flow ratio was calculated for the data at 40 krpm and the results are shown in Figure 4.18. The incompressible flow ratio appears to be a better measure of the pressure recovery since the differences are less subtle. All configurations of BLC show drastic improvement of the flow ratio over the baseline case. The suction case and the blowing case seem to be roughly equivalent in improving the flow ratio, but the combination of suction and blowing shows an even greater improvement.

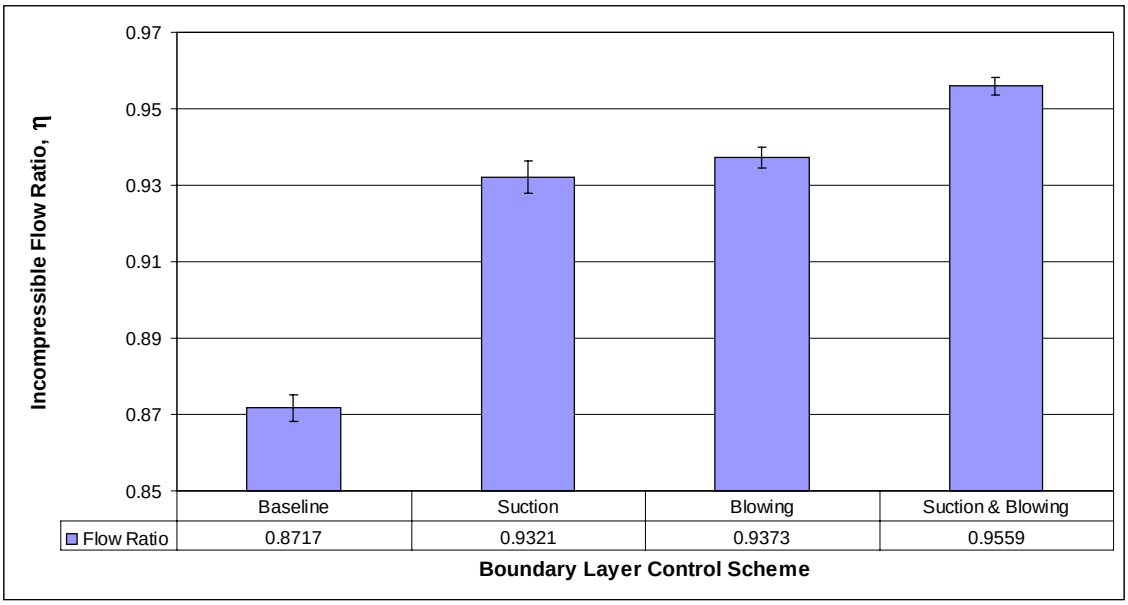

Figure 4.18: Incompressible flow ratio of the inlet at 40 krpm, a measure of the pressure recovery

In this serpentine inlet, the low pressure recovery is primarily due to the development of wide boundary layers and eventually separation. The losses that develop are due to the turbulence associated with the separated region. The use of suction improves the pressure recovery by bleeding off the lossy boundary layer just before separation. Even if the suction allowed the inlet to be isentropic, the pressure recovery would be less than unity since suction removes available energy from the inlet. Suction, however, delays the onset of separation, to which most of the losses in the baseline case are attributed. As Ball (1984) pointed out, blowing does not necessarily prevent losses from forming in the boundary layer, but it attempts to "cover-up" the losses by re-energizing the lossy parts of the flow. Again, the re-energized flow near the boundary allows the fluid to more effectively negotiate the turning and diffusion, which delays the onset of separation. When both suction and blowing are used together, their effects are combined, but as the profiles of Figure 4.6 and the inlet performance descriptors of Figure 4.15, Figure 4.16, Figure 4.17, and Figure 4.18 show, the combination is not linear.

4.1.3.4 Summary of Flow Control

Table 4.3 summarizes the improvement on distortion and pressure recovery over the baseline case. The results show that suction seems to have more influence in minimizing distortion than blowing, while blowing seems to have more influence in maximizing pressure recovery. Their combination ensures that both distortion is minimized and pressure recovery is maximized. Using ejector pumps as the source of both suction and blowing guarantees that the combination of suction and blowing is justified. For example, an engine designer with integrated ejector pumps within the inlet can use suction plus blowing for the same amount of bleed-air from the compressor as he or she could for just suction or blowing by itself. Exploring this, however, will be reserved for future work, but a set of preliminary data is presented in Appendix D.

Table 4.3: Summary of the improvement of distortion and pressure recovery

		Improvement over Baseline		
Parameter	**Baseline**	**Suction**	**Blowing**	**Suction & Blowing**
Distortion Intensity, *I*	0.00598	51.2 %	43.1 %	56.5 %
Distortion, *D*	0.01549	33.4 %	22.1 %	40.5 %
Total Pressure Recovery, *TPR*	0.9945	0.261%	0.282%	0.362%
Incompressible flow ratio, $\eta_{\sigma i}$	0.9321	6.93%	7.53%	9.66%

The measurements of distortion and pressure recovery were taken only along the spanwise centerline of the inlet's exit, immediately before the start of the transition duct. It would be inappropriate to claim with confidence that any improvements measured in distortion or pressure recovery would be matched at the engine fan-face because of boundary-layer growth and corner losses in the transition duct. This is especially true for this project with discontinuities between the inlet and transition pieces. It is appropriate, however, to claim that with a given transition duct, an improved inlet performance will improve the overall performance of the intake stages of an engine. The scope of this project was to examine the benefits of BLC on an inlet's ability to diffuse and turn the incoming flow, but the design of a transition piece that efficiently transforms the improved flow from rectangular cross-sections to circular cross-sections is left for another project.

It is also important to point out that no definitive claims can be made as to whether suction, blowing, or suction plus blowing is the generalized optimal design choice. As mentioned before, neither the suction nor the blowing holes have been optimized to provide the most effective BLC scheme. It is conceivable that blowing could outperform suction drastically if both cases were optimized, or vice-versa. It was the scope of this project only to show that suction, provided by an ejector pump, could be used with blowing to effectively improve an inlet's performance, but not to devise the optimum case. The data presented here does, however, show that even unoptimized BLC configurations have positive improvement in distortion and pressure recovery, and one can expect that optimized configurations would show even better improvements.

4.1.4 Preventing the Onset of Engine Instability

As mentioned in Section 2.1, distortion has a negative effect on the surge margin of an aircraft engine. An experiment was performed to assess the ability of the 1% suction plus blowing scheme, presented in Section 4.1.3, to delay the onset of instability in the test simulator. The experiment consisted of ramping the simulator speed up to 60 krpm with approximately 5.02 scfm of suction and 5.31 scfm of blowing, which is approximately 0.84% and 0.88%, respectively, of the estimated core flow at 60 krpm. Then, the BLC was quickly turned off to watch the simulator enter into instability. An accelerometer measured the vibration as the simulator went unstable. The accelerometer's output is shown in Figure 4.19 to triple as the simulator goes unstable after the BLC was turned off. Even though the distortion and pressure recovery improvements were only calculated along the spanwise center of the inlet, Figure 4.19 shows that the BLC has a global effect on improving the surge margin of the simulator.

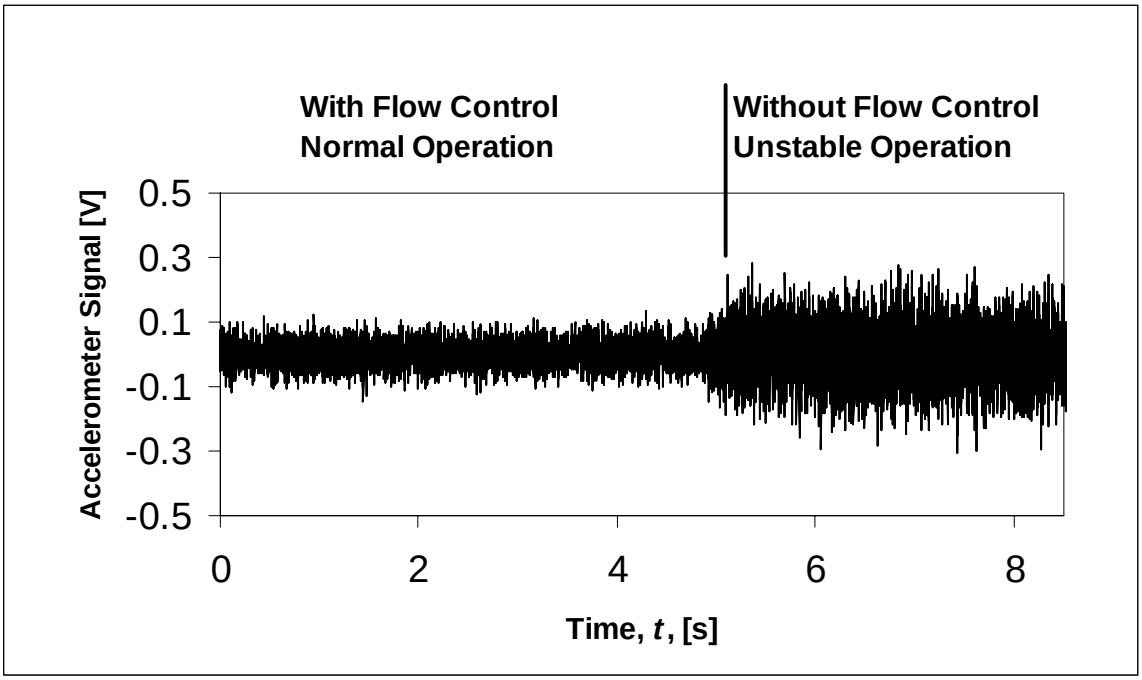

Figure 4.19: Output of accelerometer showing BLC to delay instability in the simulator

4.2 Microphone Results

As discussed in Section 3.1.4.2, two types of microphone data were taken along the inlet surface. One type examined how the microphone signal changed for attached and separating flow, and the results will be presented in the first subsection. The other type, presented in Appendix C, attempted to resolve the microphone signal into its different components: acoustic and pseudo-acoustic pressure fluctuations. The second subsection of this section will assess a microphone's ability to sense the effectiveness of the BLC in minimizing distortion and separation. Figure 4.20 shows the microphone locations along the surface.

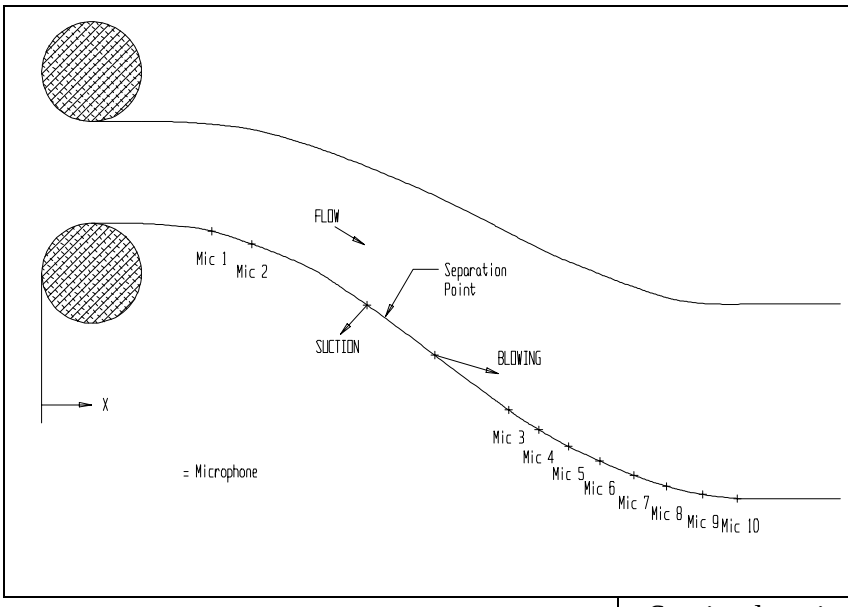

Microphone	
Num.	Distance, X [in]
1	3.41
2	4.21
3	9.36
4	9.96
5	10.56
6	11.18
7	11.87
8	12.53
9	13.26
10	13.94
Suction location	6.52
Blowing location	7.88

Figure 4.20: Microphone locations, where X is the distance from the front of the bellmouth

4.2.1 Microphone Spectrums for Attached and Separated Flow

The microphones placed along the centerline of the inlet were used to examine how pressure fluctuations changed along the inlet's surface as the flow turns and diffuses. The microphones were also used to examine the influence BLC has on the pressure fluctuations. Table 4.4 shows the BLC flowrates used for the microphone experiments, which are similar to those presented in Table 4.1 for the aerodynamic experiments.

Table 4.4: Flowrates used for boundary layer suction and blowing during microphone experiments

		Flowrate	
		[scfm]	**[%-core flow]**
Suction		5.304	1.40
Blowing		5.078	1.34
Suction & Blowing	Suction	5.247	1.38
	Blowing	5.047	1.33
Simulator at 40 krpm		758.7	

Figure 4.21 and Figure 4.22 show the spectrums of the upstream and downstream microphones, respectively, on the frequency range of 25 to 300 Hz. Figure 4.23 shows

the difference in the two signals. The microphone spectrums seem to mimic the aerodynamic data seen in Section 4.1. The spectrums of Microphone 1 upstream show little change from the baseline with suction, blowing, and suction plus blowing—just as Figure 4.4 shows only a slightly stronger inlet Mach profile with suction plus blowing. At Microphone 10, however, suction, blowing, and suction plus blowing have a definite effect on the baseline case for both the aerodynamic profiles of Figure 4.6 and the microphone spectrums of Figure 4.22. Examining the aerodynamic profiles, the suction case and blowing case seem to be equivalent in reducing the profile deficit, while suction and blowing combined offers further reductions. The microphone spectrums, however, seem to show that blowing is more effective at reducing the pressure fluctuations than suction, and that the combined use of suction and blowing seem to barely lower the fluctuations from the blowing alone case.

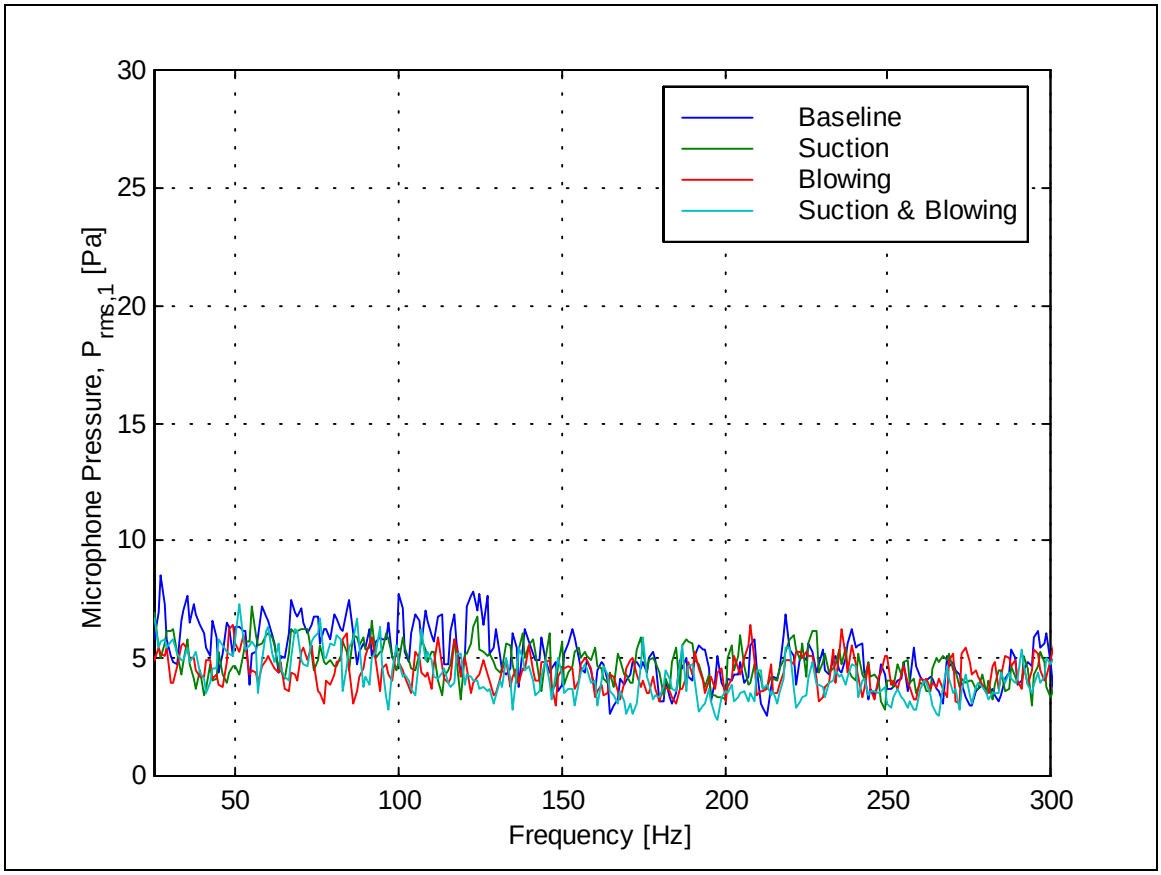

Figure 4.21: Spectrum of Microphone 1 (upstream)

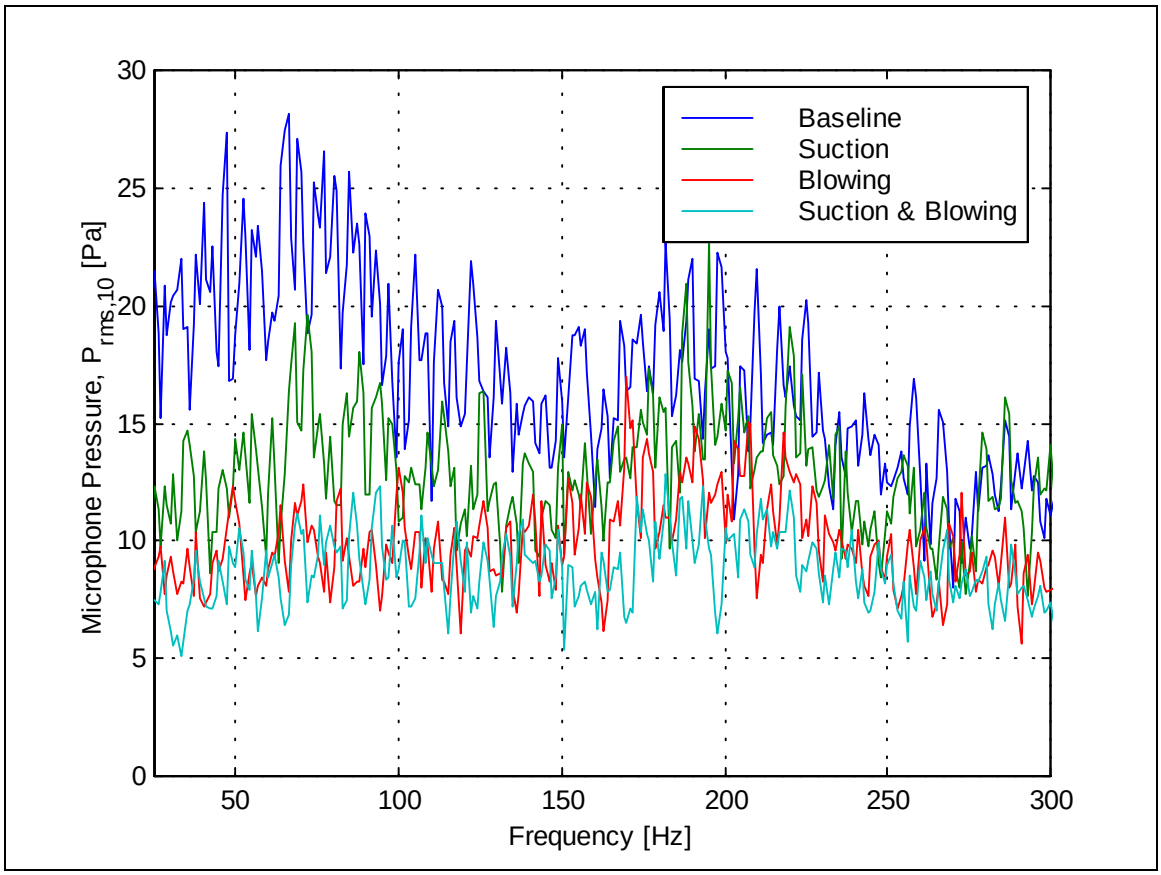

Figure 4.22: Spectrum of Microphone 10 (downstream)

Figure 4.23 shows the difference between the spectrums of Microphone 10 and Microphone 1. Suction plus blowing minimizes the difference in the spectrums at Microphone 10. It appears that minimizing the difference in the spectrums in Figure 4.23 coincides with minimizing the distortion of Figure 4.16 and maximizing the pressure recovery of Figure 4.18. This observation suggests the potential that microphones have in a feedback control system to minimize separation. Since the spectrum of Microphone 1 is similar for all three of the BLC schemes, it can be used as a reference to a clean flow structure, and the difference between Microphone 10 and Microphone 1 can therefore be used as an error signal to control a valve for an ejector pump or blowing supply.

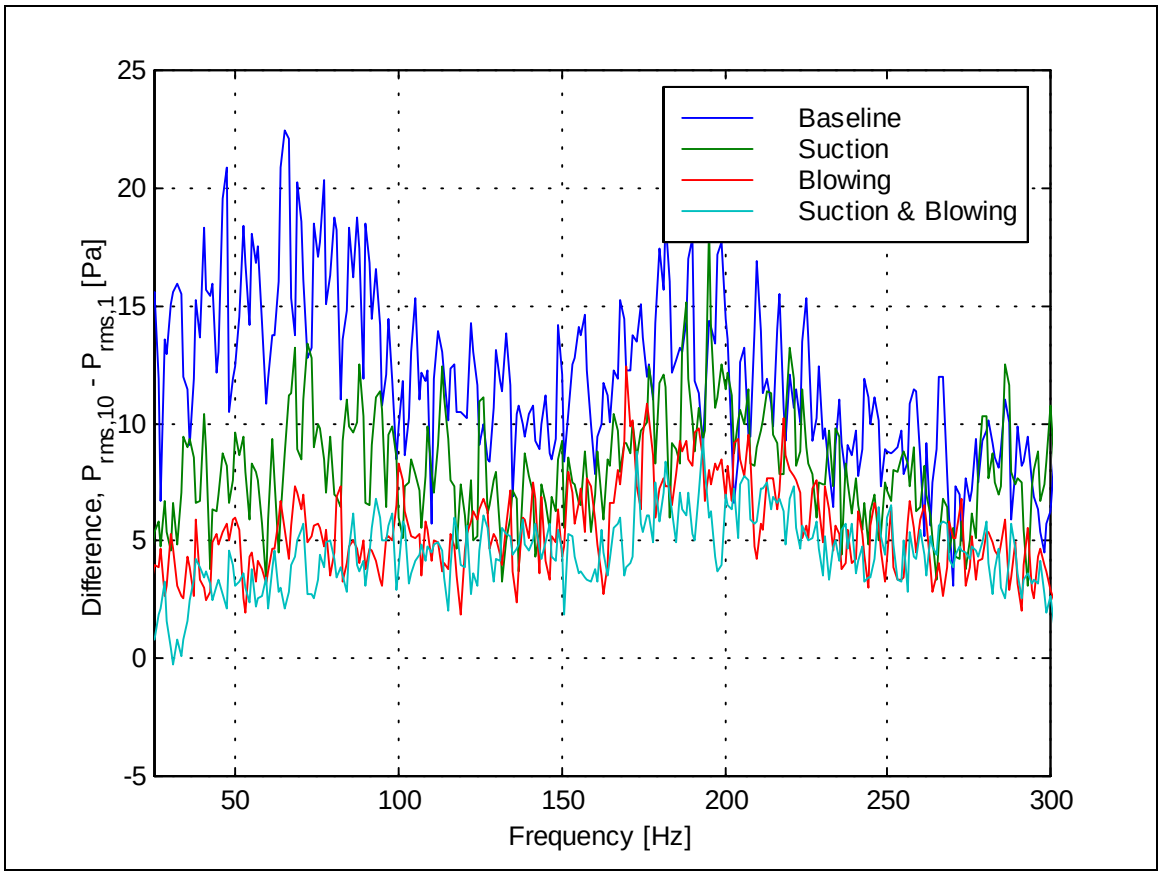

Figure 4.23: Difference in Microphone 10 (downstream) and Microphone 1 (downstream) microphone signals

In Figure 4.24 the frequency content of each microphone signal between 25 and 300 Hz was combined into one number by Equation (4.8) (Smith 2000). Note how the pressure fluctuations tend to increase as the flow is diffused and turned to create higher levels of turbulence. Even though the time-averaged static pressure is expected to rise while the flow diffuses (and slows down), the time-averaged value is not reflected in Figure 4.24 since it would only be revealed in the DC-component at zero frequency. This proposes that the rise in the combined pressure fluctuations is only due to an increase in turbulence as the flow begins to separate. Treating the boundary layer with suction and blowing minimizes the separation and therefore minimizes the pressure fluctuations. While Table 4.2 showcases how the pressure fluctuates at various positions from the wall with aerodynamic measurements, Figure 4.24 demonstrates with microphone measurements how BLC affects the fluctuations along the wall as the flow diffuses and separates.

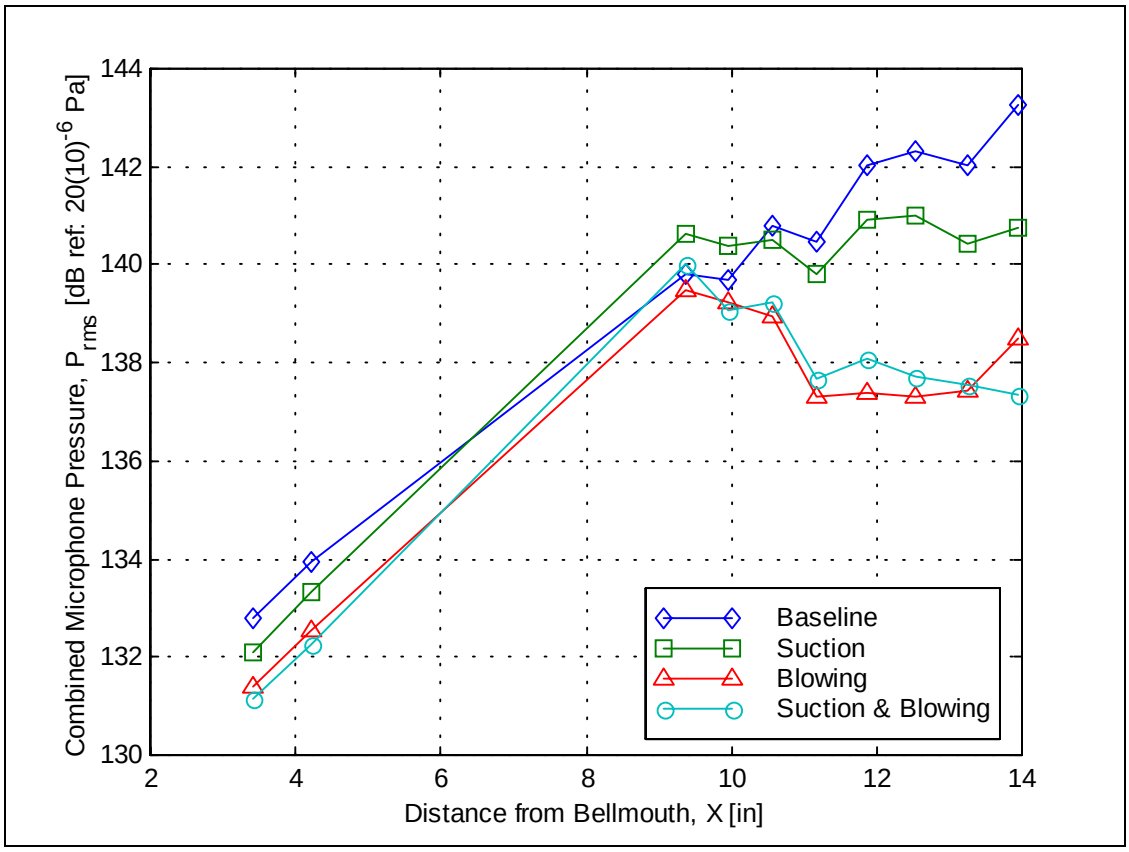

Figure 4.24: Combined microphone pressure for each microphone, showing how the pressure fluctuations change along the flow's path; the suction and blowing holes are at 6.52 in and 7.88 in, respectively

$$L = 10\log\left(\frac{1}{p_{ref}^2}\sum_{k=1}^{n}\left(p_{rms}^2\right)_k\right) \tag{4.8}$$

where L is the combined signal
n is the number of frequency bands
p_{rms} is the root-mean-square pressure at frequency f_k
p_{ref} is the reference pressure, $20(10)^{-6}$ Pa

The microphone signals in the baseline case of Figure 4.24 continue to grow sharply downstream of the suction and blowing holes. Suction, however, retards the growth of the downstream microphone signals. The blowing and suction plus blowing cases tend to actually lower the microphone signals as the flow continues to diffuse. This suggests that the turbulence levels are being diminished as the boundary layer is treated. While suction has only a local effect in delaying separation, blowing can affect the boundary layer well downstream of the blowing holes. This can explain why blowing is

shown in Figure 4.24 to have a stronger influence on the downstream microphone than suction.

The frequency range shown in Figure 4.22 is the range most heavily influenced by the flow characteristics. The blade-passing-frequency of the simulator, at a speed of 40 krpm with 18 rotating blades, is 12 kHz, which is well above the plotted frequency range. Furthermore, the tones associated with the misalignments of the inlet with the bellmouth were found to be on every spectrum, regardless of the BLC scheme, at frequencies well above 300 Hz. Figure 4.24 shows that the noise usually associated with blowing is not a large contributor to the noise at the lower frequency range since the pressure fluctuations at the microphones downstream of the blowing jets are the lowest for the suction and suction plus blowing cases. Furthermore, any unwanted effects on the spectrums due to the microphones not being exactly flush with the curved surface would be approximately the same for each BLC scheme, so they would be cancelled out in the comparisons. The differences in the spectrums, therefore, must be a result of the separated flow and the effect BLC has on the separation.

4.2.2 Assessment of Microphones as Active Flow Control Sensors

Flush-mounted Microphones have potential to offer feasible means to provide feedback in an active control scheme where other flow sensors would disturb the flow. Rioual *et al*. (1994) used flush-mounted microphones to control the transition of a boundary layer from laminar to turbulent. As Lighthill's (1951) analogy suggests, aerodynamics and acoustics have an intimate relationship.

Before microphones can be used as feedback for an active BLC scheme, the correlation between microphone spectrums and aerodynamic profiles must be determined. Therefore, an experiment was designed to assess the potential microphones have in providing actively controlled boundary layer blowing. First, a Kiel total pressure probe was traversed over 2.6 in, as described in Section 3.3.1, several times while the simulator speed was maintained at 30 krpm. The blowing rate was changed with each traverse to determine the effect it has on the total pressure profile. Some blowing rates

were chosen that created an excess of normalized total pressure near the wall. Then, microphone measurements were taken for approximately the same blowing rates.

Figure 4.25 shows the aerodynamic profiles created by the traverse. The aerodynamic profiles show that as the blowing flowrate increases, the profile deficit decreases, and the blowing rates above 1.37% actually created an overpressure when the normalized total pressure went above unity. Figure 4.26 shows the distortion, *D*, calculated at the exit of the inlet by Equation (4.4). The distortion decreases as the blowing rate increases to 1.37%, but higher flowrates generate higher distortion levels. The distortion is minimized when the profile does not exhibit overblowing.

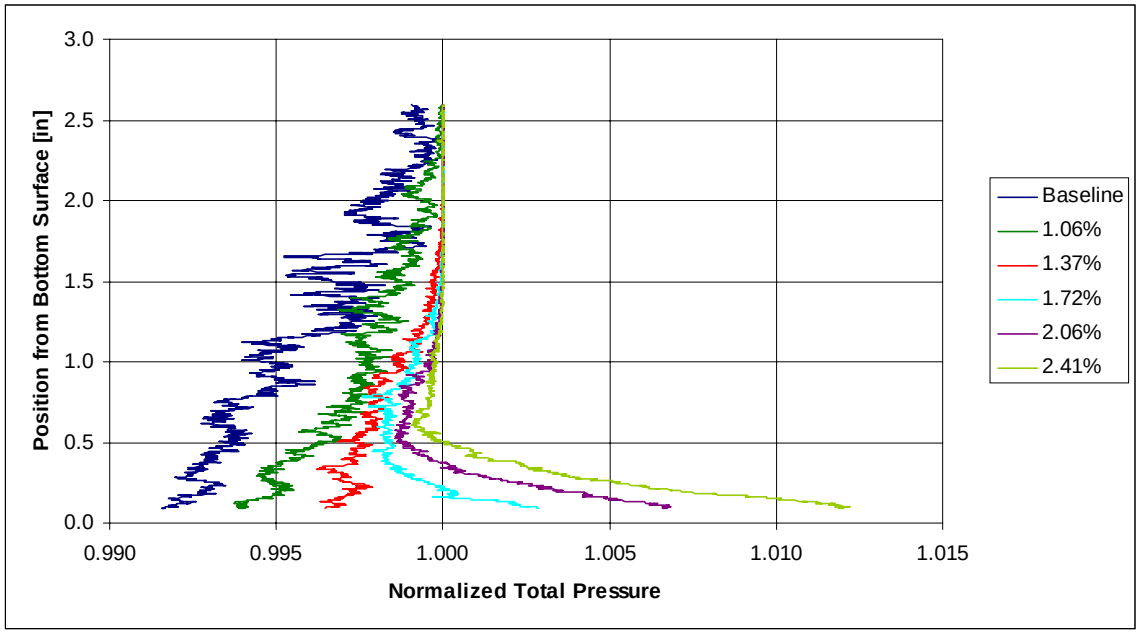

Figure 4.25: Effect of different blowing rates [%-core] on the total pressure profile, at 30 krpm

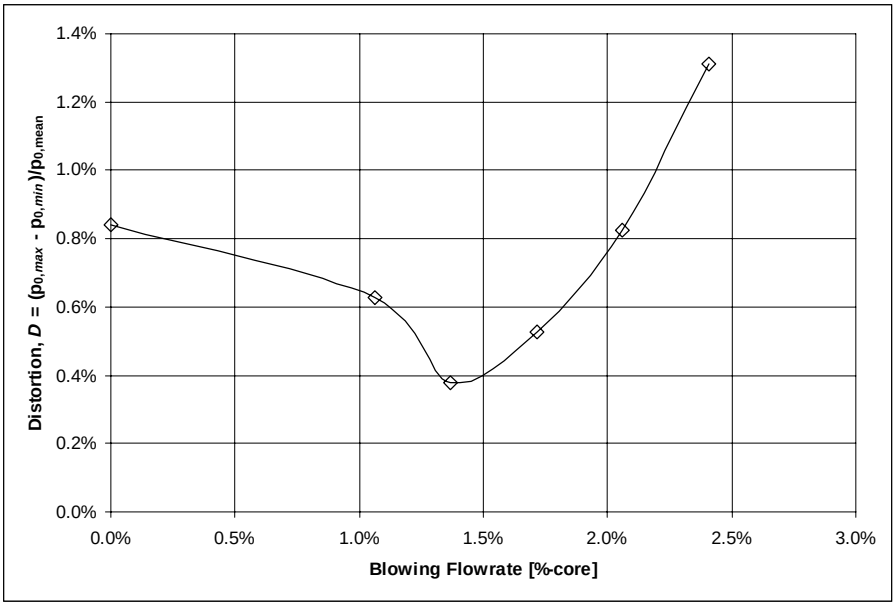

Figure 4.26: Distortion calculated at the exit of the inlet

Figure 4.27 shows the captured microphone pressure spectrums related to the aerodynamic profiles of Figure 4.25. The microphone spectrums seem to decrease in value drastically for flowrates less than 1.37%, while the higher flowrates show little or no improvement. This is reiterated in Figure 4.28 where each microphone spectrum is combined using Equation (4.8). Above 1.37%, the combined microphone signal decreases only slightly with higher blowing rates, but it does not increase as the distortion would suggest.

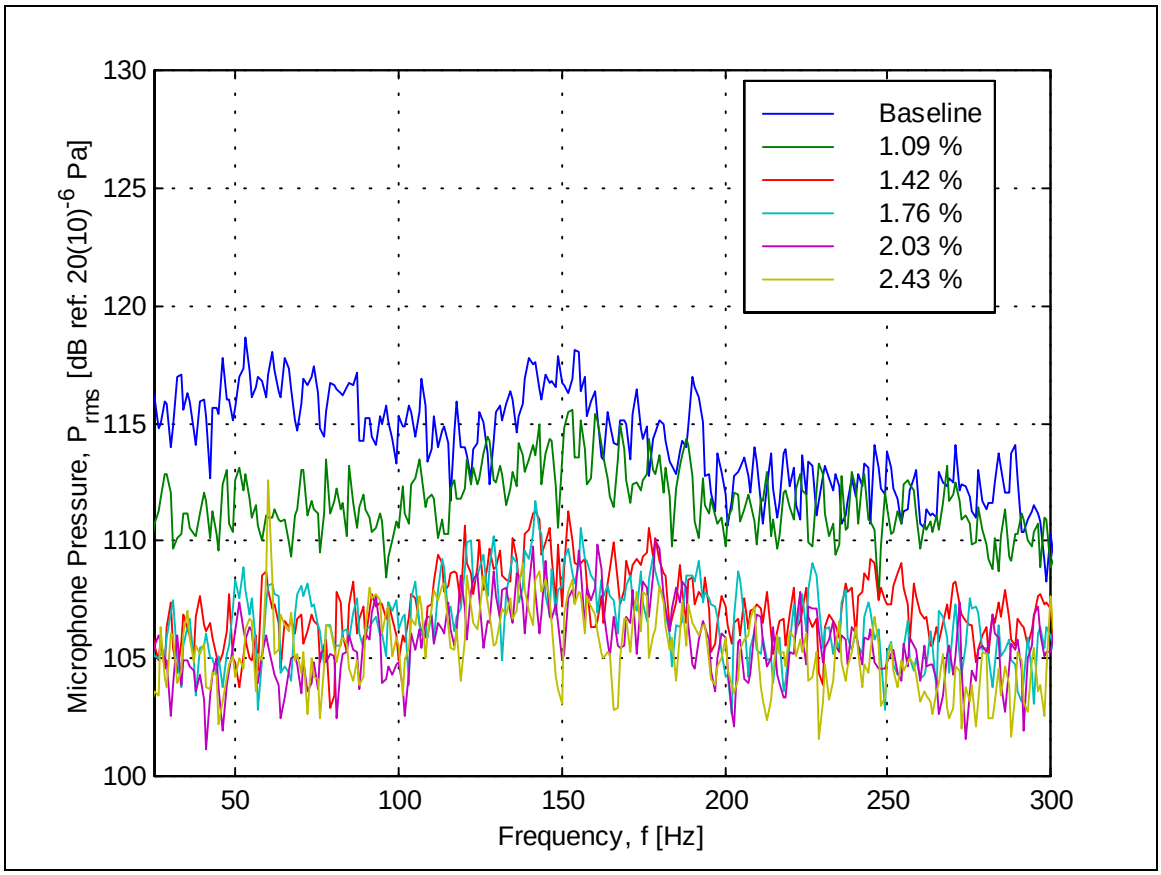

Figure 4.27: Effect of different blowing rates [%-core] on microphone pressure at 30 krpm

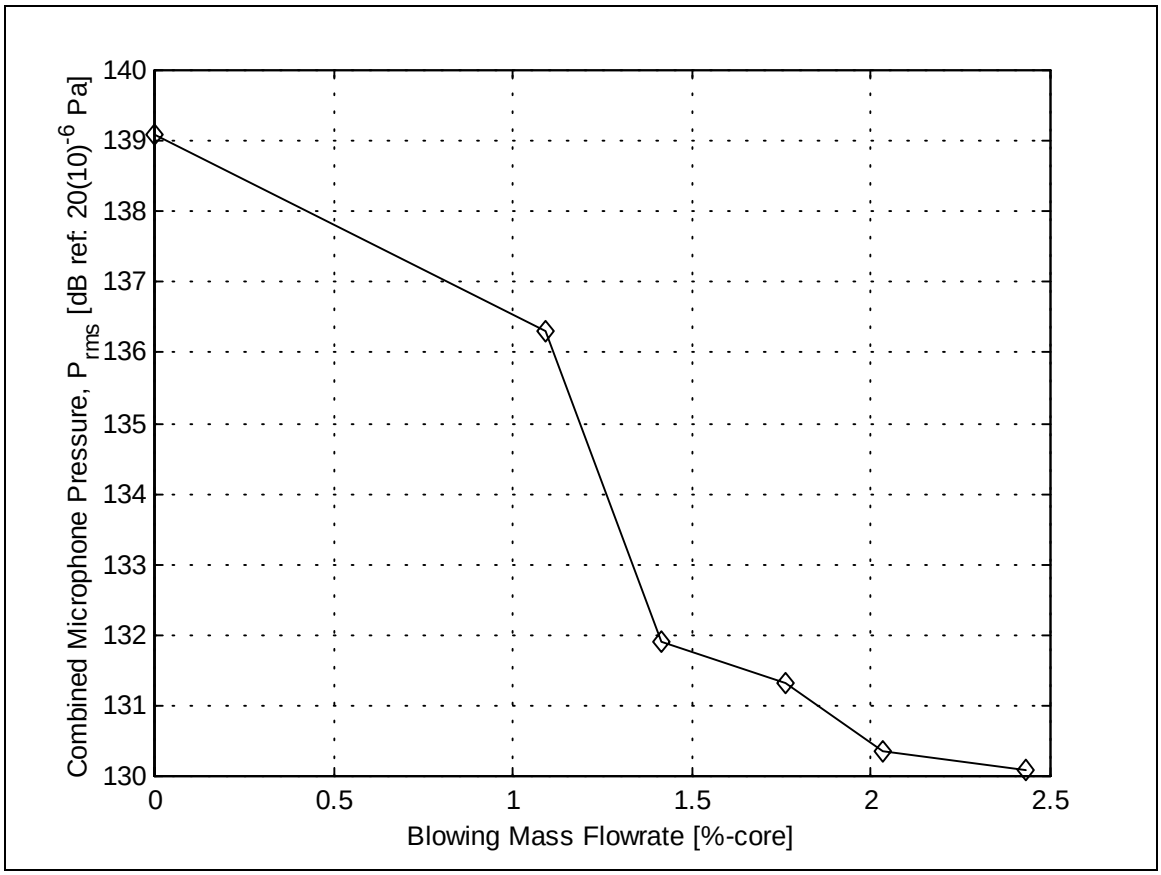

Figure 4.28: Combined microphone pressure for between 25 and 300 Hz at 30 krpm

The blowing air available for BLC on a real engine would come from the latter stages of the air compressor. The work required to compress the air to its final stages makes it difficult to justify bleeding it for non-essential features. Therefore, two constraints exist in a boundary layer blowing scheme: (1) the blowing flowrate must be kept reasonably close to 1.0% of the core flow and (2) the blowing flowrate must not create more total pressure than losses take away. Figure 4.25 shows that for blowing rates above 1.37%, an excess of total pressure was created. Using the flowrates above 1.37% is bad for two reasons: (1) more blowing air is used than is needed and (2) distortion can actually increase.

A practical active control scheme would not allow overblowing to occur. Unfortunately, if the combined microphone pressure, shown in Figure 4.28 were to be used as an error signal to be minimized in an active control scheme, the controller would ask for increasingly more blowing rates and the distortion would rise to intolerable levels.

Ideally, the combined microphone pressure would reach a minimum when the distortion, *D*, would be at a minimum.

An attempt was made to examine another method that may have promise in giving feedback to a BLC controller. Following the methods presented in Simpson *et al*. (1987) and Agarwal and Simpson (1989), which were briefly described in Section 2.3.3, the turbulent pressure spectrum was captured. The two arrays of three microphones described in Section 3.1.4.2 were used to filter out the acoustic component of the microphone signal to leave only the turbulent pressure component. Unfortunately, due to a lack of resources, the experiment was not done to a proper precision, and no conclusive results should be reported. This is not to say that a properly done experiment would show or would not show conclusive results. Appendix C describes the problems with the experiment performed and shows the data obtained.

The data suggests that a definite relationship exists between the aerodynamic profile and the microphone spectrum. Even though this particular sensing scheme may not be practical, there is hope that a practical microphone sensing scheme will be found that will not allow overblowing. Perhaps a controller, that looks only at either the turbulent or the acoustic components of the microphone pressure signal, may provide extra incite to the flow along the surface that will limit the blowing flowrate to the proper level. Or, a controller with penalties for both high blowing rates and high microphone pressure values may provide a workable solution. One promising controller might use the sensitivity of the combined pressure signal with blowing rate since Figure 4.28 shows a change in slope when the optimum blowing rate is reached.

5.0 Conclusions and Recommendations

This chapter presents the major conclusions derived from the previous chapters, and recommends work to be done in the future.

5.1 Conclusions

In this research project, the benefits of boundary layer control in a compact, highly offset serpentine inlet of a small-scale turbofan engine simulator was explored. The compactness of the inlet allows an application to unmanned air vehicles (UAVs) that require a low radar cross section (RCS) but high performance and minimal weight. Ejector pumps were also examined to be a viable source of suction, but only conventional sources of blowing were tested. Microphones were shown to accurately indicate the degree of distortion at the exit of the inlet, which gives them potential to be practical feedback sensors in an active flow control system.

BLC was shown to improve the distortion and pressure recovery of the inlet, by means of enhancing the total pressure profile at the exit, with suction and blowing flowrates of around 1% of the core flow. The suction and blowing alone cases showed roughly the same improvements in improving distortion and recovery. The combination of suction and blowing was shown to be better than either by itself. With suction plus blowing at 40 krpm, the distortion, *D*, decreased by 40.5% compared to the baseline while the flow ratio, $\eta_{\sigma i}$, increased by 9.66%. Neither the suction or the blowing configurations were optimized for efficiency, so it would be inappropriate to claim that suction, blowing, or the combination of suction and blowing is the better design choice. It would be appropriate to claim, however, that optimized configurations would show even better improvements than those documented in this thesis.

Previous work has shown that distortion from an inlet diminishes a compressor's surge margin. The enabling ability of BLC to decrease distortion and increase the simulator's operating range was tested and confirmed. The simulator was taken to 60

krpm with suction and blowing turned on without any signs of instability. Then, once the BLC was turned off, the simulator quickly drifted into a region of instability, which proves that BLC allowed the simulator to operate in a region that it would have otherwise been unable. Accelerometers captured the simulator's change in vibration from the relatively calm operating range to the relatively violent instability range.

A microphone's ability to be used as a feedback sensor to an actively controlled BLC scheme was also examined. The microphone spectrums of suction, blowing, and suction plus blowing were compared with the corresponding aerodynamic profiles. Also, the microphone spectrums of a wide range of blowing rates—without any suction—was compared with corresponding aerodynamic profiles. It was shown that as BLC minimized the deficit of the profile and improved the distortion and recovery, the magnitude of the microphone pressure decreased. It was discovered that the sensing scheme used in this research correlates well with improvements in the boundary layer, which is promising for a feedback sensor. If no modifications to the sensing scheme are made, however, the error signal would drive the controller to force higher blowing flowrates than needed or allowed in a practical setting.

5.2 Recommendations for Future Work

As with any research project, formulations of new questions and ideas arose through the course of this endeavor. One large area for a better understanding of the BLC in a serpentine inlet is to develop cookbook-type guidelines for optimizing the suction and blowing configurations, including suction and blowing hole locations, size, and orientation. Also, a detailed system study that weighs the benefits of BLC in minimizing distortion and the drawbacks of compressor bleeding in lowering the thermodynamic efficiency of the engine would tremendously aid aircraft designers.

The ejector pumps used in this research project were off-the-shelf unmodified products. There is potential, however, for a modified ejector pump to be integrated into the inlet itself so that the length of lossy suction lines can be minimized. The exhaust of such an ejector pump could be used as the source of boundary layer blowing, so that for the same bleed-rate required for just suction, both suction and blowing could be used

simultaneously. A preliminary assessment of an integrated ejector pump performance is given in Appendix D.

A refinement of the sensing scheme used in this project is necessary before it could be used in an actual application. Simpson *et al*. (1987) noticed that the turbulent pressure fluctuations, normalized by the shearing stress, peaked near the separation point. This suggests that a microphone array that is able to filter the acoustic component out of the microphone signal may provide the means to actively control the separation effectively. The attempt made within the scope of this research project, presented in Appendix C, was insufficient in its execution, but a better attempt may prove to be worthy.

References:

Agarwal, N.K. and Simpson, R.L. "A New Technique for Obtaining the Turbulent Pressure Spectrum from the Surface Pressure Spectrum," *Journal of Sound and Vibration.* v. 135, 1989, p. 346-350.

Anderson, B.H. and J. Gibb, "Vortex-Generator Installation Studies on Steady-State and Dynamic Distortion," *Journal of Aircraft.* v. 35, n. 4, 1998, p. 513-520.

Anderson, B.H., *et al*., "A Study on MEMS Flow Control for the Management of Engine Face Distortion in Compact Inlet Systems," Proceedings of the 3rd ASME/JSME Joint Fluids Engineering Conference, San Francisco, July 1999.

Ball, W.H. "Experimental Investigation of the Effects of Wall Suction and Blowing on the Performance of Highly Offset Diffusers," AIAA 83-1169, 1983.

Ball, W.H., "Tests of Wall Blowing Concepts for Diffuser Boundary Layer Control," AIAA 84-1276, 1984.

Beckwith, Thomas G., Roy D. Marangoni, and John H. Lienhard, *Mechanical Measurements*, 5th ed. Reading, Massachusetts: Addison-Wesley, 1993.

DP15 Variable Reluctance Pressure Transducer. Website: http://www.validyne.com/dp15.htm, December 1999.

Feng, Jinwei. Personal communication, February 2000.

Fox, R.W. and S.J. Kline. "Flow Regimes in Curved Subsonic Diffusers," *Journal of Basic Engineering.* v. 84, September 1962, p. 303-312.

Jones, J. *Stealth Technology*, ed. Matt Thurber. Blue Ridge Summit, PA: Tab Books, 1989.

Kerrebrock, Jack L. *et al*. "A Family of Designs for Aspirated Compressors," ASME 98-GT-19, 1998.

Kline, S.J., and F.A. McClintock. "Describing Uncertainties in Single-Sample Experiments," *Mechanical Engineering.* January 1953, p. 3.

Laufer, J., John E. Ffowcs Williams, and Stephen Childress. "Mechanism of Noise Generation in the Turbulent Boundary Layer," *AGARDograph 90*, November 1964.

Leitch, Thomas, "Reduction of Unsteady Stator-Rotor Interaction by Trailing Edge Blowing," M. S. Thesis, Virginia Polytechnic Institute and State University, Blacksburg, VA, 1997.

Leitch, Thomas. Personal communication, December 1999.

Lighthill, M. J. "On sound generated aerodynamically I. General Theory," *Proceedings of the Royal Society of London (Series A)*, v. 211, 1952, p. 564-587.

Lighthill, M. J. "On sound generated aerodynamically II. Turbulence as a source of sound," *Proceedings of the Royal Society of London (Series A)*, v. 222, 1954, p. 1-32.

Meriam Instrument, "Laminar Flow Elements Installation and Operation Instructions," File number 501:440-9; Model 50MR2-2.

Model 460 Turbofan Propulsion Simulator Products Specification, Tech Development Inc., U.S. Patent 3434679.

"PFS Pressure Catalog," PFS-604A, 1999.

Poisson-Quinton, Ph., and L. Lepage. "Survey of French Research on the Control of Boundary Layer and Circulation," in *Boundary Layer and Flow Control*, ed. G.V. Lachmann, Volume I. New York: Pergamon Press, 1961.

"Pratt & Whitney Engine Gallery," Website: http://www.pratt-whitney.com/engines/gallery/f100.220.html, April 2000.

Rao, Nikhil, ""Reduction of Unsteady Rotor Interaction by Trailing Edge Blowing Using MEMS Based Microvalves," M.S. Thesis, Virginia Polytechnic Institute and State University, Blacksburg, VA, 1999.

Rioual, J. -L., P.A. Nelson, and M.J. Fisher. "Experiments on the Automatic Control of Boundary-Layer Transition," *Journal of Aircraft*. v. 31, n. 6, November-December 1994, p. 1416-1418.

Ross, Donald. *Mechanics of Underwater Noise*. New York: Pergamon Press, 1976.

SAE Aerospace Recommended Practice 1420, Revision A. "Gas Turbine Engine Inlet Flow Distortion Guidelines", 1998.

Seddon, J. "Aerodynamic Factors in Design," in *Practical Intake Aerodynamic Design*, ed. E.L. Goldsmith and J. Seddon, p. 1-20. Oxford, UK: Blackwell Scientific, 1993.

Seddon, J. and E.L. Goldsmith. *Intake Aerodynamics.* London: Collins, 1985.

Simpson, R.L., Y.-T. Chew, and B.G. Shivaprasad. "Structure of a Separating Turbulent Boundary Layer," *Journal of Fluid Mechanics*. v. 113, 1981, p. 23-74.

Simpson, R.L, M. Ghodbane, and B.E. McGrath. "Surface Pressure Fluctuations in a Separating Turbulent Boundary Layer," *Journal of Fluid Mechanics.* v. 177, 1987, p. 167-186.

Smith, Jerome. Personal communication, April 2000.

United Sensor catalog, Bulletin No. 3.

Vaccon Vacuum Products. Website: http://www.vaccon.com/PDFs/pg14.pdf, February 2000.

Williams, D.D. "Engine Response to Distorted Inflow Conditions," AGARD CP-400, Munich, Germany, September 1986.

Williams, D.D. and L.E. Surber. "Intake Engine Compatibility," in *Practical Intake Aerodynamic Design*, ed. E.L. Goldsmith and J. Seddon, p. 21-71. Oxford: Blackwell Scientific Publications, 1993.

Appendix A: Bench Tests

Before any experiments were performed on the simulator, experiments were performed with the inlet placed on the intake of a centrifugal blower in the Flow Lab of Virginia Tech. The objective of these experiments was to develop a workable design in a simple test rig to avoid iterations on the more complicated simulator. This appendix will document the findings of the bench tests. The first section will characterize the flow to examine where the separation occurs and its severity. The second section will discuss the iterations on the suction and blowing configuration designs.

A.1 Characterizing the Inlet Flow

Once the design of the inlet was decided, the flow within the inlet had to be characterized to show that the design of the inlet was sufficient in providing a separated flow that would be controllable. The flow was characterized by three different methods: streamers on the curved surface, boundary layer traverses, and static pressure taps along the surface.

Using streamers along the curved surface was the first and easiest way to characterize the inlet. When the flow was attached, the streamers were taut and pointing downstream, but the turbulent flow in the separated region forced the streamers to violently oscillate in random directions. Unfortunately, it would be difficult to document the streamers' behavior, but they provided a preliminary assessment of the flow within the inlet.

The boundary layer traverses give the best clue as to how the flow behaves as it flows downstream. Table A.1 shows the development of the boundary layer in the inlet. The total pressure profile at the beginning, Station 10, shows a well-attached boundary layer, but the profile downstream at the exit, Station 60, shows a highly distorted profile with a vertical slope at the wall that is typical of separated flow. The profile at Station 50 indicates that separation first begins 7.0 in from the bellmouth.

Table A.1: Profiles along the inlet's surface (on blower)

Station Num.	Distance from end of bellmouth following surface [in]	Profile
10	1.1	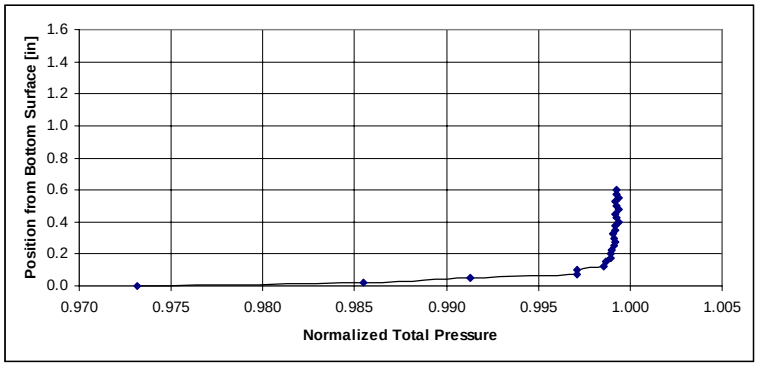
20	3.1	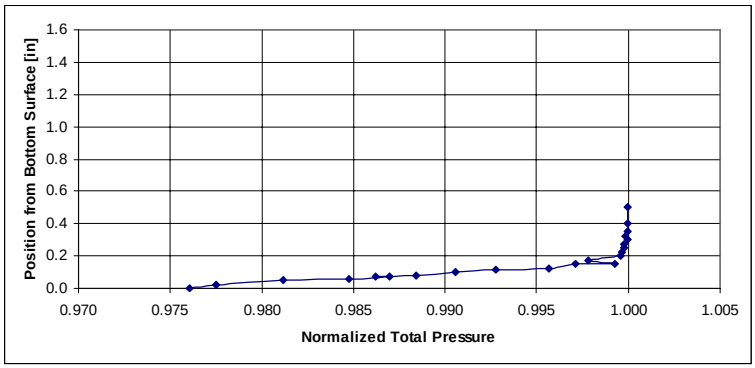
30	4.8	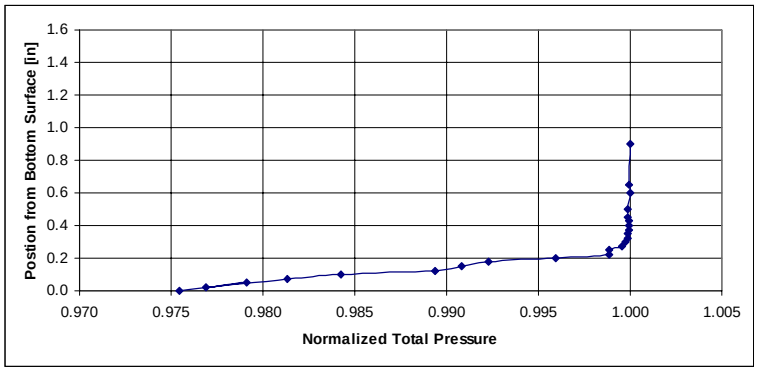

Station Num.	Distance from end of bellmouth following surface [in]	Profile
40	6.0	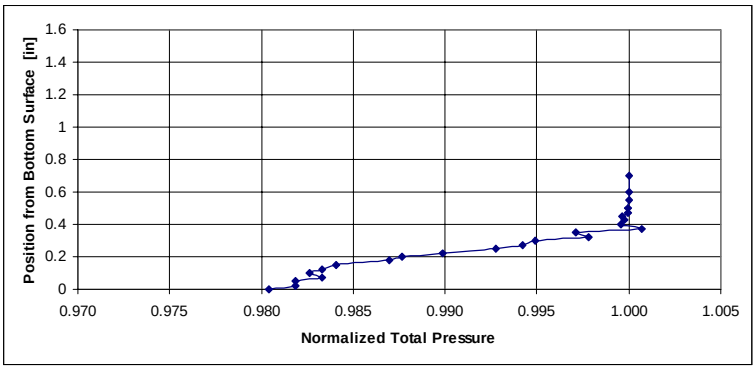
45A	6.3	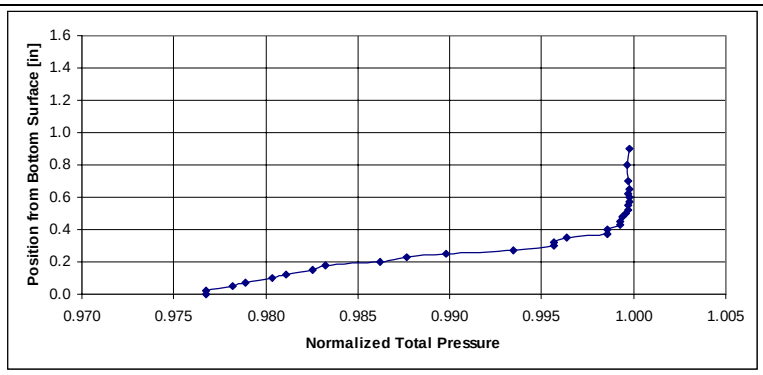
45B	6.5	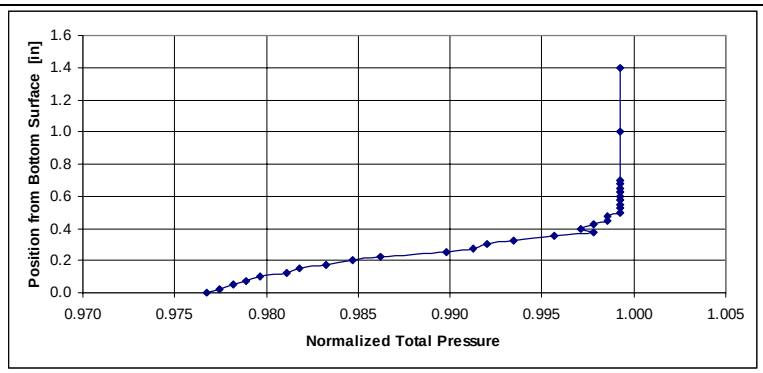
45C	6.8	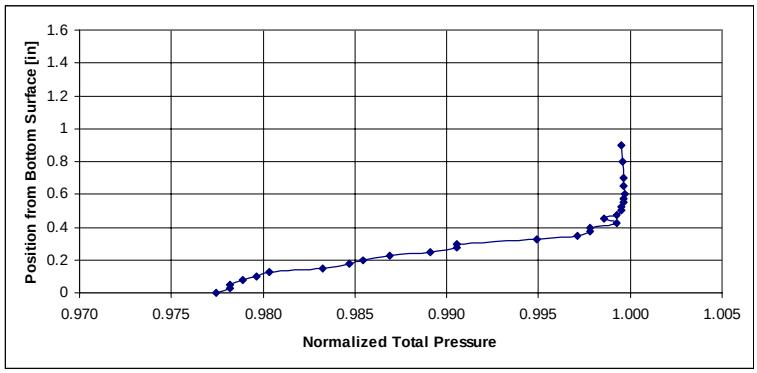

Station Num.	Distance from end of bellmouth following surface [in]	Profile
50	7.0	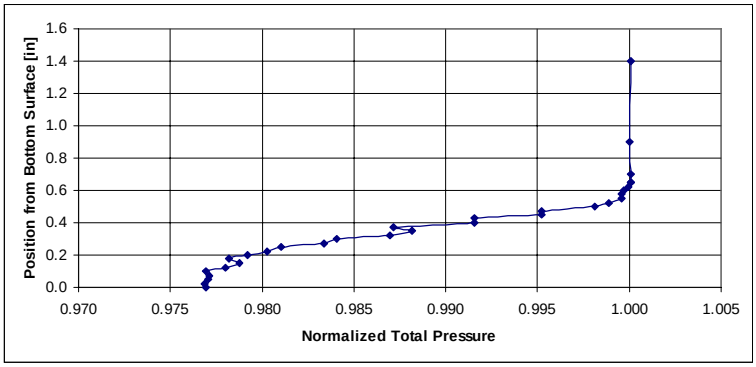
60	10.3	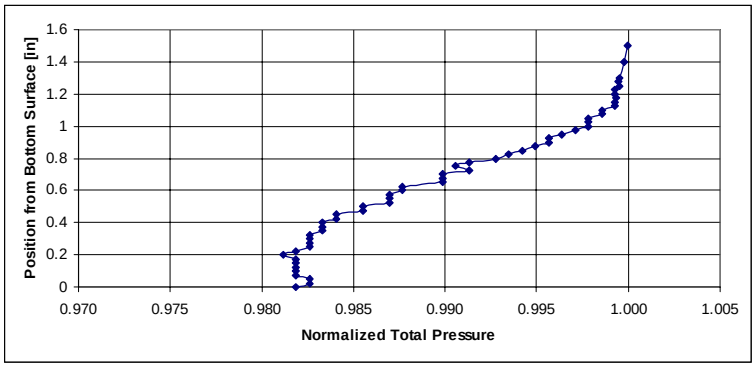

Static pressure taps, placed along the curved surface, provided one last clue as to where the flow separated. Figure A.1 shows the static pressure to increase up to the point of separation. After separation, the static pressure remains fairly constant before climbing again at a slower pace. The increase of static pressure downstream of the separated point may be due to eddies and vortices within the inlet impinging on the static pressure taps. It should be noted that the uncertainty in this measurement is significant.

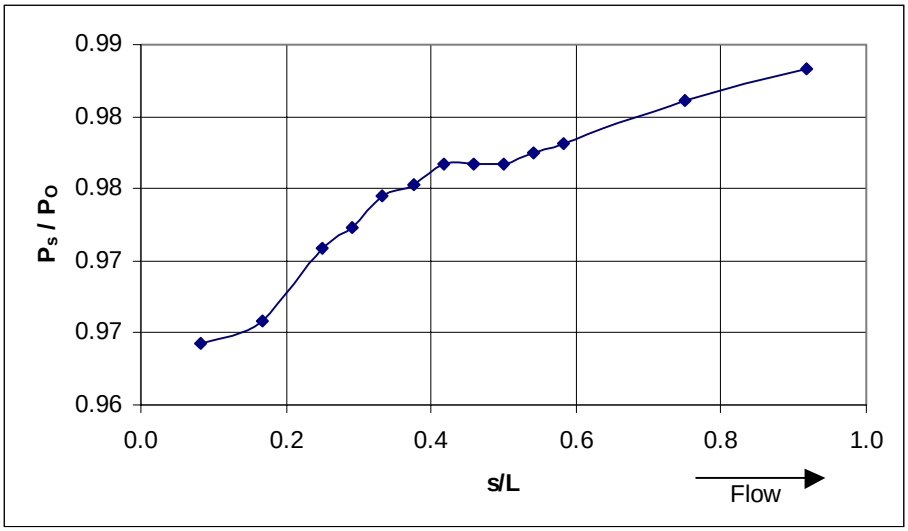

Figure A.1: Static pressure distribution along curved surface: flow separates at s/L ≈ 0.45 (on blower)

To compare the results found on the blower to what was later found on the simulator, the inlet Mach number and mass flow was measured in a similar way to that described in Section 4.1. At the center of the entrance, the Mach number on the blower was found to be 0.22, while the Mach number on the simulator was later found to be 0.23. Figure A.2 shows the Mach number profile at the entrance. Using numerical integration, the mass flowrate was found to be 869 scfm on the blower and 759 scfm on the simulator, which is a 15% difference.

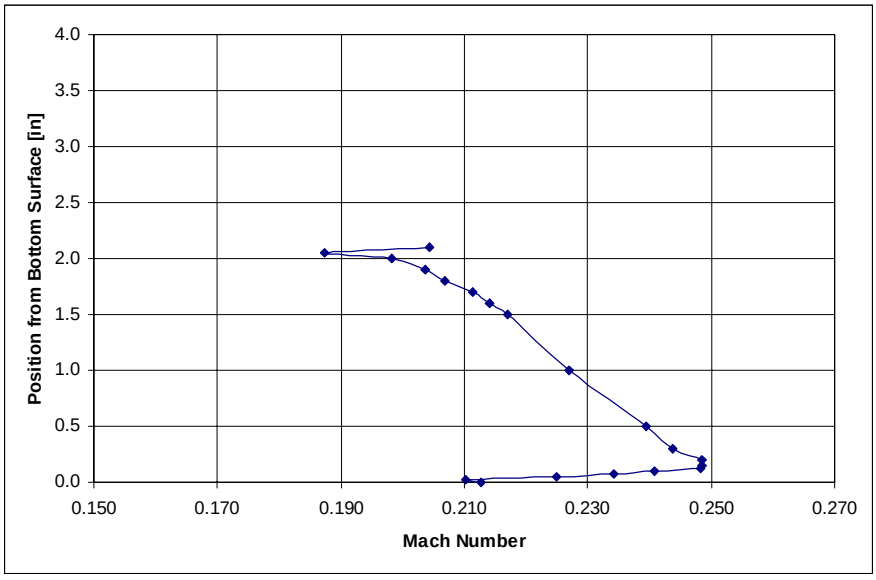

Figure A.2: Mach number profile at entrance to inlet attached to the blower

A.2 Suction and Blowing Hole Design

Once the flow inside the inlet was characterized, the suction and blowing holes had to be designed. Kerrebrock *et al*. (1998) suggested that boundary layer suction is best applied just prior to the point of separation. Therefore, the results shown in the previous section indicated that the suction holes should be placed at Station 50, which is approximately 7.0 in from the back of the bellmouth following the curved surface. Poisson-Quinton and Lepage (1961) claimed that finely perforated suction holes provide the best method to remove the boundary layer, so the diameter of the suction holes was set to be 0.055 in. Experiments were performed at the exit of the inlet to determine an appropriate number of suction holes. The Vaccon VDF 250 provided the suction for these experiments on the blower. The tested configurations included (1) 9 holes covering 2.0 in of the inlet's width, (2) 17 holes covering 2.0 in of the inlet's width, and (3) 30 holes covering 3.75 in of the inlet's width. Table A.2 compares the results, and shows that the 17-hole configuration provides the best improvement.

Table A.2: Comparison of suction holes at the exit of the inlet (on blower)

Number of holes	Width [in]	Flowrate [%-core]	Profile
9	2.00	0.94	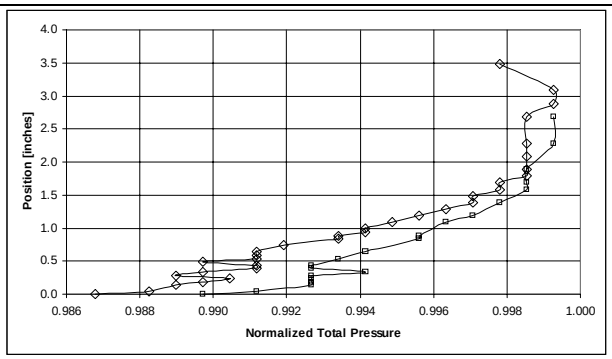
17	2.00	1.24	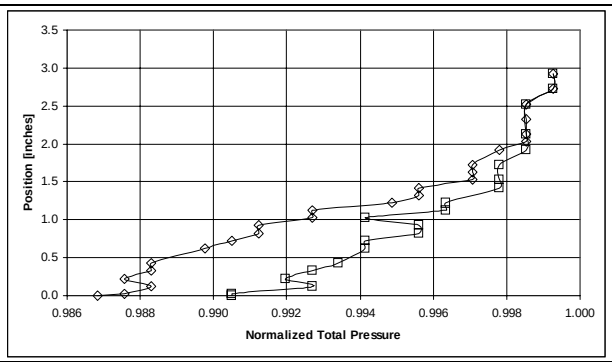
30	3.75	0.80	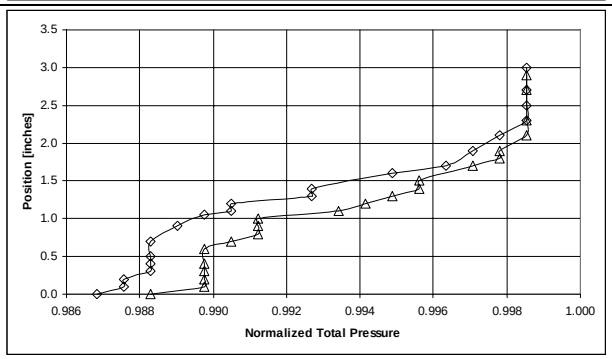

The blowing holes were placed as close as possible downstream of the suction holes. The size of the plenums provided a spatial limitation. The holes were pointed downstream and attached to the inlet as discussed in Section 3.1.2.2. Design iterations were not performed on the blowing configurations since the first iteration showed sufficient results.

The combined use of suction and blowing were examined on the blower. The results are shown in Figure A.3, and are similar to the results given in Figure 4.6.

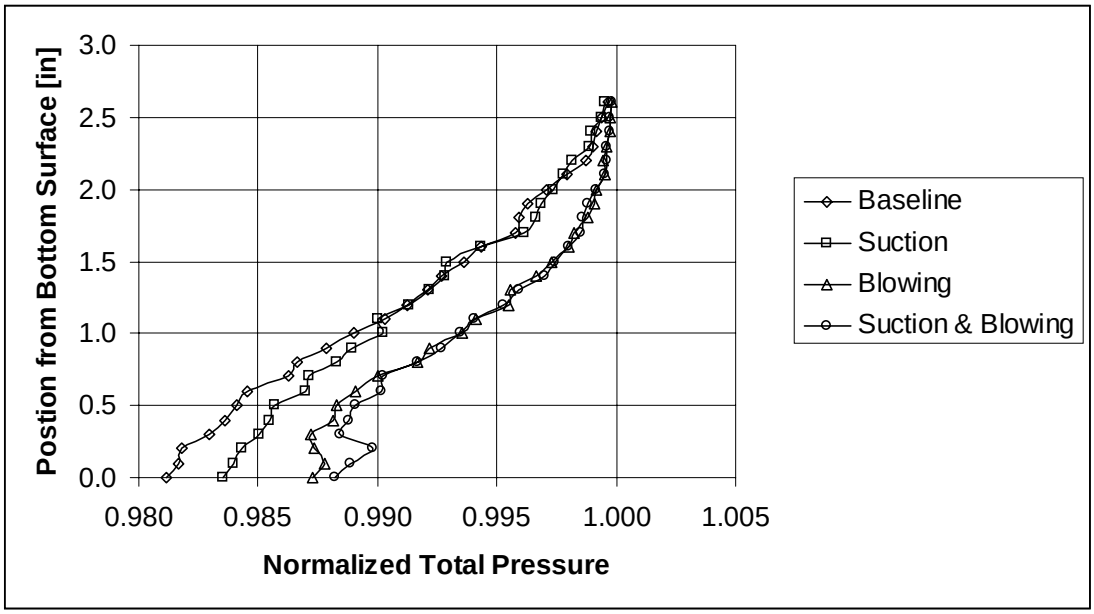

Figure A.3: Aerodynamic profiles with BLC at the exit of the inlet (on blower)

Instead of the blower, the simulator was used as the source of flow through the inlet for the data presented in Chapter 4.0. As the dissimilar baseline profiles of Table A.2 and Figure A.3 show, the blower bench tests are not highly repeatable. The blower is operated by an electric motor, and the blower speed was found to be highly sensitive to other loads on the electrical circuit. The control valve, however, can maintain the simulator's speed to within 500 rpm. Furthermore, varying the supply pressure for the simulator allows a wide range of simulator speeds and throat Mach numbers, but the speed of the blower is not variable.

Appendix B: Error Analysis

In Chapter 4.0 some measurements were given with an estimate of the uncertainty in that value. The given uncertainty was calculated based on a method presented in Beckwith *et al*. (1993 p. 82). Appendix B will attempt to outline the method.

The total uncertainty in a measurement is a function of the bias of the measurement and the precision of the measurement. Equation (B.1) algebraically defines uncertainty. Bias error is defined as the error produced by the system, while precision error is defined as the error associated with the randomness of the phenomenon being measured (Beckwith *et al*. 1993, p. 48). The bias error is usually quoted by the manufacturer of the measurement device, while the precision error is the standard deviation of a multi-sampled value.

$$u_i = \sqrt{(b_i)^2 + (p_i)^2} \tag{B.1}$$

where u_i is the total uncertainty
b_i is the bias of the measurement
p_i is the precision of the measurement (standard deviation, σ_i)

Once the uncertainty of a measured value is known, the uncertainty propagates to a calculated quantity through a formulation developed by Kline and McClintock (1953). If the desired value of an experiment is a function of a set of measurements, i.e. $y = f(x_1, x_2, \ldots, x_n)$, then the resultant uncertainty in y is given by Equation (B.2).

$$u_y = \sqrt{\sum_{i=1}^{n} \left(\frac{\partial y}{\partial x_i} u_{x_i} \right)^2} \tag{B.2}$$

where u_y is the total uncertainty in y
y is the desired calculated quantity
x_i is the measured quantity
u_{x_i} is the uncertainty in the measured quantity

In this thesis, the previous method was applied to several equations. For example, the mass flowrate of the simulator was calculated based on Equation (4.2) and the distortion intensity was calculated based on Equation (4.3). For all of these calculations, measurements of several different types had to be made: total pressure, static pressure, temperature, etc. When the DAQ system sampled the pressure for 10 s at 100 Hz, the standard deviations of the 1000 data samples provided an estimate of the precision error. Coupled with the transducer's bias error, the total uncertainty of the pressure at that point propagated through the calculations for the simulator mass flowrate, intensity, etc. The biases of the directly-measured quantities are given in Table B.1, and the resulting total uncertainties of the calculated quantities are given in Table B.2.

Table B.1: Listing of the measurement bias

Measured Quantity	**Bias of Quantity**
Total Pressure	±0.00125 psi
Static Pressure	±0.003125 psi
Ambient Pressure	±0.007 psi
Width of inlet	±0.001 in

Table B.2: Listing of the total uncertainty of the calculated quantities

Calculated Quantity	**Total Uncertainty of Quantity**
Suction mass flowrate	Less than 0.1%
Blowing mass flowrate	±1.7%
Core flowrate	±8.5 scfm
Distortion Intensity, *I*	±0.0002 minimum to ±0.00037 maximum
Distortion, *D*	±0.00040 minimum to ±0.00065 maximum
Total pressure recovery, *TPR*	±0.00010 minimum to ±0.00018 maximum
Flow ratio, $\eta_{\sigma i}$	±0.0023 minimum to ±0.0043 maximum

Appendix C: Alternate Sensing Scheme

In Section 4.2.2 the exit microphone was assessed of its potential to be a feedback sensor in an active BLC system. It was shown that a strong correlation exists between the aerodynamic profiles and the microphone pressure spectrums as the blowing rate increases. Unfortunately, even though the distortion was minimized with a blowing rate of 1.37% of the core flow, the microphone signal never reached a minimum. Therefore, without modifications, the microphone as a feedback sensor would drive the blowing rate increasingly higher to generate even higher distortion.

As mentioned in Section 2.3, there are a few components to a microphone signal within a fluid: acoustic pressure fluctuations, turbulent pressure fluctuations, and vibration. The microphone signals presented in Section 4.2.2 contain all three components. Agarwal and Simpson (1989) and Simpson *et al*. (1987) presented a method of resolving a microphone signal into its different components. The methods are presented briefly in Section 2.3.3.

A hypothesis was made that even though the entire microphone sensor is not minimized when the distortion is minimized, one of the components might be. To test this hypothesis, the experiment described in Section 4.2.2 was repeated with the two arrays of three microphones described in Section 3.1.4.2. The aerodynamic profiles are shown in Figure C.1. The corresponding distortion values are given in Figure C.2. The processed microphone spectrums are given in Figure C.3 and Figure C.4. The rms pressure within the frequency range of 25 and 300 Hz was combined with Equation (4.8), and Figure C.5 compares the time and space filter signals with the single microphone signal.

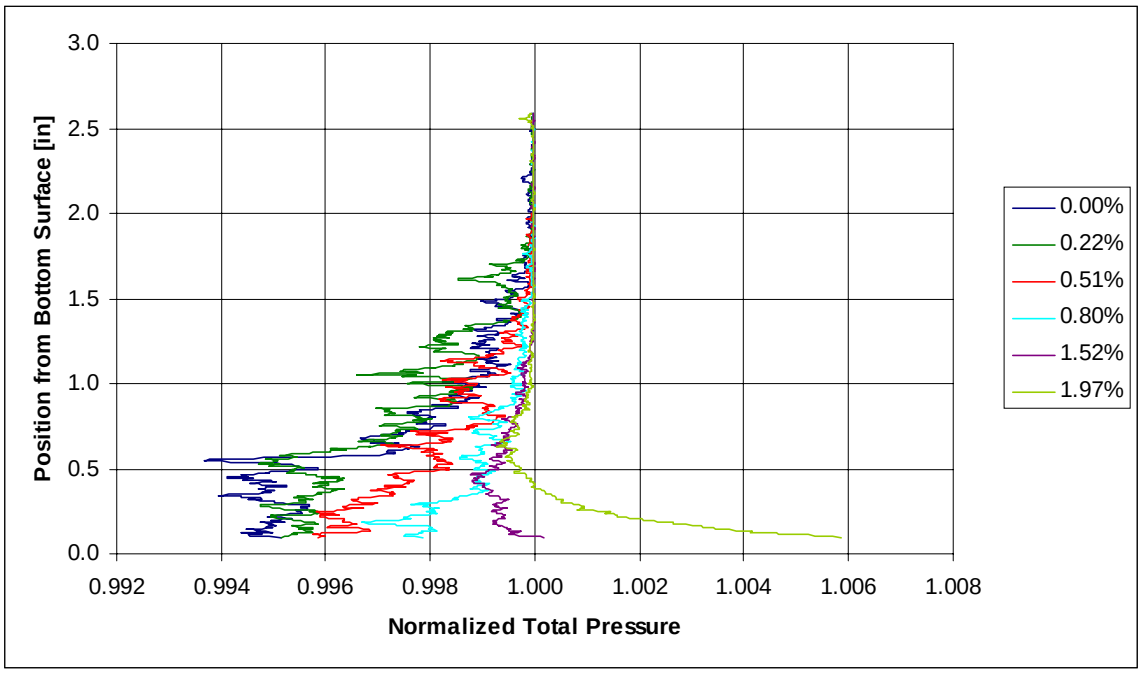

Figure C.1: Effect of different blowing rates [%-core] on the total pressure profile, at 30 krpm

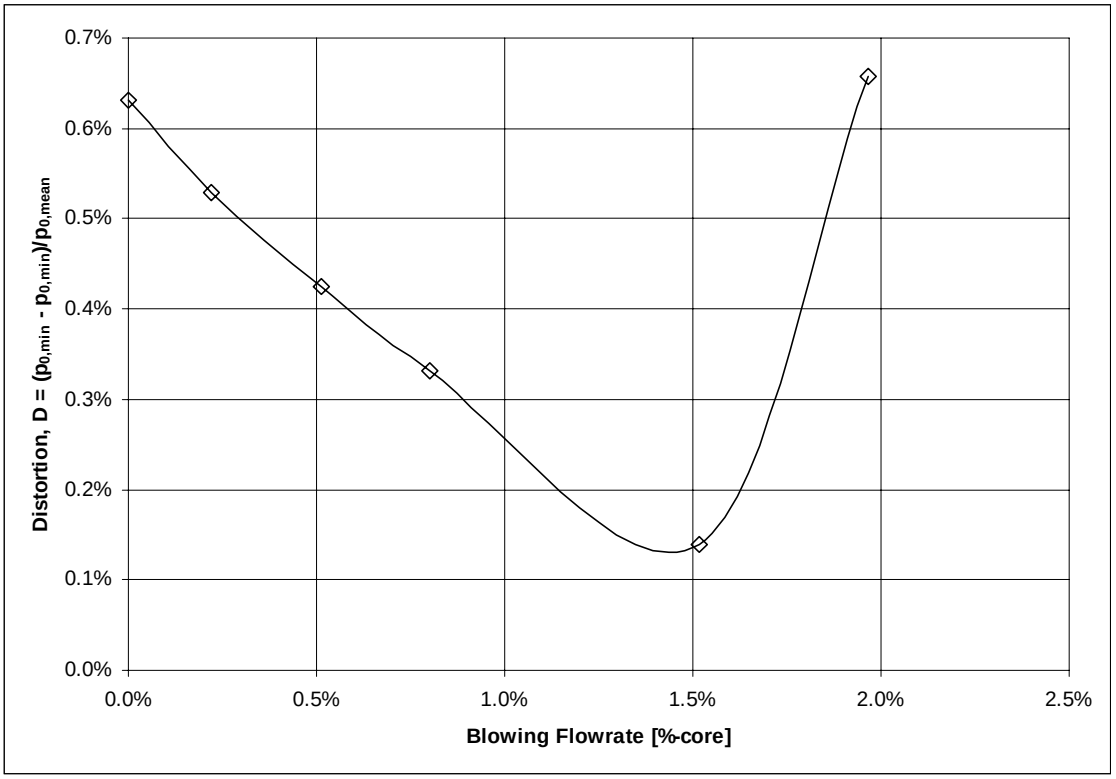

Figure C.2: Distortion calculated at the exit of the inlet, at 30 krpm

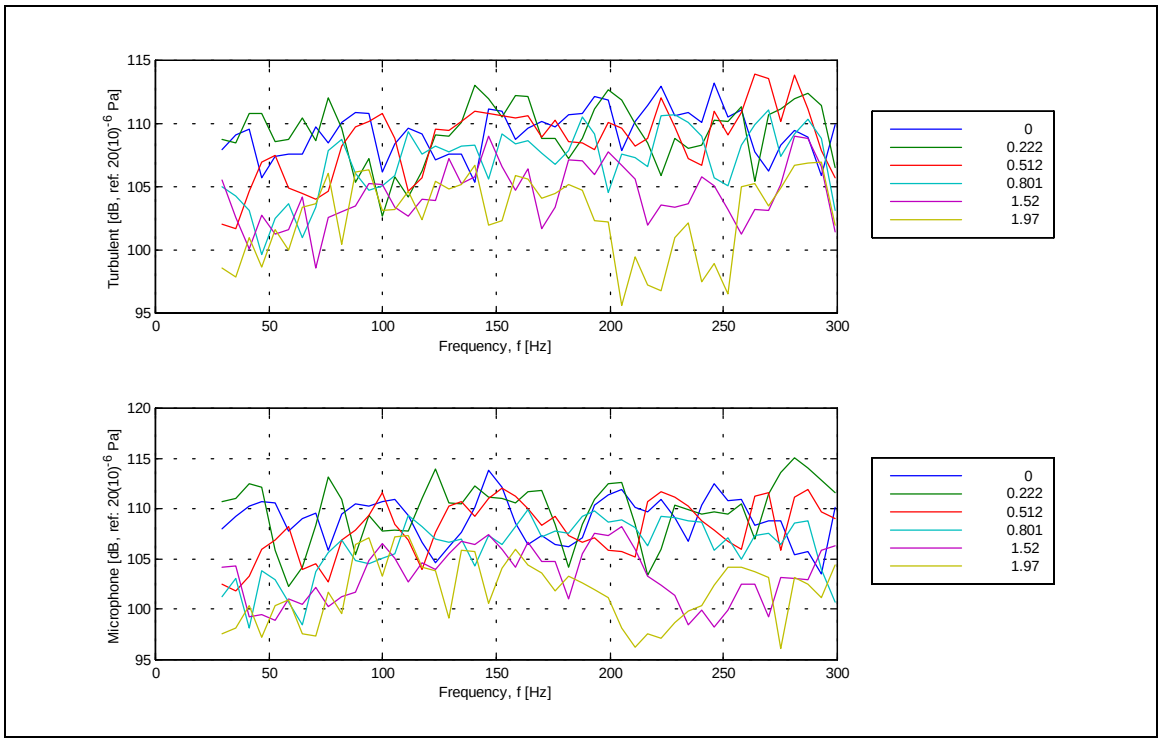

Figure C.3: Pressure fluctuations with time filter versus blowing rate [%-core], 30 krpm

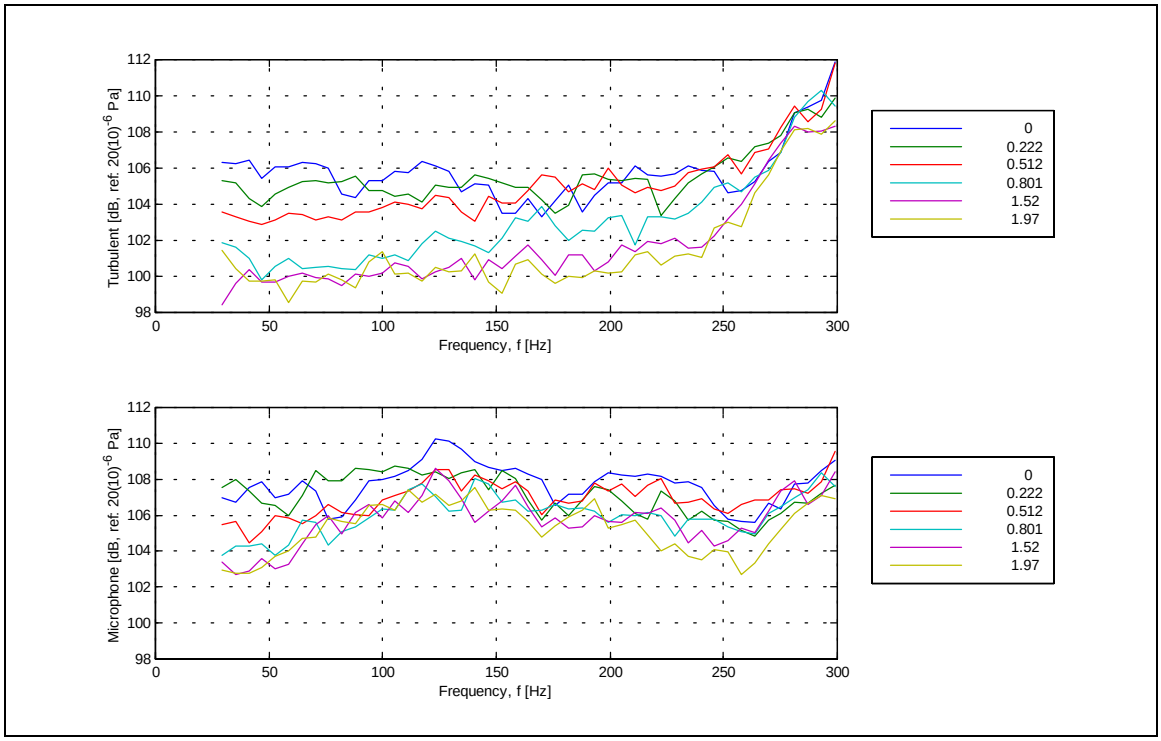

Figure C.4: Pressure fluctuations with space filter versus blowing rate [%-core], 30 krpm

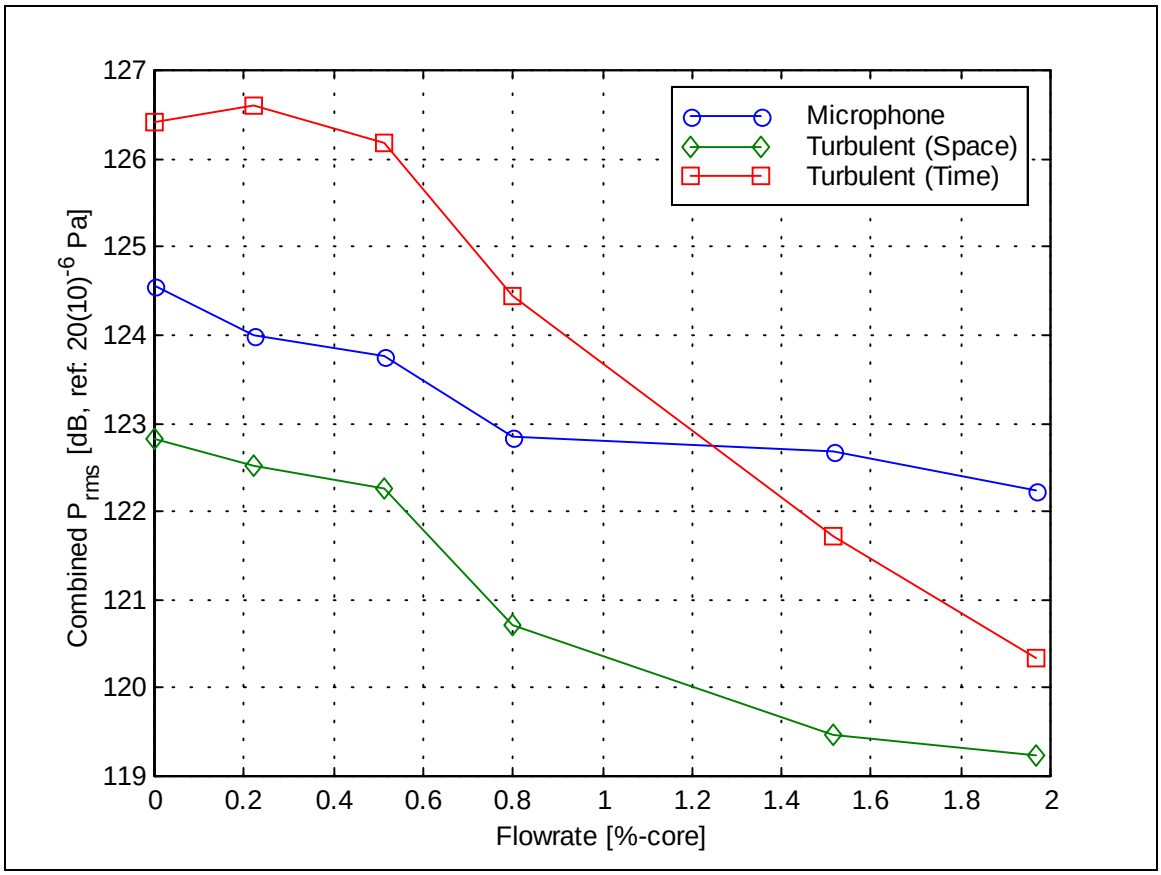

Figure C.5: Comparison of combined pressure signal between 25 and 300 Hz, 30 krpm

The results presented in the previous figures suggest that turbulent pressure fluctuations follow the same trend as the entire microphone signal. However, a lack of resources hindered the precision and accuracy of the results of the experiment. The microphones were not flush with the curved inlet surface, which is the source of most of the inaccuracies. The steps and cavities left by the microphones create flow regimes that are independent from the core flow. Therefore, the microphones within the array sense different flow phenomena and the assumptions required to obtain the turbulent pressure fluctuations fail. Figure C.6 shows that the two calibrated microphones in the space filter, for example, see entirely different flow phenomena since the amplitudes are different by a factor of two. With microphone signals so greatly different, the results presented in Figure C.5 cannot lead to conclusive results.

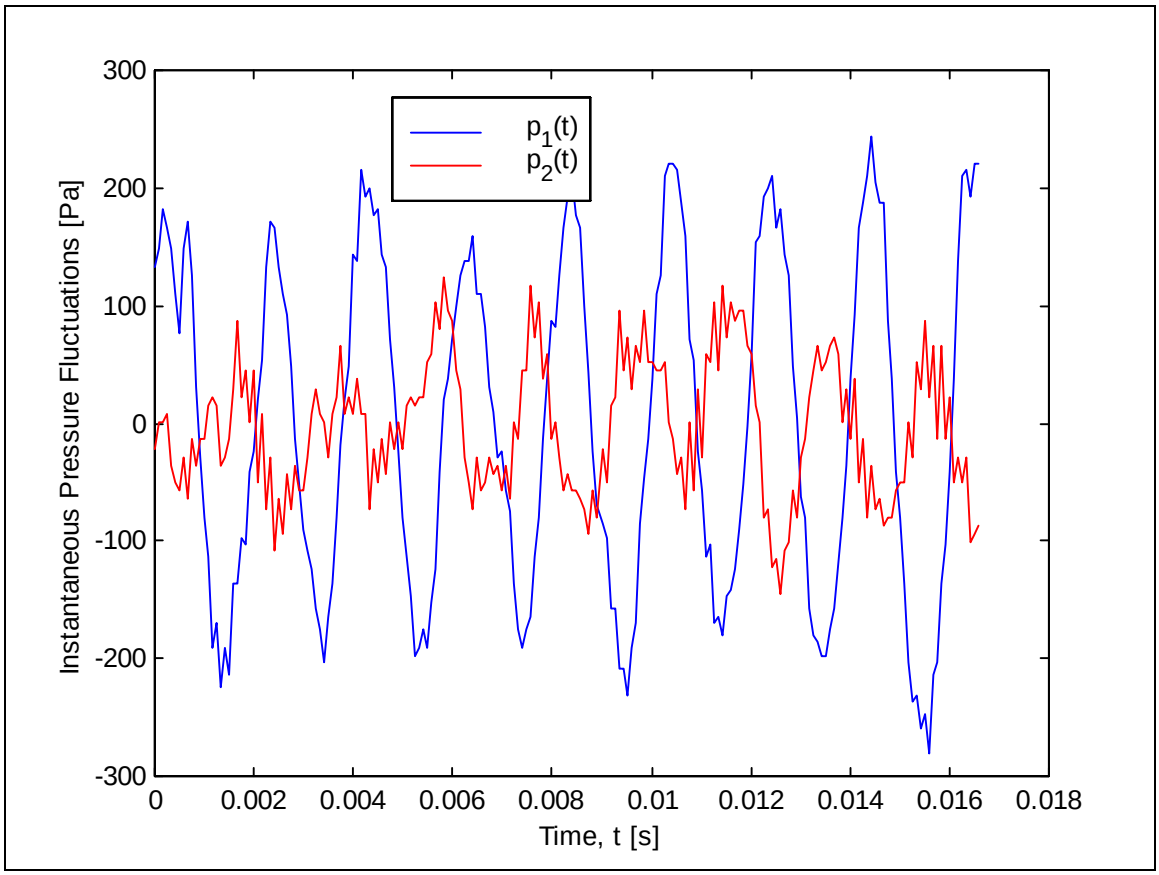

Figure C.6: Comparison of calibrated microphone signals in the time filter array

The results presented in this appendix should not discourage future projects to investigate the role that turbulent pressure may have in an active flow control scheme within an inlet exhibiting separated flow. With proper resources, the microphone arrays may prove to be a viable feedback sensor. The problem with the microphones not being flush to the curved surface can be resolved by using pinhole apertures in the surface that opens into a microphone casing. The apertures should then be calibrated with a known source and with the rest of the microphones within the array to ensure that all microphones have the same transfer function.

Appendix D: Integrated Ejector Pumps

In Section 4.1.3.4 it is mentioned that an integrated ejector pump could greatly benefit inlet designs relying on BLC. With an integrated ejector pump, only one bleed is needed from the latter stages of the compressor to provide both boundary layer suction and blowing. Appendix D will summarize the results of a preliminary assessment of the ability of an integrated ejector pump array to control boundary layer separation

A set of off-the-shelf ejector pumps was modified to fit onto the inlet. The cylindrical bodies of Vaccon JS-60 ejector pumps were milled flat to leave only the necessary material. Then, the ejector pumps were placed on the inlet as shown in Figure D.1. A high-pressure plenum was regulated to 65 psi to power the ejector pump. The suction port of the ejector pump was connected to the suction holes inside the inlet, and the exhaust port of the ejector pump was connected to the blowing holes. The ejector pumps connected to the high-pressure plenum and the inlet are shown in Figure D.2.

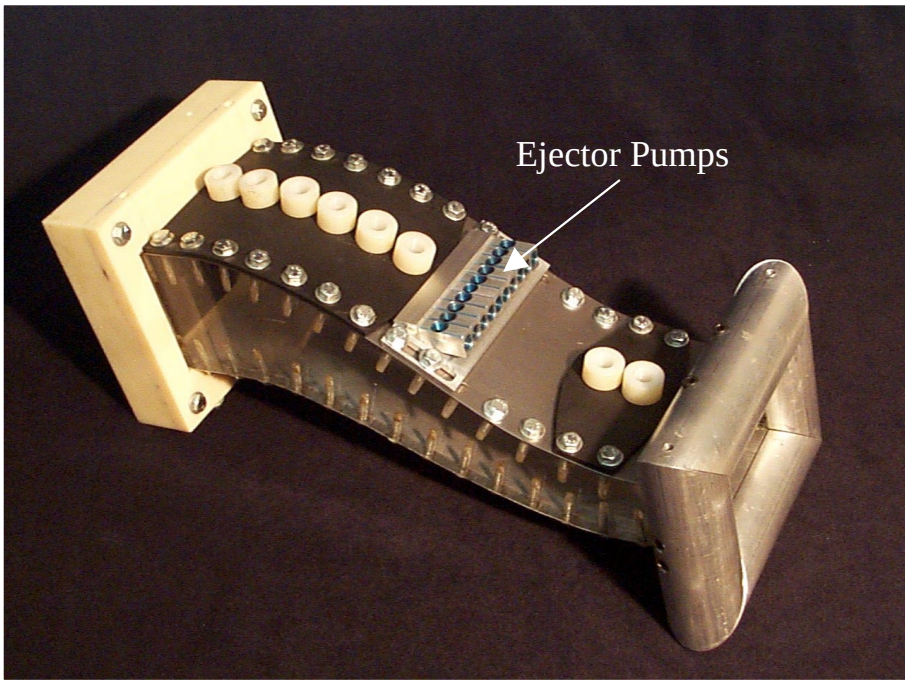

Figure D.1: Picture of inlet with modified ejector pumps

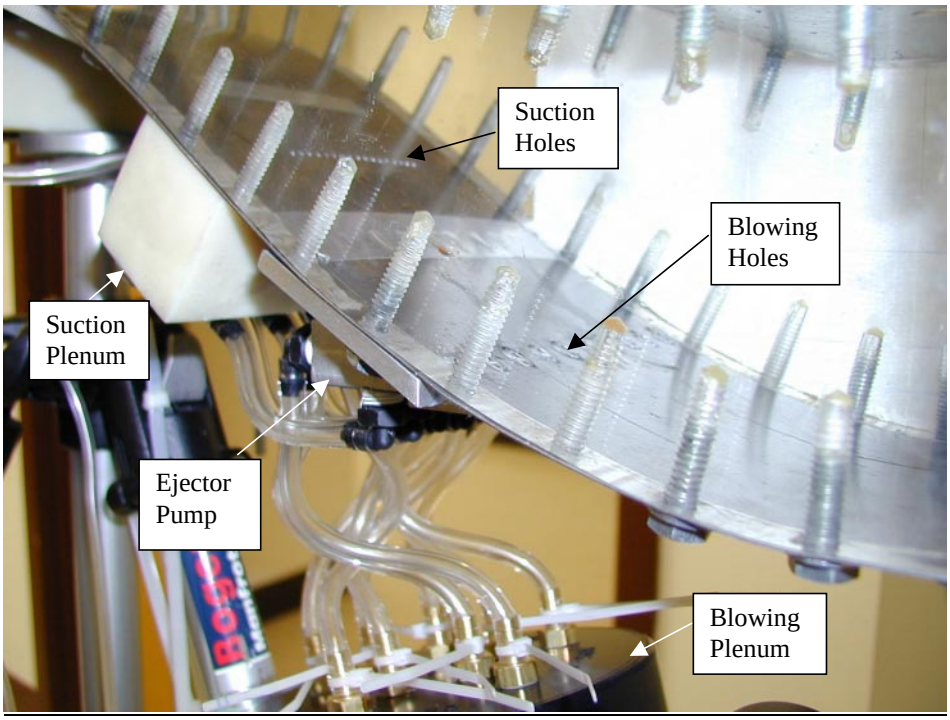

Figure D.2: Picture showing ejector pump installed on the inlet

The inlet with the modified ejector pumps was placed on the intake to a centrifugal blower, and traverses at the exit examined how well an ejector pump could provide both the boundary layer suction and the boundary layer blowing. The profiles are shown in Figure D.3, and the calculated distortion parameters are given in Figure D.4 and Figure D.5. Because of the different test conditions between the blower and the simulator, it is difficult to compare these results with the results found in Section 4.1.3. The integrated ejector pumps did, however, improve the distortion intensity by 31.9% and the distortion by 32.0% on the blower. Comparatively, the combined suction and blowing case on the simulator tests improved intensity and distortion by 56.5% and 40.5%, respectively.

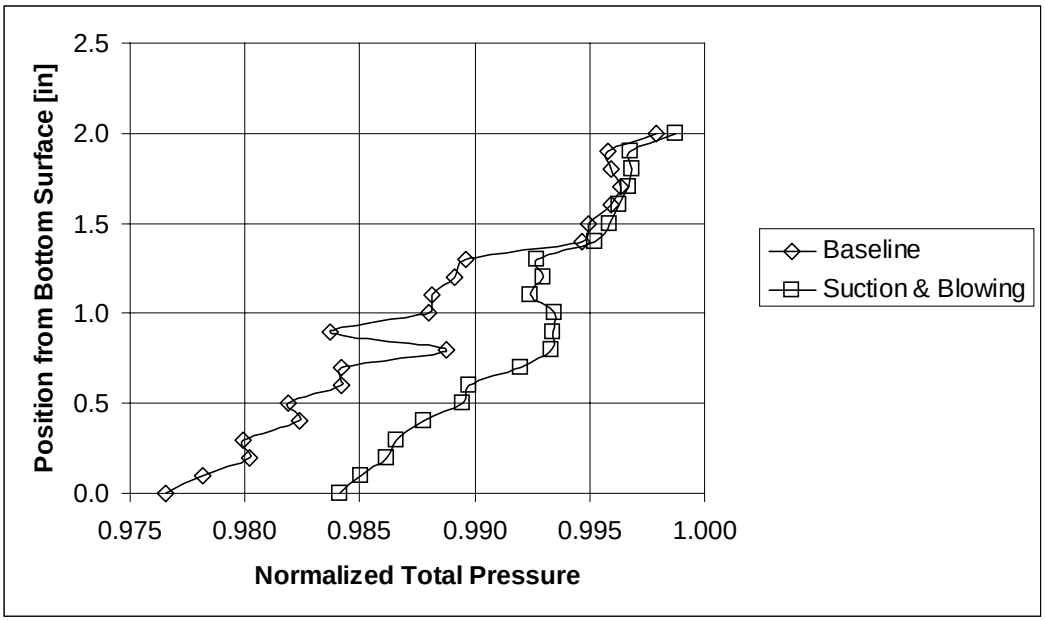

Figure D.3: Preliminary integrated ejector pump results (on blower)

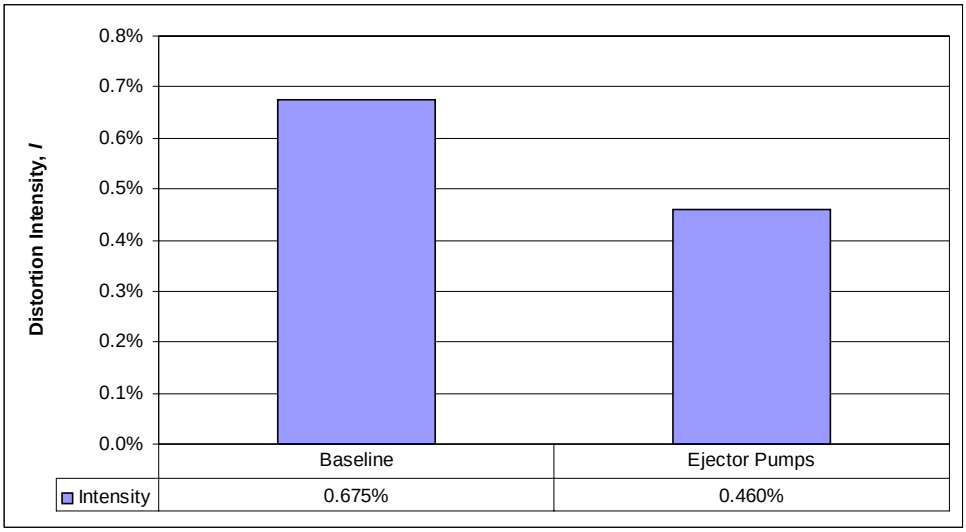

Figure D.4: Distortion intensity with integrated ejector pumps (on blower)

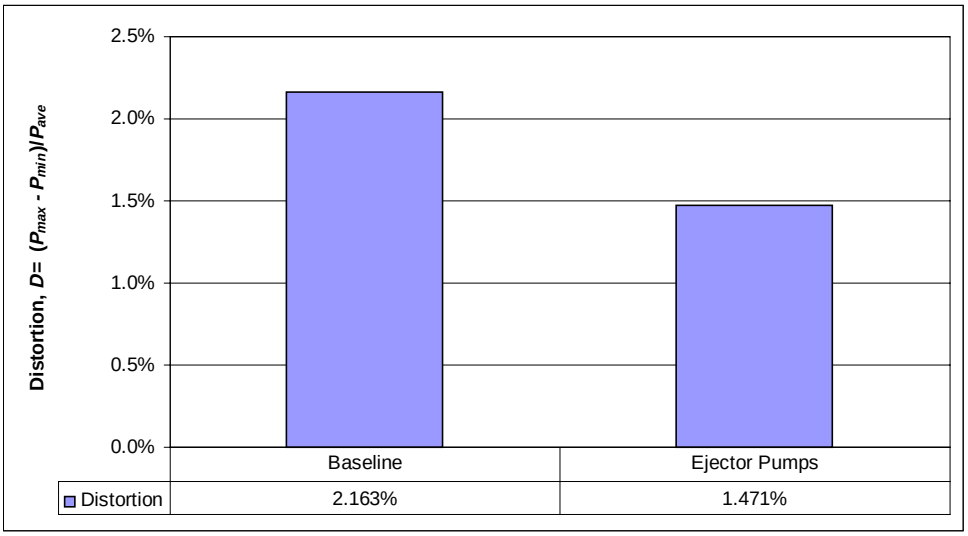

Figure D.5: Distortion with integrated ejector pumps (on blower)

Ejector pumps are susceptible to changes in back-pressure, which may explain why the integrated ejector pumps saw somewhat limited success. To further the problem, the designs of today's ejector pumps do not provide very useful exhaust flows, simply because their designers did not expect the exhaust to be used for boundary layer blowing. The development of ejector pumps that provide efficient jets of air is required before an integrated ejector pump would be viable.

Vita

David K. Harper

David K. Harper was born January 25, 1977 in South Charleston, WV, but grew up in Scott Depot, WV where he attended Winfield High School. He graduated *Summa Cum Laude* from Virginia Polytechnic Institute and State University in May 1999 with a Bachelor of Science in Mechanical Engineering. Immediately, he began his graduate studies in Virginia Tech's Mechanical Engineering Department under the direction of Dr. Wing Ng, while working for Technology in Blacksburg, Inc. as an assistant research engineer. Upon graduation, he will join the Air Compressor Group of Ingersoll-Rand in Davidson, NC. The author defended his thesis on May 4, 2000.